Regulation of human hematopoietic stem cell lineage commitment

Xiaoji Chen

A dissertation

submitted in partial fulfillment of the

requirements for the degree of

Doctor of Philosophy

University of Washington

2013

Reading Committee:

David Morris, Chair

Patrick Paddison, Co-Chair

Beverly Torok-Storb

Tony Blau

Ying Zheng

Program Authorized to Offer Degree:

Molecular and Cellular Biology

University of Washington

Abstract

Regulation of human hematopoietic stem cell lineage commitment

Xiaoji Chen

Chair of the Supervisory Committee:

David Morris

Department of Biochemistry

Understanding the molecular mechanisms that govern human hematopoiesis remains a major goal of both developmental and clinical biology. My thesis projects focus on identifying and characterizing regulatory factors involved in myeloid commitment steps for human hematopoietic stem and progenitor cells (HSPCs), so as to expand them *in vitro* or direct them into desired lineages.

I first studied the histone methyltransferases G9a and GLP, which play key roles during mammalian development through mono- and di-methylation of

histone H3 lysine 9 (H3K9me1/2), modifications associated with transcriptional repression. I found that G9a/GLP activity drives progressive, genome-wide H3K9me2 patterning in euchromatin during HSPC lineage specification. Remarkably, HSPCs continuously treated with UNC0638, a G9a/GLP small molecular inhibitor, better retain stem cell-like phenotypes and function during *in vitro* expansion. This expansion effect was further enhanced by co-treatment of SR1, an aryl hydrocarbon receptor (AHR) inhibitor. Moreover, UNC0638 treated HSPCs preferentially gave rise to megakaryocytes over other myeloid lineages when differentiating. These results suggest that G9a/GLP activity facilitates human HSPC lineage commitment and inform clinical manipulation of donor-derived HSPCs *in vitro*.

I also applied a high-throughput shRNA screening approach to identify genes controlling early myeloid differentiation of human HSPC. To aid in identification of candidate screen hits, data from the shRNA screen were compared to known hematopoietic/hematopoietic malignancy functions and mouse HSC eQTLs. Potential self-renewal and differentiation genes were validated by a secondary screen. Further functional validations will involve gene knockdown experiments followed by flow analysis, colony-forming unit assays, and *in vivo* experiments in a canine transplantation model. Ultimately our results will facilitate *in vitro* and *in vivo* manipulations of human HSPC to control lineage commitment.

ACKNOWLEDGEMENTS

This work would not be made possible without the guidance and help of many individuals. I owe the greatest thanks to my mentors Drs. Patrick Paddison and Beverly Torok-Storb for everything they have taught me in science and in life throughout these years. They have set a high standard as great scientists themselves. They always support me in good times and in bad times. I couldn't ask for better mentors. I want to thank Dr. Tony Blau for letting me explore the molecular and cellular world for the first time as an undergraduate student and continuously help me in graduate school. I would also like to thank Drs. David Morris, David Emery, Ying Zheng, and Bruce Clurman for being on my committee and for all their valuable discussions at our meetings.

I thank all my labmates in the Paddison lab and Torok-Storb lab for helping me generating ideas, carrying out experiments and encouraging me when things don't go well. Special thanks to Yang-Li Ou and Kyobi Skutt-Kakaria for closely working with me and contributing to this work.

I was very privileged to have many outstanding collaborators in the course of this work: Drs. Andrew Emili, Matthew Ferro, Keith Loeb, Shelly Heimfeld, Jerry Davison, Brent Wood, George Georges, Julio Vazquez, Lopez Punam Malik, et al. I couldn't complete this work without their intellectual inputs and technical assistances.

Last but not least, I want to thank my parents, my fiancé, and all my friends, for making me the happiest person I ever could be.

TABLE OF CONTENTS

Chapter 2. Materials and methods

Chapter 3. G9a/GLP-dependent histone H3K9me2 patterning during human hematopoietic stem cell lineage commitment

LIST OF FIGURES

LIST OF TABLES

CHAPTER 3

CHAPTER 5

LIST OF ABBREVIATIONS

AHR	Aryl hydrocarbon receptor
ANC	Absolute neutrophil counts
Angptl5	Angiopoietin-like 5
APC	Allophycocyanin
BIX	BIX01294
BM	Bone marrow
BSA	Bovine serum albumin
C/EBP	CCAAT/enhancer-binding protein
CFSE	Carboxyfluorescein succinimidyl ester
CFU	Colony-forming unit
CGI	CpG islands
ChIP	Chromatin immunoprecipitation
CLP	Common lymphoid progenitor
CMP	Common myeloid progenitor
DAPI	4',6-diamidino-2-phenylindole
DMSO	dimethylsulfoxide
DNA	Deoxyribonucleic acid
DNMT	DNA methyltransferase
EDTA	Ethylenediaminetetraacetic acid

EHMT1	Euchromatin histone methyl transferase 1 (also called GLP)
EHMT2	Euchromatin histone methyl transferase 2 (also called G9a)
EPO	Erythropoietin
ESC	Embryonic stem cell
FACS	Fluorescence-activated cell sorting
FHCRC	Fred Hutchinson Cancer Research Center
FITC	Fluorescein isothiocyanate
FLT3L	fms-related tyrosine kinase 3 ligand
G-CSF	Granulocyte colony-stimulating factor
GATA1	GATA-binding factor 1
GATA2	GATA-binding factor 2
GFP	Green fluorescent protein
GM-CSF	Granulocyte-macrophage colony-stimulating factor
GMP	Granulocyte monocyte progenitor
Gy	Gray
H3K9me2	Histone H3 lysine 9 di-methylation
HBE1	Hemoglobin, epsilon 1
HBG1	Hemoglobin, gamma A
HBG2	Hemoglobin, gamma G
HDAC	Histone deacetylase
HKMT	Histone lysine methyltransferase
HLA	Human leukocyte antigen

HOXA9	Homeobox A9
HOXB4	Homeobox B4
HSC	Hematopoietic stem cell
HSCT	Hematopoietic stem cell transplantation
HSPC	Hematopoietic stem and progenitor cell
IF	Immunofluorescence
IGF	Insulin-like growth factor 1
IGFBP2	Insulin-like growth factor binding protein
IgG	Immunoglobulin G
IL-3	Interleukin-3
IL-6	Interleukin-6
IMDM	Iscove's modified Dulbecco's media
iPSC	Induced pluripotent stem cell
JMJD	Jumonji domain-containing protein
LCR	Locus control region
LDA	Limiting dilution assay
LINE	Long interspersed repetitive element
LMO2	LIM domain only 2
LOCK	Large organized chromatin K9me2 modification
Meg	Megakaryocyte
MEP	Megakaryocyte erythrocyte progenitor
miRNA	microRNA

MLP	MSCV-LTRmiR30-PIG
MPL	Myeloproliferative leukemia virus oncogene, also known as CD110
MPP	Multi-potent progenitor
NOD/SCID	Non-obese diabetic/severe combined immunodeficient
NSG	NOD/Scid/IL-2 receptor-γ null
PBMC	Peripheral blood mononuclear cell
PBS	Phosphate buffered saline
PCR	Polymerase chain reaction
PE	Phycoerythrin
PF4	Platelet factor 4
PIC	Protease inhibitor cocktail
PMSF	phenylmethanesulfonylfluoride or phenylmethylsulfonyl fluoride
PRMT	Protein arginine methyltransferase
RBC	Red blood cell
RNA	Ribonucleic acid
RNAi	RNA interference
RT-qPCR	Real time quantitative PCR
Runx1	Runt-related transcription factor 1
SAM	S-adenosyl-methionine
SCF	Stem cell factor
SDF1	Stromal-derived factor-1
SDS	Sodium dodecyl sulfate

shRNA	Short hairpin RNA
SINE	Short interspersed repetitive element
siRNA	Small interfering RNA
SR1	StemRegenin 1
SRC	SCID-repopulating cell
TBI	Total body irradiation
TET	Ten-eleven translocation
TPO	Thrombopoietin
TSS	Transcription start site
UCBT	Umbilical cord blood transplantation
UNC	UNC0638
ZNF	Zinc finger

CHAPTER 1

INTRODUCTION

1.1 Hematopoiesis

During mammalian development, hematopoiesis first takes place in the yolk sac, and then moves to the aorta-gonad mesonephros (AGM) region, the fetal liver and finally the adult bone marrow (Orkin and Zon 2008). The mammalian hematopoietic system is hierarchically organized such that the developmental potential to produce lineages and terminally differentiated cells is progressively restricted. In the current model, hematopoietic stem cells (HSCs) initially give rise to multipotent progenitors (MPPs), which are no longer capable of long-term self-renewal but maintain full hematopoietic lineage differentiation capacity (Bystrykh et al. 2005; Christensen and Weissman 2001; Morrison and Weissman 1994). MPPs differentiate into common lymphoid progenitors (CLPs) and common myeloid progenitors (CMPs) (Akashi et al. 2000; Kondo et al. 2001; Serwold et al. 2009). These cells, in turn, further differentiate into bi- and mono-potent lymphoid and myeloid restricted progenitors, respectively. For myeloid lineages, these include bipotent granulocyte/monocyte progenitors (GMPs) and megakaryocyte/erythrocyte progenitors (MEPs). In the final step, fully lineage

restricted precursor cells (e.g., pro-megakaryocyte, pro-B-cell) mature into terminally differentiated effector cells. Thus, similar to other adult stem cell systems, partially restricted progenitors are responsible for generating all of the lineage-specific effector cells (i.e., erythrocytes, platelets, granulocytes, monocytes/macrophages, T-cells, etc.) (Orkin and Zon, 2008). In humans, this includes the daily production of >2x10^11 hematopoietic cells representing ~11 lineages, all of which arise from a small pool of self-renewing adult HSCs (Fig. 1.1) (Novershtern et al. 2011).

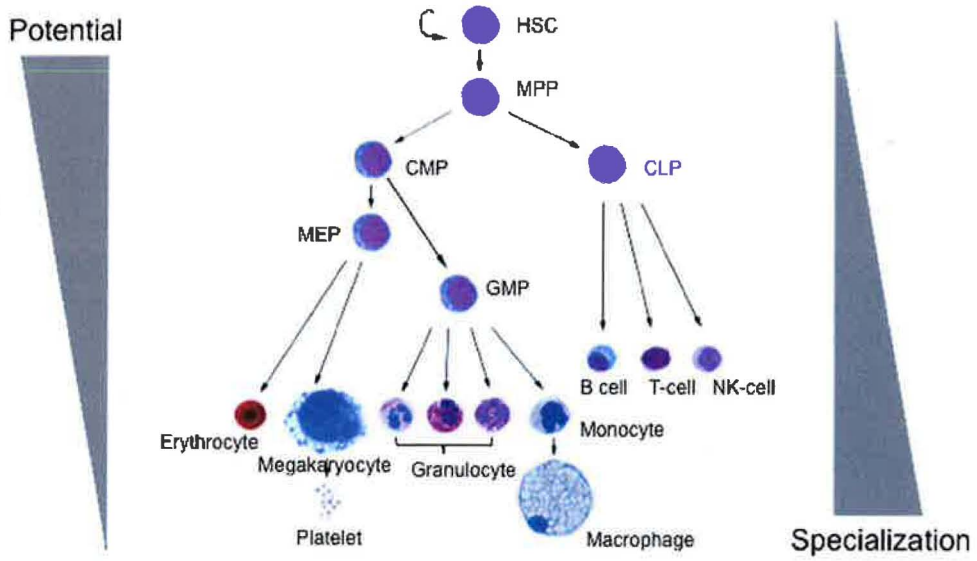

Figure 1.1. Model of human hematopoiesis. HSC give rise to two lineage restricted progenitor cells: CMP that gives rise to MEP GMP, which in turn differentiate into different types of myeloid blood cells; and CLP that gives rise to T cell, B cells, and nature killer cells. Cellular potential is gradually lost as the cells undergo specialization. (Figure modified from: *https://daley.med.harvard.edu/assets/Willy/hematopoiesis.jpg*)

1.1.1 Hematopoietic stem cell

It was first discovered over 50 years ago that there was a rare population of cells in the bone marrow, which, when injected into irradiated mice, could form colonies in the recipient spleens (Zon 2001). They were named colony-forming units-spleen (CFU-S). It was later found that transplantation of a single purified HSC into a lethally irradiated mouse was able to reconstitute the mouse's entire hematopoietic system (Ema et al. 2005).

Previous studies indicated that human HSC could be identified by their ability to efflux of a mitochondrial dye, rhodamine 123 (Baum et al. 1992). They can also be characterized by cell surface markers $Lin^{-}CD34^{+}CD38^{lo/-}$ $CD90^{+}CD45RA^{-}$ (Majeti et al. 2007). Based on these phenotypes, HSC can be isolated by fluorescence-activated cell sorting (FACS).

HSC is the most well studied human adult stem cell. As other stem cells, it can both self-renewal to maintain themselves, as well as differentiate into all lineages of blood cells. HSC are able to undergo asymmetric divisions, where one of the daughter cells remains a stem cell while the other one differentiates. A balance of HSC self-renewal and differentiate is determined by both intercellular factors and signals from the microenvironment. It is the most critical regulation particularly when the system is challenged (i.e. after stem cell transplantation). It is imperative that regardless of blood cell demand, the stem cell pool will be maintained.

Three decades of research on mammalian HSCs has resulted in their prospective isolation and the identification of gene products and cognate

signaling pathways that affect cell growth and differentiation. However, our understanding of the complexity of the signaling events controlling these cell fate decisions is only just emerging, and methods to control stem cell fate remain elusive. This has significantly limited the successful application of new approaches for HSC transplantation, including clinical transplantation procedures for patients with cancer, marrow failure, hemoglobinopathies, auto-immune diseases, or any other clinical condition that could benefit from an infusion of HSCs or their progeny.

1.1.2 Intrinsic and extrinsic factors regulating hematopoiesis

Loss-of-function and gain-of-function studies have revealed critical roles of transcriptional factors in controlling HSC self-renewal, proliferation, and lineage-specific differentiation. Dysregulation of the transcriptional network is often associated with hematopoietic disorders such as leukemia.

Runt-related transcription factor 1 (Runx1, also named AML1), LIM domain only 2 (LMO2), and T-cell acute lymphocytic leukemia 1 (tal-1/SCL) are required for HSC survival and self-renewal (Fig. 1.2) (Orkin and Zon 2008). Runx1 is expressed in all HSCs in the mouse embryo as well as in the adult bone marrow (North et al. 2002). Mouse HSC that lacks of Runx1 failed to generate erthrocytes, myeloid cells, and lymphocytes (North et al. 2002). Translocation and point mutation of Runx1 are found in leukemia (Ng et al. 2010). Both LMO2 and tal-1/SCL are essential for embryonic hematopoiesis *in vivo*. Mice homozygously deleted LMO2 or tal-1/SCL are "bloodless" and die at an early

stage in utero (Shivdasani and Orkin 1996). Abnormal activation of tal-1/SCL is frequently found in acute T-cell leukemia (Shivdasani et al. 1995).

On the other hand, several transcription factors have more lineage-restricted roles. GATA binding protein 1 (GATA1) is a major regulatory factor controlling globin gene expression in erythroid differentiation. GATA1-null mice showed severe anemia (Gutierrez et al. 2008). shRNA knockdown of GATA1 in $CD34^+$ cord blood cells inhibits STAT5-induced erythropoiesis (Wierenga et al. 2010). A murine GATA1- erythroid cell line was generated to better study the function and mechanism of GATA1 in erythropoiesis (Suh et al. 2006). GATA2 is expressed in HSC as well as erythrocytes. GATA2-deleted mouse embryonic stem cells (ESCs) form significantly less erythroid colonies *in vitro* than the wild type control (North et al. 2002). PU.1 and CCAAT/enhancer-binding protein C/EBPα favor the commitment to granulocytes and monocytes (Friedman 2007). Ablation of PU.1 prevents the generation of granulocytes, monocytes, and T and B lymphocytes (Laslo et al. 2006). Deletion of C/EBPα in mouse fetal liver resulted in increased number of erythroid cells and reduced number of myeloid cells, while overexpression of C/EBPα in HSC induced myeloid differentiation at the expense of erythroid differentiation (Suh et al. 2006).

Transcription factors physically and functionally interact with each other to form a regulatory network to control hematopoiesis. A good example is that, in cell fate choice of GMP, PU.1 actives Egr-2 and Nab-2, which induce macrophage and repress neutrophil differentiation. In contrast, C/EBPα up-regulates Gfi-1, which promotes neutrophil and inhibits macrophage

differentiation. In addition, Egr/Nab-2 and Gfi-1 repress each other (Laslo et al. 2006). Another example is that EKLF and Fli-1 antagonize each other to dictate erythroid versus megakaryocytic in lineage choice of MEP (Laslo et al. 2008).

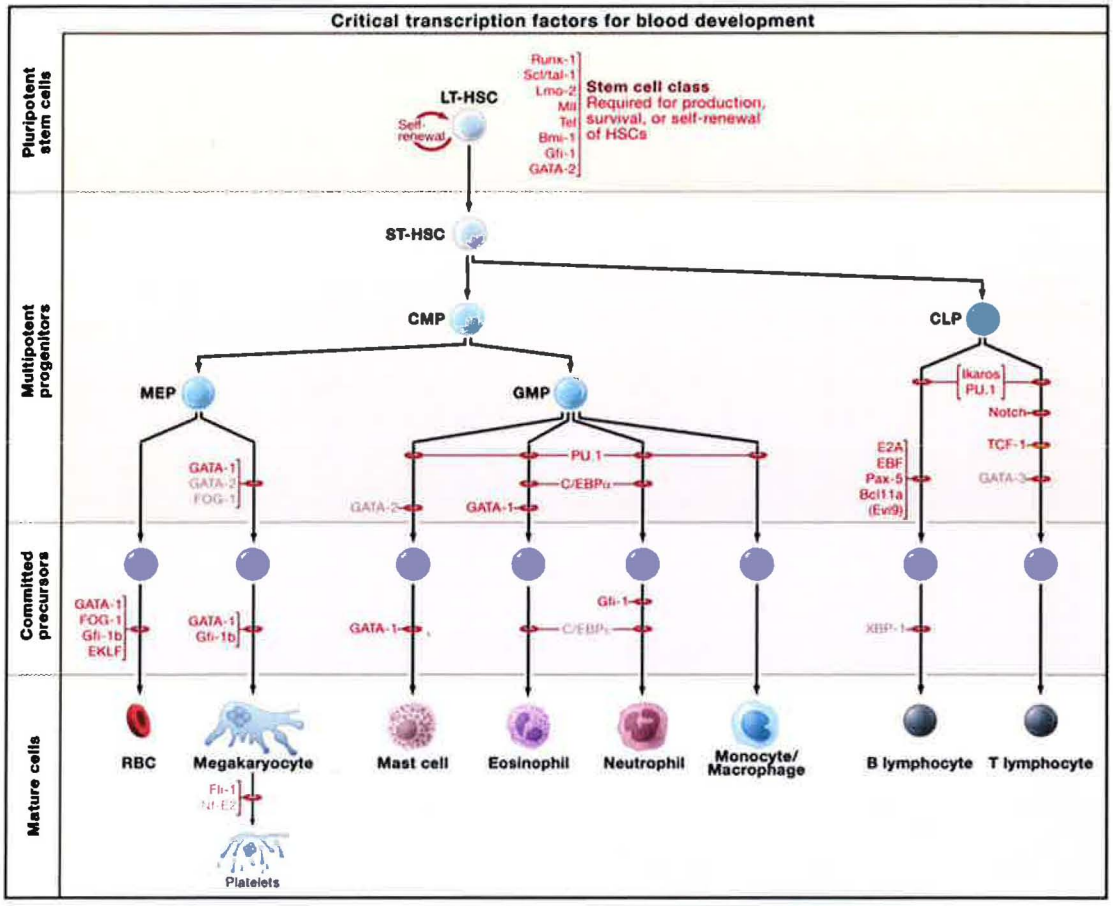

Figure 1.2. Transcriptional control of hematopoiesis.

(Figure adapted from Orkin, S.H. and Zon, L.I., 2008)

Genome-wide gene expression analysis has made it feasible to map transcriptional profiles in different populations of blood cells. A global gene expression study has shown that the more immature long-term HSC largely expresses molecules related to their interaction with the microenvironment; short-

term HSC preferably expresses genes involved in cell cycle initiation; while myeloid and lymphoid cells express lineage-specific markers (Ivanova 2002). Novel transcription factors that are up-regulated in HSCs vs. committed cells are being discovered, such as E2F1, SPIB, CNOT2, and HIF1A (Gomes et al. 2002).

Furthermore, in an adult human, HSCs reside within a special bone marrow microenvironment, or the niche, which is composed of osteoblasts, macrophages, adipocytes, and fibroblasts (Fuchs et al. 2004). Direct and indirect interactions and molecular cross-talks between HSCs and niche cells are essential in maintaining HSCs in a quiescent, undifferentiated state. Niche cells secret chemokines that are necessary for the maintenance of the HSC, including Kitl (also known as kit ligand, stem cell factor, or steel factor), Interleukin-6 (IL-6) and stromal-derived factor-1 (also known as SDF1, or CXCL12), jagged, BMP4, angioprotein (Renstrom et al. 2010). Disrupting the niche results in impaired hematopoiesis (Perry and Li 2007).

HSCs are able to attach to the niche through adhesion receptors (e.g. N-cadherin) and ligand-receptor interactions (e.g. Notch-Jagged) (Wilson and Trumpp 2006). Notch ligand Jagged1 is expressed by cells within the bone marrow niche, while Notch1 and Notch2 are both expressed on the hematopoietic progenitor cells (Kumano et al. 2001). This indicates a role of Notch signaling in regulation HSC. In fact, activation of Notch1 inhibits differentiation and enhances self-renewal of HSC *in vitro* (Stier et al. 2002). Another niche-dependent signaling pathway, the Wnt/beta-catenin pathway, also plays a key role in promoting HSC self-renewal in the absence of differentiation

(Renstrom et al. 2010). Wnt3a deficient mice died at embryonic day 12.5, and Wnt3a-/- HSCs showed impaired proliferation and differentiation (Luis et al. 2009).

HSC can be mobilized from their bone marrow niche to the peripheral blood by G-CSF. G-CSF induces proteases to cleave adhesion molecules on HSC (Greenbaum and Link 2010). In response to G-CSF treatment, HSC proliferate, detach from the niche, and enter into the circulating blood, from where they can be collected for purposes such as transplantation (Copelan 2006). G-CSF-mobilized HSC differ from those in the bone marrow in that they are more uniformly quiescent. A DNA microarray comparing $CD34^+$ cells from bone marrow vs. G-CSF mobilized peripheral blood has revealed different expression levels of genes involved in cell cycle (Graf et al. 2001).

1.1.3 *Ex vivo* manipulation of HSCs

One holdback of therapeutic application of human HSC is their inability to self-renewal and expand *in vitro*. Inadequate numbers of donor HSC is a major limitation of successful HSC transplantation (HSCT). One strategy clinicians use in umbilical cord blood transplantation (UCBT) to overcome this issue is to co-fuse UCB cells from a second donor. Double UCBT correlates with a lower rate of relapse (Smith and Wagner 2009), which suggests that an increase in the number of HSC is benefit clinical outcomes. Great efforts have been made to expand HSC *ex vivo*. A mixture of cytokines, such as stem cell factor (SCF), and fms-related tyrosine kinase 3 ligand (FLT3L), are commonly added to the culture

of human HSC in order to support their growth and expansion. However, no more than a four-fold expansion of HSC has been achieved with combinations of cytokines, and a gradually loss of HSC potential was observed (Sorrentino 2004).

Hox transcription factors are implicated in regulating HSC proliferation and differentiation. Previous studies have found that overexpression of HOXB4 or HOXA9 in HSC resulted in an increased self-renewal and extensive expansion of HSC *ex vivo*, while retaining their normal developmental potential (Antonchuk et al. 2002; Kirito et al. 2004). Considering that Notch and Wnt pathways are both present in the HSC niche and play a role in regulating HSC fate determinations, activation of these pathways is likely to result in expansion of the HSC pool. It has been shown that over-expression of Notch1 caused an increased self-renewal in HSC (Renstrom et al. 2010). However, an increase HSC numbers was not achieved in a clinical setting of *ex vivo* expansion using Notch ligand (personal communication). Incubation of HSC with Wnt proteins WNT5A and WNT3A is also associated with an increased expansion of HSC (Sorrentino 2004). A more recent study based upon a small molecular screen has discovered an aryl hydrocarbon receptor (AHR) antagonist, StemRegenin 1 (SR1), which was able to promote *ex vivo* expansion of human HSCs, while retaining their normal developmental potential (Boitano et al., 2010).

1.1.4 Megakaryopoiesis

Megakaryocytes are big (50-100 μm in diameter) cells with polyploid nuclei (up to 64N) (Szalai et al. 2006). During megakaryopoiesis (Fig. 1.3), HSCs first generate CMPs, which then differentiate into MEPs. MEPs are bi-potent, and can give rise to erythrocyte or megakaryocyte precursors. Megakaryocyte precursors then undergo a series of changes including endomitosis, organelle synthesis and cytoplasmic expansion. Mature megakaryocytes are no longer able to proliferate. During the formation of proplatelets, microtubules slide and overlap to drive proplatelet elongation. Besides, platelet granules and cellular organelle are transported to the end of proplatelets, from which platelets are released (Patel et al. 2005). One megakaryocyte can generate ~10^4 platelets. ~10^{11} platelets are produced daily in a human adult (Kaushansky 2007) and play important roles in hemostasis and thrombosis. Megakaryocytes are characterized by cells surface markers CD41 (integrin αIIb), CD42 (glycol-protein Ib) and CD61 (integrin β3) (Fig. 1.3 yellow arrows). TPO, a ligand to myeloproliferative leukemia virus oncogene (MPL, also known as CD110), is an essential cytokine for both HSC proliferation and megakaryocyte differentiation from HSC (Fig. 1.3 green arrows).

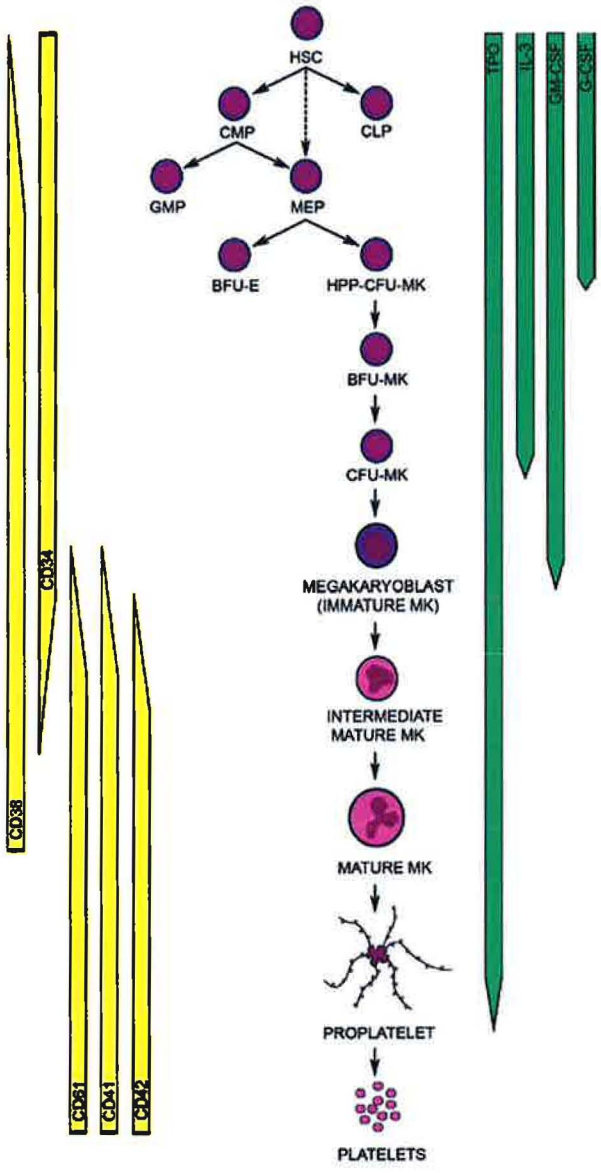

Figure 1.3. Megakaryopoiesis. Shown are also cell surface markers (yellow arrows) and important cytokines (green arrows) in different developmental stages of megakaryopoiesis.

(Figure adapted from Szalai et al., 2006)

Thrombocytopenia patients have a low platelets count, which increases the risk of severe bleeding. It is one of the major complications post high-dose chemotherapy followed by HSCT (Nash et al., 1996). 4 million platelet transfusions are performed yearly in the USA to treat thrombocytopenia (Goodnough et al., 2003). Nevertheless, in addition to the challenge of obtaining adequate numbers of donors, efficacious platelet support is also confounded by immune response to the donor platelets and by the fact that platelets can only be stored at room temperature, which increases the risk of bacterial contamination (Gandhi et al., 2005). Developing an approach to produce and expand large number of autologous megakaryocytes *ex vivo*, which can then be reinfused with HSCT, has great clinical potential to accelerate platelets reconstitution.

2.1 Epigenetic regulation

Transcription factors and other regulatory genes have critical roles in controlling of hematopoiesis. However, they cannot address all the questions raised in HSC lineage differentiation. For example, given that all the cells share the same genetic information, what causes the heterogeneous phenotypes during development? And what ensures that differentiation only occurs in one direction and committed cells do not convert back to the stem cell in normal condition? These questions bring up another critical regulatory factor of the cell—epigenetic regulation.

Epigenetics refers to inherited alternations in gene expression through chromatin modulations that are independent of the DNA sequence

(Christopheren and Helin 2010). There are a variety of epigenetic modifications including: DNA methylation, histone methylation and acetylation, nucleosome remodeling, and noncoding RNA. These modifications interact with each other and form a complex regulatory network to control the cell fate decisions. Growing studies have suggested that epigenetic regulations are largely involved in cell fate determination, not only during the onset of differentiation but also in maintaining the differentiated state once it is set.

The lineage-priming model of stem cell differentiation claims that stem cells, such as HSCs, maintain a relatively open chromatin (Attema et al., 2007; Gaspar-Maia et al., 2011) with less repressive marks compared to their mature progenies. This open chromatin structure allows for multilineage genes to be expressed at low levels. Proper differentiation requires up-regulation of preferred lineage-specific genes as well as shutting down genes of alternative lineages. Interfering in either way could result in altered cell fate (Orkin, 2003). During commitment, chromosomes become largely condensed, associated with DNA methylation, histone deacetylation, and increased levels of repressive marks histone H3 lysine 9 dimethylation (H3K9me2) and lysine 27 trimethylation (H3K27me3). Although generally stable, condensed chromosomes can be "re-opened" in case of reprogramming or tumorgenesis (Gaspar-Maia et al., 2011).

2.1.1 DNA methylation

DNA methylation occurs at the 5' position of cytosine and predominantly in the dinucleotide CpG (Ginder et al. 2008). Most CpGs in the mammalian genome are methylated excepted for the CpG islands (CGIs), which are CpG-rich regions often found near the gene promoters (Deaton and Bird 2011). DNA methylation inhibits gene transcription through direct interfering with the binding of transcription factors or through acting with methyl cytosine-binding proteins (MCBPs) and forming a complex that inhibits transcription initiation (Ginder et al. 2008). DNA methylation can also recruit other epigenetic modifiers, such as histone methyltransferase, to the locus and cause long-term gene silencing in X chromosome inactivation, genomic imprinting, retrotransposon silencing, etc. (Bhutani et al. 2011).

DNA methylation is carried out by DNA methyltransferases (DNMTs), which transfer the methyl group from S-adenosyl-methionine (SAM) to cytosine. There are two types of DNMTs: *de novo* methyltransferases DNMT3a and DNMT3b, which add methylation to completely unmethylated DNA, and maintenance methyltransferase DNMT1, which methylate DNA when the other strand is already methylated (Ginder et al. 2008). 5mC can be converted to 5-hydroxymethycytosine (5hmC) by the TET (ten-eleven translocation) family of proteins (Tahiliani et al. 2009), which may further lead to DNA demethylation (Tammen et al. 2012) (Fig. 1.4).

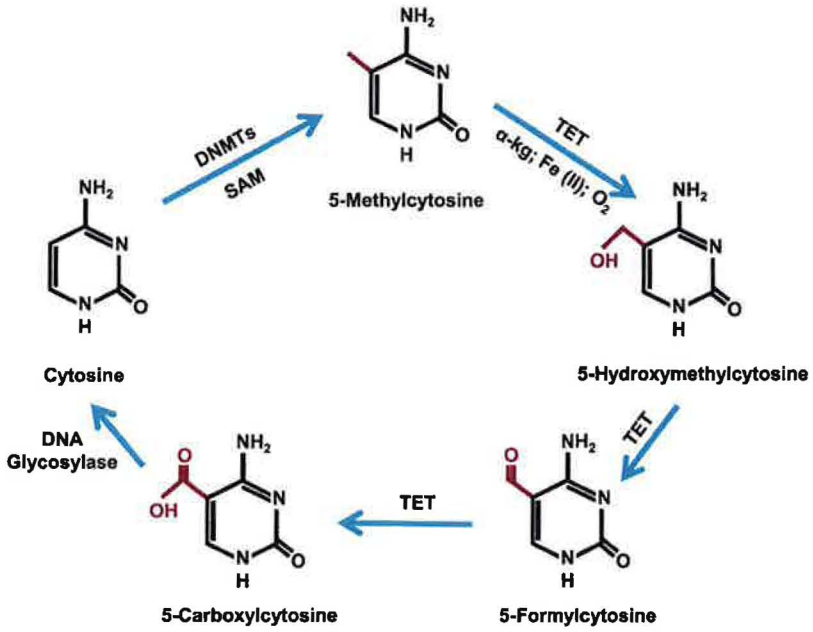

Figure 1.4. DNA methylation dynamics.

(Figure adapted from Tammen et al. 2012)

DNA methylation plays an important role in hematopoiesis. Previous studies have found that the *de novo* DNA methyltransferases Dnmt3a is required in mouse HSC differentiation (Challen et al. 2012). *Dnmt3a*-null HSCs have increased self-renewal ability but impaired differentiation due to inability to silencing their HSC genes (Challen et al. 2012). DNA methylation is dynamic during development. Hematopoietic genes whose expressions are repressed by DNA methylation in ESCs are demethylated in hematopoietic lineages (Calvanese et al. 2011). A decrease in Dnmt3a and Dnmt3b and global demethylation were observed during mouse erythropoiesis *in vivo* (Shearstone et

al. 2011). DNA methylation landscape also changes during HSC aging and is largely dependent on the proliferative history of HSCs. (Beerman et al. 2013).

2.1.2 Histone methylation

Another major mechanism for epigenetic regulation of the genome is histone modification. The N-terminal tails of histone that protrude from the nucleosome can be covalently modified by mechanisms such as acetylation, methylation, phosphorylation, and ubiquitination (Allis et al. 2007). Histone methylation plays a role in transcriptional regulation by either activating (e.g. H3K4me3, H3K27me1) or repressing (e.g. H3K9me2, H3K9me3, and H3K27me3) gene expressions (Vakoc et al. 2005). It is catalyzed by two types of methyltransferases—the protein arginine methyltransferases (PRMTs) and the histone lysine methyltransferases (HKMTs) (Allis et al. 2007).

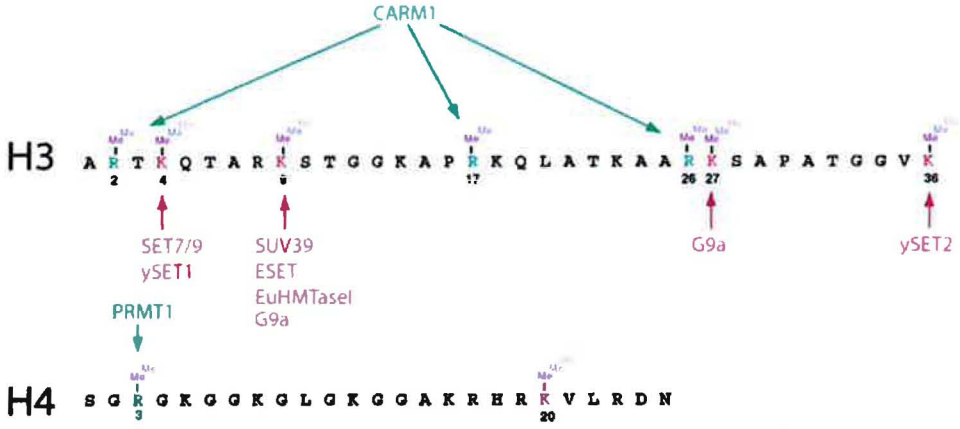

Figure 1.5. Known methylation sites on H3 and H4, and associated histone methyltransferases.

(Figure adapted from Bannister et al. 2002)

Histone methylation has a critical role in normal development and its disrupt is related to diseases such like cancer. Previous studies on ESCs have indicated that pluripotent stem cells maintain an open chromatin state (Gaspar-Maia et al. 2011). During differentiation, chromatins become condensed, associated with DNA methylation, histone deacetylation, and increased levels of H3K9me2 and H3K27me3. This chromosomal condensation can be reverted during reprogramming or tumorgenesis (Gaspar-Maia et al. 2011). Homozygous mutation of the H3K9 methyltransferase Eset in mice results in preimplantation lethality (Meissner 2010). H3K4 methyltransferase MLL1 is translocated in leukemia, and SMYD3 is overexpressed in colorectal cancer, liver, breast and cervical cancers (Malik and Bhaumik 2010).

2.1.3 Histone methyltransferases G9a/GLP

G9a/EHMT2 and GLP/EHMT1 are conserved protein lysine methyltransferases that play key roles in regulating gene expression and chromosome structure during mammalian development through *de novo* mono- and di-methylation of histone H3 lysine 9 (H3K9me1/2) [reviewed in (Collins and Cheng, 2010)], histone marks associated with transcriptional silencing (Litt et al., 2001; Noma et al., 2001; Su et al., 2004; Wen et al., 2009). G9a and GLP contain nearly identical Su(var)3-9 family SET methyltransferase domains, with which they bind and methylate H3K9me0/1, and ankyrin repeat domains that create a methyl-lysine binding module which allows binding of H3K9me1/2 marks

separately from their catalytic domains (Fig. 1.5) (Collins et al., 2008). Thus, G9a and GLP have separable "reading" and "writing" functions and can "read" its own marks, which may allow nucleation and spreading of H3K9me2 marks along chromatin (Collins and Cheng, 2010).

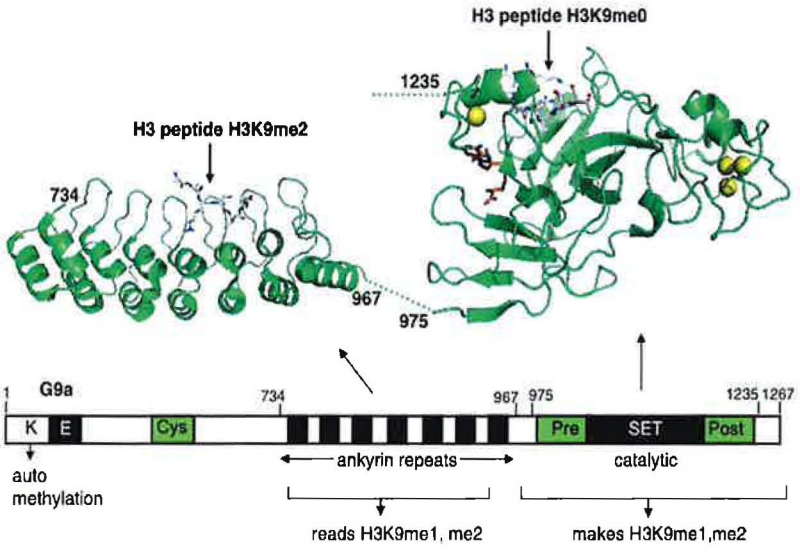

Figure 1.6. Structure of G9a.

(Figure adapted from Collins and Cheng 2010)

G9a is essential for early mouse embryo development and embryonic stem cell (ESC) differentiation (Tachibana et al., 2002). Its loss abolishes methylated H3K9 in euchromatic regions (Rice et al., 2003; Tachibana et al., 2002) and increases in H3K9 acetylation and H3K4 dimethylation (Tachibana et al., 2002), both associated with transcriptional activation. However, H3K9 trimethylation (me3) (Peters et al., 2003), a transcriptional repressive mark found

in heterochromatic regions, is unaffected by G9a loss, and is maintained by other methyltransferases, e.g., Suv39h or Setdb1 (Peters et al., 2003; Rice et al., 2003). G9a and H3K9me2 have been associated with euchromatic gene silencing in a number of cellular contexts: Oct4 gene in differentiating mESCs (Feldman et al., 2006), NRSF/REST-mediated silencing of neuronal genes in non-neuronal lineages (Roopra et al., 2004), and PRDI-BF1 silencing during B-cell differentiation (Gyory et al., 2004). The H3K9me2 mark can be found in isolated regions near genes and also in large Mb chromatin blocks that can be lineage-specific and/or lost in cancer cell lines, which may be indicative of structural roles in maintaining epigenetic memory during lineage formation (Wen et al., 2009). However, precise roles for G9a/GLP-H3K9me2 patterning in stem cell self-renewal and lineage commitment and during human hematopoiesis have yet to be determined.

BIX01294 (BIX), a chemical inhibitor of G9a, was previously reported to improve reprogramming efficiency of terminally differentiated cells into induced pluripotent stem cells (iPSCs) (Shi et al., 2008a; Shi et al., 2008b). Recent efforts to improve the effectiveness of BIX has led to the discovery of UNC0638, a BIX analogy with improved potency and reduced toxicity (Vedadi et al., 2011). UNC0638 selectively inhibits G9a and its closely related partner GLP and significantly reduced H3K9me2 on endogenous genes and microRNAs (Vedadi et al., 2011).

2.1.4 RNA interference

It was first observed in plant that introduction of a transgene, which was supposed to deepen the color of the flowers, surprisingly resulted in bleached color (Napoli et al. 1990). This phenomenon is named "co-suppression". It was later found in Caenorhabditis elegans that sequence-specific silencing was induced by injection of double-stranded RNAs (dsRNA) (Fire et al. 1998). Further studies have confirmed that co-suppression in plants and gene silencing in C. elegans were caused by a similar mechanism, which was later termed RNA interference (RNAi) or post-transcriptional silencing. RNAi is evolutionarily conserved from worms to plants to mammals. Cells utilize RNAi as a mechanism to protect themselves from RNA virus, and to regulate expressions of endogenous protein-coding genes (Hannon 2002). The first published indication that small dsRNA could trigger RNAi in mammals came from Tucshl and colleagues, who demonstrated that short RNA duplexes resembling the cleavage products of Dicer could trigger sequence-specific silencing in mammalian cell lines (Elbashir et al. 2001).

microRNA (miRNA) and small interfering RNA (siRNA) are two major small RNAs that are involved in RNAi (He and Hannon 2004) (Fig. 1.6). They are around 21-25-nucleotide long. miRNAs are derived from large pri-miRNA that forms a stem loop structure. Pri-miRNA is cleaved by two RNase III enzymes, Drosha and Dicer, sequentially. Mature miRNAs can load onto a RNA-induced silencing complex (RISC), which binds to the 3' UTR of its complementary mRNA and leads to post-transcriptional repression. On the contrary, siRNAs are derived

from long dsRNAs that can be introduced exogenously, and processed by Dicer into 21-25nt long mature siRNAs. Unlike miRNA, which form an imperfect duplex with mRNA, siRNA form a perfect duplex with its targeting mRNA, and thus leads to the cleavage of the target.

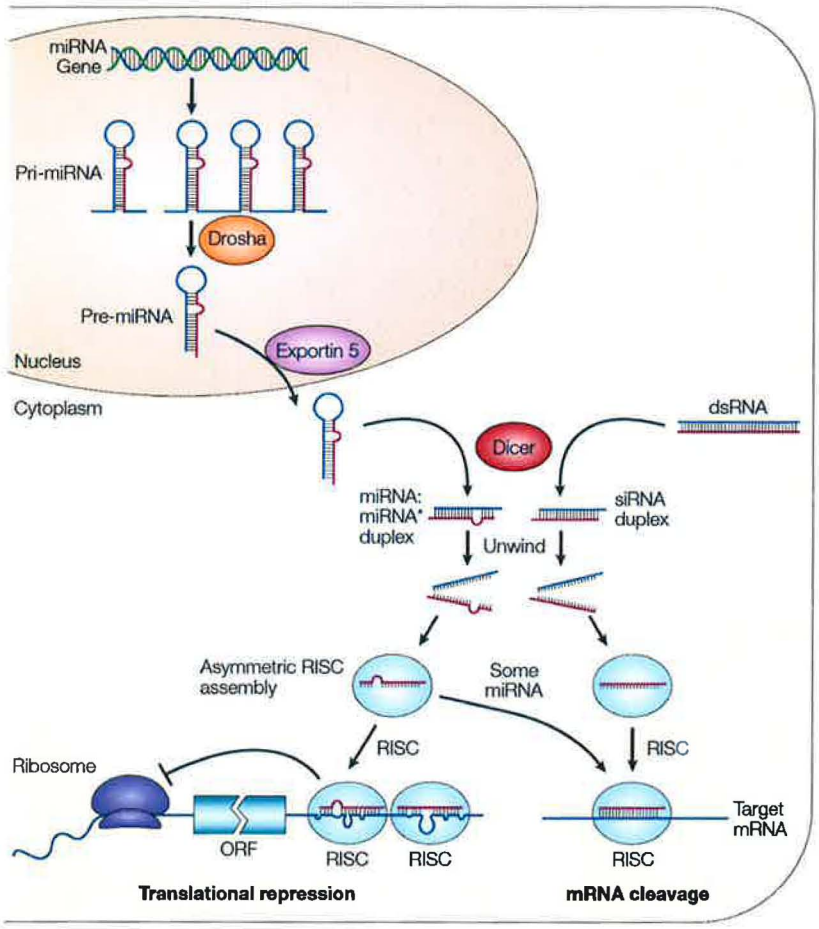

Figure 1.7. RNA interference.

(Figure adapted from He and Hannon 2004)

It was previously suggested that many lineage-specific genes are expressed at mRNA level in HSC. However, their translations are "held back" by miRNAs until differentiation happens (Georgantas et al. 2007). Microarray analysis of miRNAs discovered an enrichment of 11 miRNAs in mouse HSC, including miR-125a-5p, -196b, -99a, -130a, -125b-5p, -542-5p, -181c, -155, -193b, -126a-3p, and let7e (O'Connell et al. 2010). A recent study has identified miRNA-125b-2 as a positive regulator of megakaryopoiesis and its overexpression is related to megakaryoblastic leukemia (Klusmann et al. 2010). More miRNAs have been found to play a role in human and mouse hematopoiesis: miR-221 and -222 down-regulate human erythropoiesis (Georgantas et al. 2007). miR-150 is up-regulated by TPO during human megakaryocytic differentiation (Barroga et al. 2008). miR-155 blocks human megakaryocytosis by targeting Ets-1 and Meis1 (Romania et al. 2008), whereas miR-27a inhibits Runx1 and promotes megakaryopoiesis in mice (Ben-Ami et al. 2009). miR-181 and miR-146 drives mouse CLP differentiation to B lymphopoiesis and T lymphopoiesis, respectively (Georgantas et al. 2007). It will be of great interest to further study roles of more miRNAs in hematopoiesis.

siRNAs are synthesized *in vitro*, and can be delivered directly into cells by electroporation or lipid-mediated transfection, which leads to transit knockdown of targeting genes. In contrast, short hairpin RNAs (shRNAs) are produced endogenously through RNA polymerase III promoters, and then processed by Drosha and Dicer. shRNAs can be cloned into a viral vector to allow delivery and integration into the cell genome, which results in stable expression of shRNAs

and long-term knockdown of their targets (Rao et al. 2009). shRNA expression in the cell can be further manipulated using an inducible vector and/or selective markers.

RNAi has become a methodology of choice for knocking down gene expression in a variety of biological systems, including mammals. In the past 6 years, the use of RNAi in cultured mammalian cells has delivered new insights into potential cancer drug targets (Aza-Blanc et al. 2003; MacKeigan et al. 2005; Berns et al. 2004), apoptosis (Paddison and Hannon 2002), cell survival (Kittler et al. 2004), p53-induced cell cycle arrest (Westbrook et al. 2005), 26s proteasome function (Bartz et al. 2006) cell division (Ali et al. 2009), transformation of human mammary epithelial cells (Hope et al. 2010), and chemotherapeutic sensitization (Chen et al. 2012). Collectively, these studies, along with those in invertebrates, have demonstrated the utility of RNAi in probing gene function in unbiased, systematic ways.

RNAi has also been applied to the study of human and mouse hematopoiesis (Schaniel et al. 2009; Silva et al. 2005). Sauvageau and colleagues recently examined shRNA-mediated knockdown of 20 mouse polarity factors in an in vivo engraftment screen for mouse HSC activity (Silva et al. 2005) and identified three genes this approach, including Msi2, Pard6a, and Prkcz, required for HSC repopulation and maintenance. Another study by Larsson and colleagues targeted ~1300 human genes using shRNAs in human cord blood cells (Schaniel et al. 2009) to identify shRNAs that affect colony-forming cell (CFC) activities of HSPCs during ten weeks of in vitro outgrowth. Three genes

were identified, including EXT1, PLCZ1, and STK38, whose knockdown affected the frequency of CFC-CFUs and other phenotypes, including increases in erythrocyte progenitor activity, long-term culture initiating cell activity, and NOD/SCID repopulating cell activity. Both studies demonstrate the potential power of RNAi as a tool for studying mammalian hematopoiesis. However, they also highlight the shortcomings, including the necessity of using small screening pools to accommodate heterogeneous progenitor pools and protracted biological assays to indirectly measure stem cell activity. The ability to routinely and rigorously apply RNAi to human HSPCs would facilitate further understanding of self-renewal, lineage commitment, and hematological disease.

CHAPTER 2

MATERIALS AND METHODS

2.1 Cell culture

Human $CD34^+$ cells (> 90% purity) from granulocyte colony-stimulating factor (G-CSF) mobilized peripheral blood or bone marrow of healthy adults were purchased from the Fred Hutchinson Cancer Research Center (FHCRC) Cell Processing Shared Resource. Cells were maintained in either serum-containing medium [IMDM with 10% fetal calf serum, supplemented with 1X antibiotics and 100 ng/ml stem cell factor (SCF), interleukin-6 (IL-6), Flt3 ligand (Flt3L), thrombopoietin (TPO), G-CSF, and 200 ng/ml interleukin-3 (IL-3)] or the serum-free medium (StemSpan® SFEM from StemCell Technologies), supplemented with 1X antibiotics and 100ng/ml SCF, IL-6, Flt3L, TPO). UNC0638 (Sigma) and SR1 (AMRI) were resuspended in DMSO and used at indicated concentrations. Cells were cultured at 37°C in 5% CO_2/95% air at a density between 0.5-1.5 million cells/ml. Bone marrow and peripheral blood mononuclear cells prepared from samples obtained from healthy adult donors after informed written consents using forms approved by the FHCRC IRB in accordance with the Declaration of Helsinki.

2.2 Flow cytometry and FACS sorting

Cells were harvested, washed, and re-suspended in 2% calf serum. Flow cytometric analysis and FACS sorting was performed using the following antibodies: CD3-FITC (BD, # 555332), CD11b (Beckman Coulter, # IM0530), CD14 (BD, # 347493), CD15 (BD, # 555401), CD19 (BD, # 560994), CD34-APC (BD Biosciences, # 555824), CD38-PerCP-Cy 5.5 (BD, # 551400), CD45 (BD, # 340943), CD45.1 (eBioscience, # 25-0453-82), CD45RA-FITC (Invitrogen, # MHCD45RA01), CD45RA-Pacific Blue (Invitrogen, # MHCD45RA28), CD49f-FITC (BD, # 561893), CD56 (BD, # 340723), CD90-PE (BD, # 555596), CD123-PE (BD, # 554529), CD235a (Beckman Coulter, # IM2212U). Cells were analyzed on FACSCanto flow cytometer (BD) and sorted on FACSAria cell sorter (BD). Data analysis was performed using FlowJo (Three Star), or the software developed by the laboratory of Brent Wood that allows for high-level multicolor flow analysis (Wood, 2006).

2.3 ChIP-sequencing

3-5 million cells were harvested and fixed with 1% formaldehyde at room temperature (RT, 10 min), followed by glycine (125 mM) to stop the crossing linking reaction (RT, 5 min). Cells were then washed twice with ice cold PBS containing 1X PMSF, and then resuspended in cell lysis buffer (1% SDS, 10 mM EDTA, 50 mM Tris, pH 8.1) containing 1X protease inhibitor cocktail (PIC, Roche) and PMSF, and rotated (4°C, 30min). Extracts were sonicated using a

Bioruptor (Diagenode) set on "HIGH" for 30 cycles of 30 sec ON and 30 sec OFF according to manufacturer's instructions to achieve chromosome fragment lengths of 200-400 bp. After sonication, samples were spun down (4°C, 10 min) and the supernatant was transferred to a new tube for ChIP. 100 µl sonicated cell extract was then diluted in 400 µl ChIP Dilution Buffer (Magna ChIP^{TM} G kit, Millipore, # 17-611) containing 1X PIC and PMSF, and incubated with 1 µg of anti-H3K9me2 (Abcam, # ab1220) at 4°C for 1 hour while rotating. 20 µl protein G magnetic beads were then added per sample and incubated at 4°C overnight while rotating. ChIP samples were then washed with low and high salt buffers, reverse-crosslinked, and purified. Samples are prepared for Illumina-based sequencing using Encore NGS Library System I (NuGEN, # 300-08). High-throughput sequencing-by-synthesis (HT-SBS) was performed on an Illumina HiSeq 2000 sequencer available at the FHCRC Genomics Shared Resource. This procedure yielded between 96-284 X 10^6 sequence reads per sample, ~80% of which aligned to human genome version CRCh37/hg19 (UCSC Genome Bioinformatics Group).

2.4 ChIP-sequencing data analysis

Uniquely mapping and properly paired sequencing reads of 49 bp were aligned to the human genome (hg19) assembly using the Burrows-Wheeler Aligner (bwa-0.5.9) (Li and Durbin 2009) and converted to BAM files using SAMtools (v1.4) (Li et al. 2009). Peaks were called and WIG read density graphs were created using Model-based Analysis for ChIP-Seq (MACS v1.4.2) as

described (Zhang et al. 2008) using a p-value cutoff of 1×10^{-6} and a 350 bp bandwidth to match the average DNA fragment length. Genomic overlaps were defined as peaks sharing at least 100bp, determined using GenomicRanges (R package version 1.6.7) (Aboyoun et al.). In order to limit the number of false positives, a peak had to replicate to be passed to further analysis. Replication was defined as sharing at least 100bp in biological replicate. The peak centers distance to transcription start sites was annotated using ChIPpeakAnno (R package version 2.2.0) (Zhu et al. 2010). ChIP-Seq peaks are displayed using the Broad Integrative Genome Viewer. Hive plots were created using HiveR (R package version 0.2-1) (Hanson 2011). These plots were designed as an improved way to visualize gene interaction networks; however, they are also well designed to look at genomic information on multiple samples simultaneously. The axes are scaled with accurate genomic distance, nodes are sized relative to peak width and edges connect overlapping peaks. Nodes that are unique to a given condition do not have edges attached. Centers located within 5kb upstream or downstream of the TSS were qualified as TSS-associated. Centers within the gene body at least 5kb from TSS were qualified as intragenic and centers outside of the gene bodies and at least 5kb from TSS were considered intergenic. Features were obtained from UCSC Genome Browser, the retroelements data was created by the program RepeatMasker as described (Smit AFA and Green P. 1996-2010.) and the CpG Islands are defined as DNA regions greater than 200bp, more than 50% GC content and a ratio of GC dinucleotides greater than

0.6 expected based on G's and C's in sequence (Gardiner-Garden and Frommer 1987).

2.5 ChIP-qPCR

ChIP DNA from H3K9me2 (Abcam), H3K9me3 (Abcam), RNA pol II (Millipore) or a negative control rabbit immunoglobulin (IgG) were used as template for qPCR. qPCR was performed using SYBR® Green PCR Master Mix (Applied Biosystems) and 7900HT Fast Real-Time PCR System (Applied Biosystems). DNA isolated from 10% ChIP input was used for normalization. Fold enrichment was determined by $2^{-\Delta Ct}$ method (n = 3). Pre-validated ChIP-qPCR primers (QIAGEN) were used to amplify TSS regions of genes of interest, and GAPDH as a control.

2.6 Immunofluorescence

Cytospin preparations were made, fixed with 4% formaldehyde for 15 min at RT, permeabilized and blocked with 0.3% Triton X-100, 5% goat serum in PBS for 60 min at RT, then incubated with anti-H3K9me2 (Cell Signaling, # 4658S) rabbit antibody over night at 4 degrees. Primary antibodies were detected with goat anti-rabbit IgG (H+L) conjugated with AlexaFluor 488 nm (Invitrogen, # A11070). The nuclei were counterstained with mounting medium with 150 ng DAPI (Vector Labs, # H-1200). Whole slides were scanned, and images were acquired at both GFP and DAPI channels using the TissueFAXS microscopic system (TissueGnostics). All images acquired were normalized to the

background using ImageJ and then analyzed using TissueQuest. Mean GFP intensity was obtained from each cell. We also used the DeltaVision microscope (60X water objective) to take Z-series images, which were then deconvoluted and visualized using maximal intensity projection.

2.7 CFSE cell division assay

1 million $CD34^+$ cells were suspended in 1 ml warm PBS with 0.1% BSA and labeled with 3 μM CFSE (Invitrogen, # C34554) at 37 °C for 10 min. 5 volumes of ice cold PBS with 0,1% BSA was added to stop labeling. Cells were incubated on ice for 5 min and then washed and cultured with or without UNC0638 and SR1 for later analysis. Flow cytometry was performed on day 1 and day 7 with anti-CD34-APC antibody. 100% of the cells were labeled and within a single peak on day 1.

2.8 Colony-forming unit assay

500 cells were plated in 1 ml MethoCult® H4434 (StemCell Technologies, #04434) methylcellulose medium in a 35 mm dish, and incubated with a open water dish in a 150 mm culture dish at 37°C in 5% CO2/95% air. All CFUs were plated in triplicates. Burst forming unit-erythroid (BFU-E), CFU-granulocyte/ macrophage (CFU-GM) and CFU- granulocyte/erythrocyte/monocyte/ megakaryocyte (CFU-GEMM) were scored 14-16 days after plating by two persons independently.

Note that CFU-C assay is useful in the way that it measures the frequency of hematopoietic progenitor/precursor cells in a population. However, it is limited for several reasons. First, the most primitive hematopoietic stem cells are quiescent, and will not divide in respond of the growth factors in the medium. Second, CFU-C assay only measure colonies formed up to 3 weeks, while primitive hematopoietic cells need a longer time to differentiate into mature progenies.

2.9 Gene expression microarray

Human PBMC $CD34^+$ cells, were thawed and treated the next day with the following conditions for 48 hours: 0.02% DMSO, 1 μM SR1, 2 μM UNC0638 or 1 μM SR1 plus 2 μM UNC0638. Total RNA was extracted using TRIzol® Reagent (Invitrogen) and subjected to The HumanHT-12 v3 Expression BeadChip (Illumina). To establish differential expression, t-tests were performed using 'limma' (R package 3.12.0) (Smyth 2005). Genes that were changed in expression in any of the three conditions with a minimum unadjusted p-value of 0.001 were used to create a differential expression gene list. Multi-dimensional scaling was performed using the 'MASS' (R package 7.3-18) (Venables and Ripley 2002). GO-term and UniProt-Tissue analysis was performed by Database for Annotation, Visualization and Integrated Discovery (DAVID) (Huang da et al. 2009). Gene expression profiling was performed using the Broad Institute's Molecular Signatures Database (MiSig) (Su et al. 2004; Subramanian et al. 2005).

2.10 Western blot

1-2 million human $CD34^+$ cells from bone marrow or G-CSG mobilized blood were treated with 1 μM or 2 μM UNC0638 for 48 hours and lysed with RIPA buffer (150 mM NaCl, 50 M Tris, pH 7.5, 2 mM $MgCl_2$, 0.1% SDS, 2 mM DTT, 0.4% deoxycholate, 0.4% Triton X-100, 1X protease inhibitor, and 1X benzonase nuclease) before subjected to SDS-PAGE and western blot using antibodies to H3K9me1 (1:1000, Active Motif, # 39249), H3K9me2 (1:1000, Cell Signaling, # 4658), H3K9me3 (1:1000, Abcam, # ab8898), H4 (1:2000, Abcam, # ab17036) and β-actin (1:1000, Cell Signaling, # 3700).

2.11 Limiting dilution assay

Human PBMC $CD34^+$ cells were expanded with 0.01% DMSO, 1 μM SR1, 1 μM UNC0638, or 1 μM SR1 plus 1 μM UNC0638 in serum-free medium with cytokines for 14 days. 0.2 million, 1 million, or 6 million expanded cells from each treatment group were then injected intravenously into sublethally irradiated NSG mice (n = 5). Flow cytometric analysis of human $CD45^+$ cells in the mice blood was performed at weeks 2, 4, and 7 to determine human cell engraftment. Mice were sacrificed at week 8 and bone marrow was harvested from the femurs. Human $CD45^+$ cells in the mice bone marrow were analyzed by flow cytometry. Mice that contained over 0.1% human $CD45^+$ cells in the bone marrow were scored positive. The frequency of SCID-repopulating cell (SRC) was calculated using the software L-Calc (StemCell Technologies) (Boitano et al. 2010).

Note that this method is limited because its readout mainly depends on the homing ability of the grafts (i.e. if the cells fail to reach a proper niche, they cannot generate progenies). Another weakness of the NOD/SCID mouse model is the development of thymomas in a few months, which prevent long-term studies [4]. Besides, mice are small animals whose hematopoietic system is distinctive from that of humans, given that the blood one mouse makes in its whole life is similar to the amount of a human makes in one day. This may affect the study of human hematopoiesis in the mouse as well. Larger animals such as dog, sheep and cynomolgus monkeys are also investigated to study long-term hematopoiesis [71].

2.12 Canine autologous transplantation

Canine bone marrow was aspirated and cells were selected for $CD34^+$ with the canine-specific monoclonal antibody 1H6 as previously described (Bruno et al. 1999). The $CD34^+$ cells were isolated and analyzed using BD FACS Aria cell sorter (BD Biosciences, San Jose, CA) and $CD34^+$ purity was >95.5%. $CD34^+$ cells were plated in 1 ml aliquots of 100,000 cells/mL in 24-well plates in StemSpan media (StemCell Technologies, Vancouver, BC, Canada) supplemented with recombinant human (rh)FLT3-L, rhTPO (Life Technologies, Grand Island, NY), recombinant canine (rc)SCF and rcIL6 (Kingfisher Biotech, St. Paul, MN), all at 100 ng/mL. Cells were treated with StemRegenin (SR1, Cellagen Technology, San Diego, CA) and UNC0638 at 1 μM each, incubated for 14 days at 37°C and 5% CO2, and subcultured as needed to maintain cell

density of 1-2 x106 cells/mL. On day 14 cells were collected, centrifuged at 150xg for 10 minutes, suspended in RPMI media (without supplements or phenol red) and immediately infused into the conditioned recipient (9.2 Gray TBI). Dog H501 was given supportive care with antibiotics, intravenous fluids and transfusions as described (Georges et al. 2010).

2.13 shRNA cloning

shRNAs were digested from the pGIPZ lentiviral vector (Open Biosystems) between EcoRI and XhoI sites, gel purified and ligated into the same sites in the MSCV-LTRmiR30-PIG (MLP) retroviral vector (Open Biosystems). The MLP vector also contains a GFP reporter and puromycin as a selectable marker. Clones were verified by sequencing and plasmids were extracted by Maxiprep (Qiagen).

2.14 Transduction

Non-tissue culture treated 6-well plate was coated with CH296 (RetroNectin, from ClonTech) at the concentration of 2 mg/cm^2 for 2 hours at room temperature. CH296 was then moved and replaced with a similar volume of sterile 2% BSA in HBSS. After incubation at room temperature for 0.5 hour, BSA solution was moved and replaced by a similar volume of 2.5% 1 M Hepes, pH 7.0 in HBSS. Coated plate can be sealed with parafilm and stored at 4° C before use for several weeks. Hepes solution was removed before infection. Filtered virural supernate (through a 0.45 µm filter) or concentrated virus was added on to

the plate. Human $CD34^+$ cells were then added on top of the virus dropwise (1ml/well). Protamine sulfate was added at 8 mg/ml. 1X fresh medium was added 48 hours post infection. GFP^+ cells were sorted 72 hours post infection to determine knockdown.

2.15 Quantitative real-time PCR

Cells were harvested or sorted from *ex vivo* cultures and washed with PBS twice. Total RNA was extracted by TRIzol® Reagent (Invitrogen). cDNA was synthesized using the SuperScript® III First-Strand Synthesis System (Invitrogen). qPCR primers were designed using a online tool Primer3 (http://frodo.wi.mit.edu) or ordered from Qiagen QuantiTect Primer Assays. qPCR was performed using SYBR® Green PCR Master Mix (Applied Biosystems) with 7900HT Fast Real-Time PCR System (Applied Biosystems). Beta-actin was used as an endogenous control. Relative transcript abundance was analyzed using $2^{-\Delta\Delta Ct}$ method.

2.16 DNA methylation analysis

DNA was isolated using the Gentra Puregene Cell Kit (Qiagen). 1 microgram of DNA was treated with bisulfite using the Zymo EZ DNA Methylation Gold kit (Zymo Research) according to the manufacturer's protocol. Samples were run using the Infinium Human Methylation 450 BeadChip (Illumina), according to the manufacturer's instructions. Arrays were scanned on an Illumina HiScan scanner and the average % methylation was calculated using Illumina's

GenomeStudio Methylation module, without sample normalization or backgrounding.

CHAPTER 3

G9A/GLP-DEPENDENT HISTONE H3K9ME2 PATTERNING DURING HUMAN HEMATOPOIETIC STEM CELL LINEAGE COMMITMENT

3.1 G9a/GLP-mediated H3K9me2 patterning is progressive during HSPC lineage commitment and reversed by UNC0638 treatment

To investigate roles for G9a and GLP methyltransferase function during human HSPCs lineage specification, we first examined global chromatin H3K9me2 patterning using chromatin immunoprecipitation (ChIP) (O'Geen et al. 2011). To this end, H3K9me2 ChIP-sequencing analysis was performed on the following cell populations: HSC-enriched $CD34^{+}CD90^{+}CD38^{lo}CD45RA^{-}$ cells (Majeti et al. 2007), unfractionated $CD34^{+}$ cells (which contain mainly committed progenitors), $CD41^{+}CD61^{+}$ committed megakaryocytes (Megs) (Novershtern et al. 2011), $CD3^{+}$ T-cells (Majeti et al. 2007), and the HS-5 human bone marrow stromal cell line (Graf et al. 2002) (Fig. 3.1).

To ensure that H3K9me2 ChIP-seq peaks were specific to H3K9me2 and G9a/GLP activity, in control ChIP-seq experiments in unfractionated $CD34^{+}$ cells, we used a recently developed chemical probe, UNC0638, which potently and

selectively inhibits both G9a and GLP methyltransferase activity by blocking substrate access to their SET methyltransferase domains (Vedadi et al. 2011).

The ChIP-seq analysis revealed an unexpected series of results (Chen et al. 2012) (Fig. 3.1). The most primitive HSCs displayed small and fewer H3K9me2 peaks. Unfractionated $CD34^+$ cells, containing mainly committed progenitors, showed higher, defined peaks that generally occur at CpG islands. In differentiated Megs and T-cells, peaks arising in $CD34^+$ cells were elaborated on and expanded to form nearly identical H3K9me2 territories in genic regions. Figure 1A and Supplemental Figure S2A show representative samples of 80 kb of chromosome 11 and chromosome 19 from the ChP-Seq data. Virtually all genic regions showed a similar pattern.

Evidence for this pattern arose from multiple analyses of the ChIP-seq data. First, the frequency of sequence reads per H3K9me2 peak (when examining either peak height or width) showed progressive increases from more primitive to differentiated cells, which were blocked and reversed by UNC0638 treatment of $CD34^+$ HSPCs (Fig. 3.1B).

Second, examination of the H3K9me2 peaks arising in $CD34^+$ HSPCs revealed approximately 95% overlap peaks in Megs and T-cells (Fig. 3.1C-E). Figure 1D shows this result for the entirety of chromosome 11 using a hive plot representation (Hanson 2011), where green lines show H3K9me2 marks shared between HSPCs, Megs and T-cells and red lines show marks that have expanded in Megs and T-cells. The results show that almost all H3K9me2 marks

found in HSPCs are transmitted to Megs and T-cells. Hive plots for other chromosomes showed identical results (data not shown).

Third, another dramatic result revealed in the hive plots was that there are no lineage-specific H3K9me2 patterns transmitted from HSPCs to Megs or from HSPCs to T-cells. These patterns would appear as purple lines between HSPCs and Megs or HSPCs and T-cells. This was true for all other chromosomes as well (data not shown). This notion is supported by correlation of peak overlaps in different populations: Megs and T-cells share >90% of overlap (Fig. 3.1E). These analyses support a model for H3K9me2 patterning in HSPC differentiation that is progressive, but not lineage specific, at least within the cell types we examined. However, further analysis of other lineages needs to be done to confirm that H3K9me2 patterning is not lineage specific.

Fourth, H3K9me2 peaks formed in $CD34^+$ cells spread to surrounding regions in chromatin. As shown in Figure 1A, H3K9me2 marks appear to be nucleated at CpG islands and then spread through genic regions in between. Spreading is suggested by the fact that the differentiated populations are derived from $CD34^+$ HSPCs. In fact, for this experiment the Meg population was derived during *in vitro* differentiation directly from the $CD34^+$ HSPCs used for ChIP-seq. Moreover, these patterns were not due to *in vitro* differentiation artifacts, since uncultured T-cells (from two different donors) gave the same highly reproducible pattern as the Megs. Thus, the results indicate that H3K9me2 marks nucleated in $CD34^+$ cells spread to surrounding regions to form larger territories.

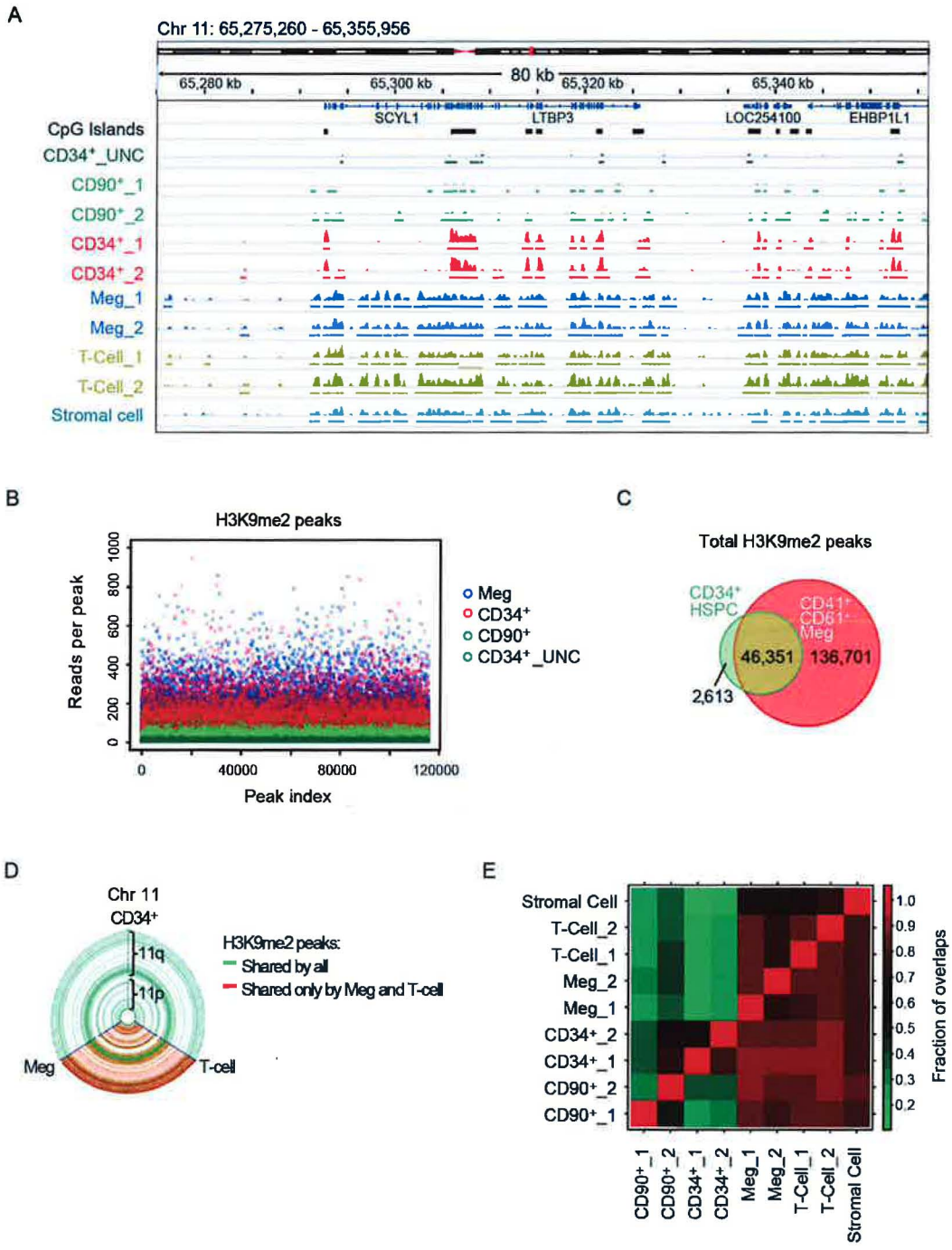

Figure 3.1. ChIP-Seq analysis of H3K9me2 patterning during HSPC lineage commitment. ChIP-Seq was performed on cells from two independent donors

with antibody against H3K9me2 in progressive stages of the hematopoietic lineages or treated with UNC0638. $CD34^+CD90^+CD38^{lo}CD45RA^-$ HSCs (denoted here as "$CD90^+$"), and $CD41^+CD61^+$ megakaryocytes were sorted from the same donors as the $CD34^+$ HSPCs on day 4 and day 10 of primary cell cultures, respectively. $CD3^+$ T-cells were sorted from the blood of two different donors. $CD34^+$_UNC indicates HPSCs treated with 2 μM of UNC0638 for 48 hrs. **(A)** Representative tracks from the Integrated Genome Viewer. The y-axis indicates the number of reads (from 0 to 50) detected in 50 bp windows. "_1" and "_2" indicate biological replicates. **(B)** The numbers of reads for each peak, limited by the sample with the fewest called peaks. **(C)** Venn diagram showing peak overlap between $CD34^+$ HSPCs and $CD41^+CD61^+$ Megs. Overlapping peaks share >100bp. **(D)** Hive plot representing chromosomes 11. The peaks are displayed with accurate genomic distances as blue nodes along the length of the axes, while peak overlaps are displayed as connected lines. Green lines represent peaks shared between $CD34^+$ HSPC, Meg and T-cell. Red lines represent peaks shared only between Meg and T-cell. Unshared peaks by the three populations would appear as purple lines. **(E)** Heat map representing the fraction of overlaps between different samples. Overlaps are defined as read density peaks sharing at least 100 bp. The number of peaks overlapping is divided by the total number of peaks in that sample and displayed as a value between 0 and 1. Comparisons are made to the samples in the rows.

3.2 H3K9me2 nucleation sites in HSPCs are enriched at H3K4me3 sites and CpG islands

We next examined H3K9me2 HSPC peak overlap with nine epigenetic marks and other genetic landmarks in HSPCs and differentiated cells. For epigenetic marks, we used the data from the work of (Cui et al. 2009), who examined multiple histone marks in $CD133^+$ human HSPCs and also differentiated $CD36^+$ erythrocytes (Fig. 3.2A). The most frequent overlap occurred with H3K4me3. This mark is found at transcription start sites (TSSs) and is associated with active transcription when present with histone H3K36me3, which is found in gene bodies (Kolasinska-Zwierz et al. 2009), or epigenetic bivalency when found in combination with repressive marks (Attema et al. 2007; Gaspar-Maia et al. 2011). Interestingly almost 50% of the H3K4me3 peaks in either $CD133^+$ or $CD36^+$ cells overlapped H3K9me2 peaks in $CD34^+$ HSPCs. This result is also consistent with H3K9me2 being enriched at TSSs (Fig. 3.2B,C), and may suggest roles for G9a/GLP in facilitating chromatin structure and bivalency at promoters primed for expression in HSPCs.

Another interesting overlap was H4K20me1 (~21% of peaks in $CD36^+$ cells) (Fig. 3.3A). In contrast to H3K4me3, this mark is found away from TSSs and has been implicated in regulating DNA damage responses, mitotic condensation, and also gene expression (Beck et al., 2012).

However, the most striking overlap was with CpG islands (CGIs) (Fig. 3.2D,E), which are DNA regions of high CpG density and are less likely to be methylated (Gardiner-Garden and Frommer 1987; Hodges et al. 2011). CGIs are

generally near the gene promoters and are associated with regulation of gene expression (Saxonov et al. 2006). There are 28,691 predicted CpG islands in the human genome (Cocozza et al. 2011). Of these, 79% are associated with an H3K9me2 peak in CD34$^+$ HSPCs (Fig. 3.2D), which represents 47% of total H3K9me2. This result strongly suggests that nucleation of H3K9me2 peaks is coordinated with CpG islands in CD34$^+$ HSPCs.

Taken together, these results demonstrate: that H3K9me2 patterning is progressive during HSPC lineage specification; that H3K9me2 nucleation frequently occurs at CpG islands in HSPCs; that patterning events are dependent on G9a/GLP methyltransferase activity; and that UNC0638 treatment alters H3K9me2 patterning to better resemble those observed in primitive HSCs.

A

Histone modifications	CD133$^+$ HSPC			
	Intergenic	Intragenic	TSS	Overlap with H3K9me2
H2-AZ	64%	17%	19%	14%
H4K20me1	50%	42%	8%	13%
H3K36me3	66%	33%	1%	2%
H3K27me1	63%	34%	3%	5%
H3K27me3	71%	20%	9%	13%
H3K9me1	59%	38%	3%	7%
H3K9me3	80%	18%	2%	3%
H3K4me1	61%	33%	6%	8%
H3K4me3	21%	16%	63%	50%

Histone Modification	CD36$^+$ Erythrocyte			
	Intergenic	Intragenic	TSS	Overlap with H3K9me2
H2-AZ	64%	17%	19%	12%
H4K20me1	51%	45%	4%	21%
H3K36me3	59%	39%	2%	5%
H3K27me1	69%	30%	1%	1%
H3K27me3	66%	23%	11%	15%
H3K9me1	59%	39%	2%	3%
H3K9me3	81%	17%	2%	4%
H3K4me1	58%	35%	7%	9%
H3K4me3	14%	16%	70%	46%

B

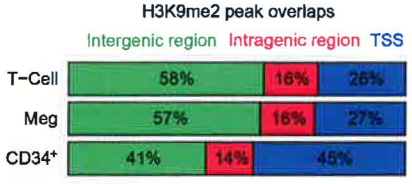

C

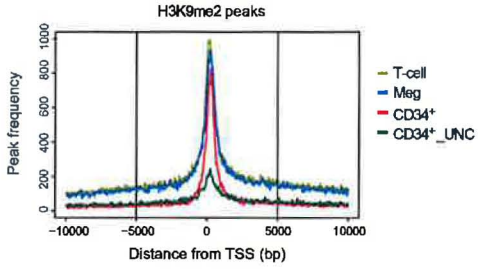

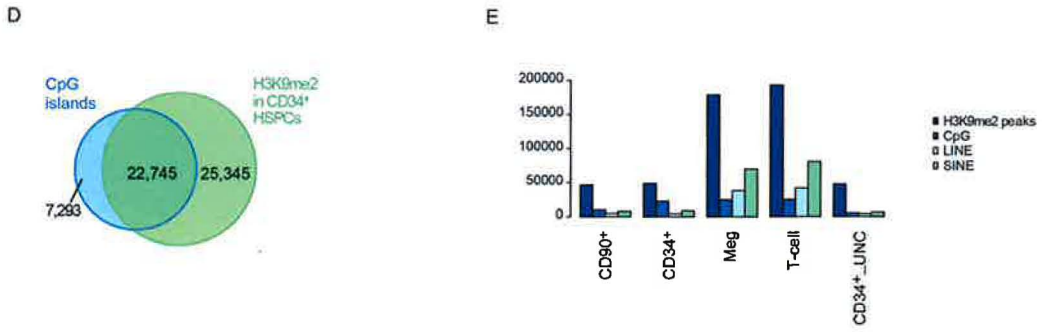

Figure 3.2. Overlaps between H3K9me2 and other epigenetic marks and genetic landmarks. **(A)** Overlap between H3K9me2 peaks in $CD34^+$ HSPCs and 9 other histone marks in $CD133^+$ HSPCs using data from the work of Cui et al., 2009. **(B)** Percentage of H3K9me2 peak associations with gene bodies and transcription start site (TSS). $CD34^+$ cells show enrichment at the TSS and deficiency in intergenic regions. **(C)** H3K9me2 peak frequency relative to TSS of genes. **(D)** Overlap between H3K9me2 peaks and UCSC CpG islands in $CD34^+$ HSPCs. **(E)** Overlaps between H3K9me2 in $CD34^+$ population and CpG islands, LINEs and SINEs are displayed as a number of H3K9me2 peaks.

3.3 G9a/GLP-H3K9me2 patterning is not required for maintenance of global DNA methylation in HSPCs

The strong overlap of H3K9me2 nucleation sites in $CD34^+$ cells with CpG islands suggested the possibility that H3K9me2 patterning may be coordinated with DNA methylation. For example, G9a is shown to directly bind to maintenance DNA-methyltransferase, DNMT1, during S phase in Cos-7 cells (Estève et al. 2006), and G9a deficient mouse embryonic stem cells display DNA hypomethylation (Ikegami et al. 2007). Therefore, we performed DNA methylation array analysis probing 99% of RefSeq genes and 96% of CpG islands in $CD34^+$ cells with and without UNC0638 treatment (Fig. 3.3). However, UNC0638 treatment did not lead to global changes in DNA methylation. In fact, only ~0.02% methylation probes showed over 2-fold difference compared to the DMSO control. These results suggest that inhibition of G9a/GLP activity and H3K9me2 patterning does not grossly perturb DNA methylation patterns in HSPCs, consistent with previous observations in human cancer cell lines (Vedadi et al. 2011).

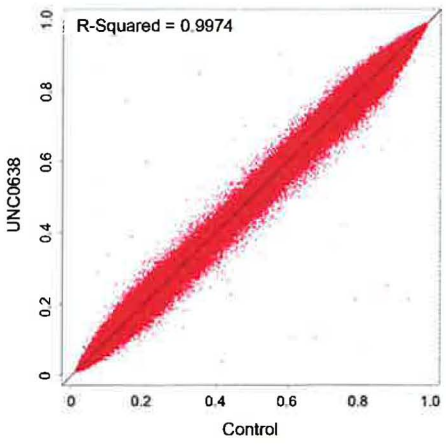

Figure 3.3. Treatment of UNC0638 did not alter global DNA methylation levels in HSPCs. Shown are absolute values of methylation levels (0 indicates unmethylated and 1 indicates completely methylated) of $CD34^+$ HSPCs treated with UNC0638 or DMSO control by DNA methylation array.

3.4 Nuclear staining of H3K9me2 confirms progressive patterning in committed HSPCs

In order to confirm that H3K9me2 patterning is progressive during HSPC lineage commitment, we next performed immunofluorescence (IF) staining of H3K9me2 marks in primitive and committed HSPCs. This analysis revealed that sorted $CD34^{+}CD90^{+}CD38^{lo}CD45RA^{-}$ HSCs showed significantly less nuclear staining than total $CD34^{+}$ population (Fig. 3.4A,B). Cells stained with secondary antibody only were used as negative control (Fig. 3.4C). Moreover, H3K9me2 staining in total $CD34^{+}$ cells revealed the emergence of nuclear speckles or foci. As noted above, UNC0638 treatment revealed that increases in H3K9me2 staining and nuclear speckling arose as a result of G9a/GLP activity (Fig. 3.4A). The quantification of staining did not examine foci per se but the entire nuclear staining intensity (Fig. 3.4B); the difference in foci formation is likely to be more dramatic than total nuclear staining. The formation of H3K9me2 foci in committed HSPCs is consistent with progressive H3K9me2 patterning and development of H3K9me2-depependent higher order chromatin changes during lineage specification.

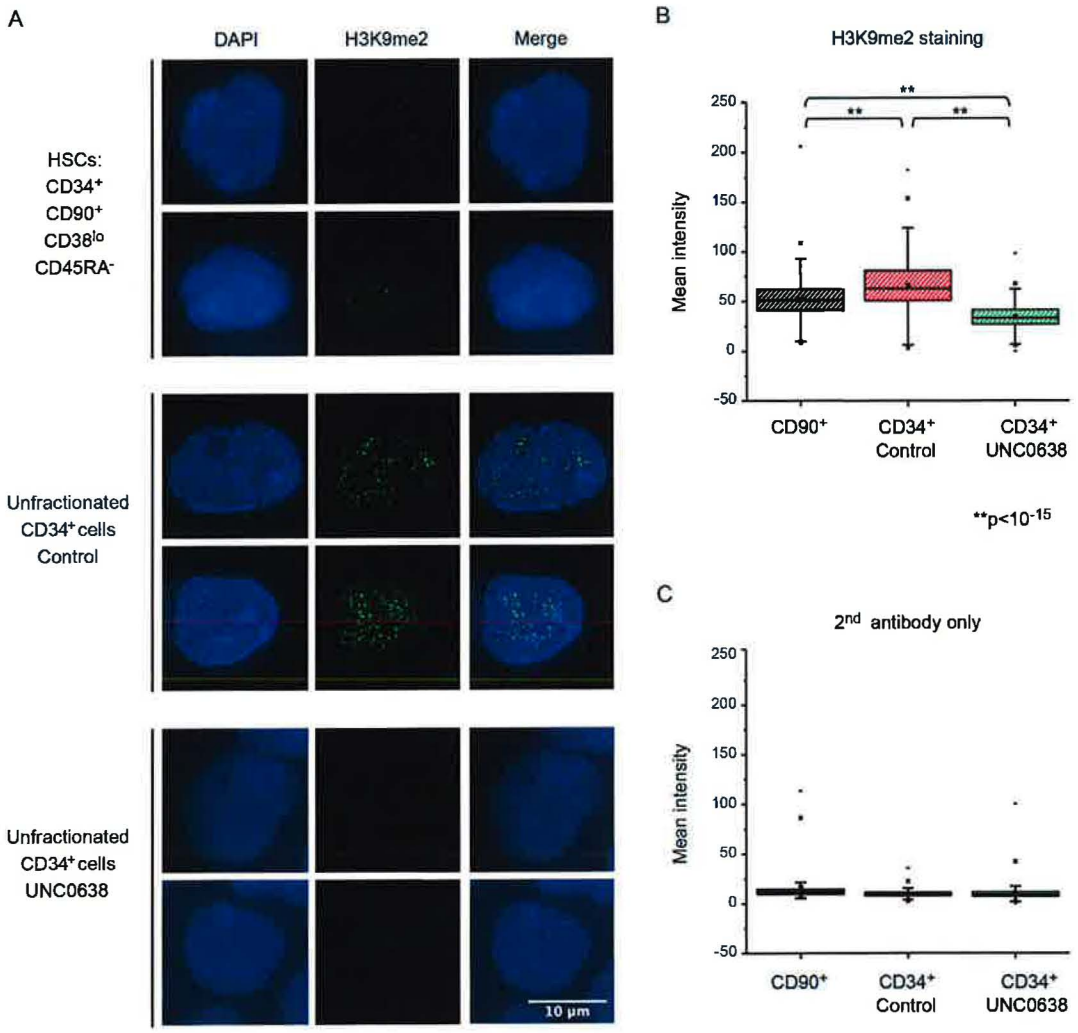

Figure 3.4. Nuclear staining of H3K9me2. **(A)** Deconvoluted z-section pictures of H3K9me2 staining (green) in $CD34^+CD90^+CD38^{lo}CD45RA^-$ HSCs (top panels), unfractionated $CD34^+$ cells (middle panels) and UNC0638 treated $CD34^+$ cells (bottom panels). Nuclei were counterstained DAPI. **(B-C)** Mean intensity of H3K9me2 staining (B) or a secondary antibody only staining (C) (n >380; $^{**}p<10^{-15}$).

3.5 Inhibition of G9a/GLP in HSPCs results in promiscuous transcription of lineage-specific genes and affects transcriptional regulation of certain gene clusters

To evaluate the effect of G9a/GLP-dependent H3K9me2 on regulation of gene expression we performed microarray gene expression analysis on unfractionated $CD34^+$ cells with or without treatment with UNC0638 (Fig. 3.5). Only 158 genes showed significant alterations in expression (Table 3.1). Interestingly, among the 103 genes up-regulated by UNC0638 were those normally expressed in more mature hematopoietic cells and also other tissues, including lung, liver, and brain, as assessed using the Uniprot-tissue database (Fig. 3.5A), and the Novartis normal tissue compendium (Fig. 3.5B). Portions of these results were confirmed by RT-qPCR analysis (Fig. 3.5C).

Among the most significantly up-regulated genes by UNC0638 were the embryonic and fetal hemoglobin genes, HBE1, HBG1, and HBG2 (Bauer and Orkin 2011) (Fig. 3.5C,E). These genes are found in a cluster of embryonic, fetal and adult hemoglobin genes on Chr11p15.5, which are progressively activated and repressed during development by a DNA element up stream of the cluster called the locus control region (LCR) (Chaturvedi et al. 2009). Consistent with our results, G9a/GLP-H3K9me2 has been shown to facilitate silencing of HBE1, HBG1, and HBG2 during mammalian development by altering chromatin secondary structure of LCR and the fetal hemoglobin genes (Chaturvedi et al. 2009).

SYMBOL	log2FC	P.Value
HBG2	1.945674	1.96E-11
CD96	1.487514	1.81E-10
HBG1	1.828907	2.20E-10
CD96	1.293908	5.90E-10
TCN1	1.519349	1.18E-09
FCER1A	1.241277	3.44E-09
MS4A2	1.14863	4.51E-09
HBE1	1.279155	6.24E-09
PRG3	1.060402	7.74E-09
ZNF274	-1.00866	2.13E-08
BEX1	1.001096	3.66E-08
ZSCAN18	-0.99646	4.37E-08
GZMB	1.409646	4.40E-08
CLECL1	1.240812	1.26E-07
CLEC5A	1.223797	4.51E-07
RHAG	0.813105	6.48E-07
	0.80976	6.70E-07
MX2	0.733394	1.05E-06
ALAS2	1.201562	1.13E-06
LOC649143	0.731518	1.91E-06
HCP5	0.876209	1.93E-06
BEX2	1.04146	2.11E-06
SEZ6L2	0.720057	2.84E-06
	0.67449	2.86E-06
HTATIP2	0.712222	2.93E-06
CBS	-0.85272	2.93E-06
PRTN3	-0.6621	3.60E-06
ZNF185	0.779629	4.82E-06
LPAR5	0.641131	5.54E-06
ZNF544	-0.72526	5.68E-06
CD93	0.627368	6.30E-06
MYCN	-0.67028	6.38E-06
LOC730051	-0.72763	6.47E-06
ZNF274	-0.64109	6.58E-06
CHGB	0.63188	6.79E-06
CRIP1	-0.62889	7.33E-06
CCL23	0.850026	7.75E-06
FCF1	-0.62257	7.84E-06
AKR1C3	0.633024	8.78E-06
	0.634274	1.19E-05
CCL23	0.654996	1.26E-05
HAVCR2	0.652208	1.75E-05
RNASE3	0.738275	1.80E-05
CCL5	1.037313	1.91E-05
GALC	0.584149	1.94E-05
CCL5	0.682667	2.45E-05
PSAT1	-0.60133	2.60E-05
HLA-DRA	0.701363	2.65E-05
TIMP1	0.629228	2.76E-05
HLA-DMA	0.568867	2.79E-05
ZDHHC19	-0.63472	2.87E-05
ASCL2	-0.57242	3.04E-05
MLLT11	0.547312	3.43E-05
SKAP1	0.616643	3.80E-05
DHRS9	0.602386	3.97E-05
PTMS	0.568305	4.07E-05
TAF7	-0.53736	4.51E-05
FHL2	0.6204	4.59E-05
TPSAB1	0.56491	5.28E-05
ZNF329	-0.60072	5.75E-05
ST8SIA6	0.600464	5.97E-05
UAP1L1	0.560081	6.66E-05
TPSAB1	0.678078	7.02E-05
CD44	0.500936	7.84E-05
ZNF615	-0.49782	8.05E-05
GAL	-0.53844	8.31E-05
KIR2DL3	0.5086	8.44E-05
MARCKS	0.533842	8.80E-05
RHOBTB3	0.502988	9.10E-05
ZNF285A	-0.53763	9.54E-05
CPA3	0.546216	9.69E-05
ATP6V0E2	0.5036	0.000101
CEBPD	-0.50484	0.000102
TIGD7	-0.48624	0.000106
C3orf14	0.86113	0.000107
CTXN1	-0.49855	0.000107
HNRNPA3	-0.48456	0.000109
NAT8B	0.484796	0.000117
CPS1	0.541865	0.000124
TMEM22	0.492805	0.000124
ETS1	0.472632	0.00014
HLA-DMB	0.471571	0.000143
F12	-0.51532	0.000153
HLA-DPA1	0.491586	0.000153
PRR6	-0.46492	0.000158
FCGRT	-0.46312	0.000164
FBN2	-0.50131	0.000176
HBD	-0.57721	0.000177
ZNF529	-0.52376	0.000179
ENSA	-0.55879	0.000183
	0.536172	0.000186
ZNF562	-0.55858	0.000189
ZIK1	-0.49058	0.000196
HBBP1	1.504344	0.000227
ID2	0.505444	0.000227
AKR1C4	0.442951	0.000243
MYL4	0.809072	0.000273
FCAR	0.460292	0.000281
GAMT	-0.44942	0.000284
DLC1	0.447538	0.000288
WBP5	0.461076	0.00029
ZNF256	-0.48427	0.000302
TMSL8	0.499805	0.000302
	0.438039	0.00032
TAF15	-0.54505	0.000329
LRFN3	0.469626	0.000335
ADORA3	0.448017	0.000355
MAD1L1	0.43788	0.000363
SLC16A3	-0.4959	0.000368
NPC1	0.517713	0.000382
SIPA1L2	0.42515	0.000386
GIMAP5	0.426359	0.000389
ZNF260	-0.42599	0.000404
FAM90A1	0.416989	0.000441
CD74	0.417821	0.000476
PPM1E	0.418218	0.000487
ZFP82	-0.43401	0.000488
SNURF	-0.40967	0.000495
LXN	0.496934	0.000504
	0.436466	0.000512
ACVR1	0.445424	0.000513
DUSP23	0.434965	0.000522
SYNGR1	-0.42986	0.000547
B4GALT5	-0.41608	0.000588
C10orf58	0.524144	0.000595
ADNP2	-0.42545	0.000598
ZNF671	-0.40627	0.000606
BTF3	0.468794	0.000608
ICOS	0.436346	0.000632
JARID2	-0.47883	0.000661
ADCYAP1	0.542196	0.000669
CD69	-0.41568	0.000672
PPP2R2B	0.417332	0.000685
P2RY10	0.4037	0.000686
	0.418504	0.000691
HNMT	0.397756	0.000698
FMO1	0.404501	0.0007
TUBB3	0.441754	0.000705
MUC1	-0.41748	0.000707
AMHR2	0.608267	0.000712
ZNF17	-0.39742	0.000714
CEACAM6	0.424659	0.000743
TCEAL3	0.390881	0.000748
IL18BP	0.401412	0.00075
ZNF773	-0.44313	0.000773
TRO	0.454252	0.00078
CCDC26	0.885214	0.000786
INPP1	0.396757	0.000794
MGC61598	-0.40046	0.000805
LYAR	-0.38856	0.000827
AQP2	0.395925	0.000882
CCDC42	0.467678	0.000896
FCF1	-0.46447	0.000908
VLDLR	-0.38845	0.000948
	-0.39926	0.000952
S100A8	-0.74134	0.000955
C1orf59	0.461413	0.000956
CLC	-0.38544	0.000984

Table 3.1. 158 genes whose expressions were significant altered by UNC0638 ($p<0.001$).

In addition, we found evidence for G9a/GLP-dependent regulation of other gene clusters, including Chr6p21 (HLA-DRA/HLA-DPA1), ChrXq22 (BEX1/BEX2), Chr17q11 (CCL5/CCL23) and Chr19q13 (ZNF329/ZNF544) (Fig. 3.5D-H). For the latter zinc finger (ZNF) cluster, UNC0638 treatment resulted in repression of gene expression, rather than de-repression (Fig. 3.4F), suggesting that G9a/GLP activity is required for the maintenance of their expression in HSPCs. Previous studies have found a protein motif called Kruppel-associated box (KRAB) domain in the majority of ZNF genes on chromosome 19, which is critical for protein-protein interaction (Eichler et al. 1998). KRAB-ZNF genes are largely involved in transcriptional repression (Eichler et al. 1998).

These results suggest, first, that inhibition of G9a/GLP by UNC0638 results in promiscuous transcription of hematopoiesis-affiliated and non-hematopoiesis-affiliated genes in HSPCs, and, second, that G9a/GLP affects local structure of chromatin at specific gene clusters in HSPCs. Primitive HSCs have been hypothesized to have a more "open" chromatin structure that promotes promiscuous transcription of both non-hematopoietic and hematopoietic differentiation genes (Hu et al. 1997; Månsson et al. 2007; Miyamoto et al. 2002). Our data indicate that G9a/GLP and H3K9me2 patterning may help restrict transcriptional promiscuity during HSPC differentiation. Thus, one intriguing implication is that H3K9me2 helps facilitate adoption of alternate chromatin structures required for lineage commitment and specification. If true, inhibition of G9a/GLP and H3K9me2 patterning may block or delay lineage commitment.

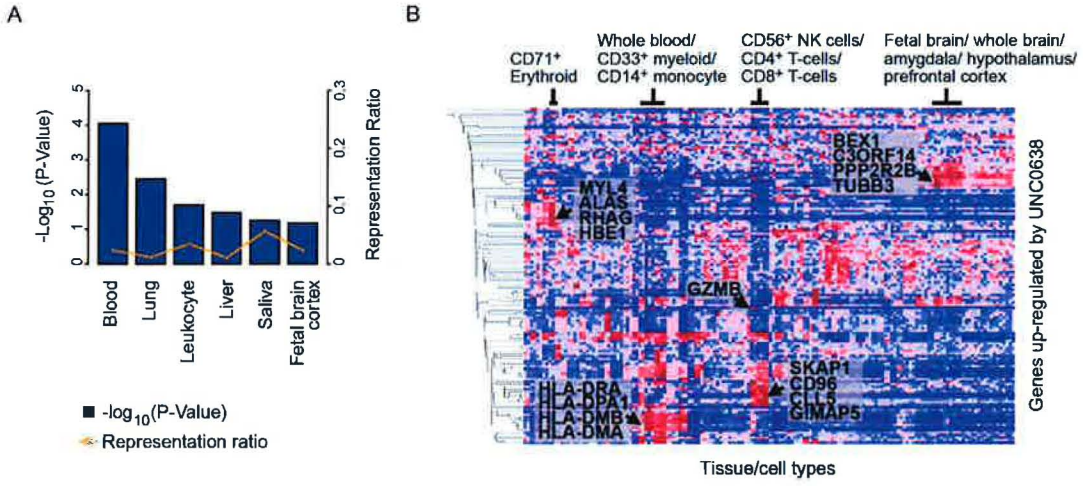
A
-Log10 (P-Value)
Representation Ratio
Blood
Lung
Leukocyte
Liver
Saliva
Fetal brain cortex
-log10(P-Value)
Representation ratio
B
CD71+ Erythroid
Whole blood/ CD33+ myeloid/ CD14+ monocyte
CD56+ NK cells/ CD4+ T-cells/ CD8+ T-cells
Fetal brain/ whole brain/ amygdala/ hypothalamus/ prefrontal cortex
BEX1
C3ORF14
PPP2R2B
TUBB3
MYL4
ALAS2
RHAG
HBE1
GZMB
SKAP1
CD96
CCL5
GIMAP5
HLA-DRA
HLA-DPA1
HLA-DMB
HLA-DMA
Genes up-regulated by UNC0638
Tissue/cell types

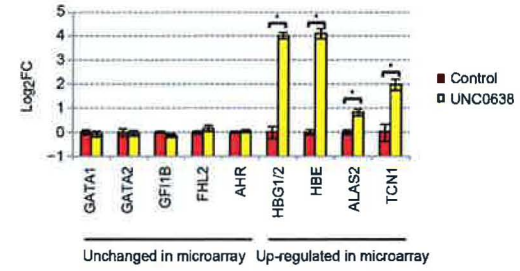
C
Log2FC
Control
UNC0638
GATA1
GATA2
GFI1B
FHL2
AHR
HBG1/2
HBE
ALAS2
TCN1
Unchanged in microarray
Up-regulated in microarray

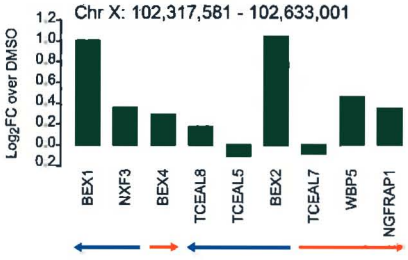
D
Chr X: 102,317,581 - 102,633,001
Log2FC over DMSO
BEX1
NXF3
BEX4
TCEAL8
TCEAL5
BEX2
TCEAL7
WBP5
NGFRAP1

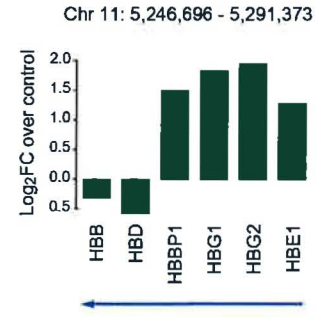
E
Chr 11: 5,246,696 - 5,291,373
Log2FC over control
HBB
HBD
HBBP1
HBG1
HBG2
HBE1

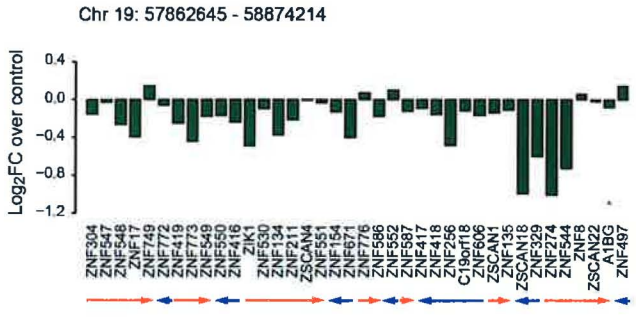
F
Chr 19: 57862645 - 58874214
Log2FC over control

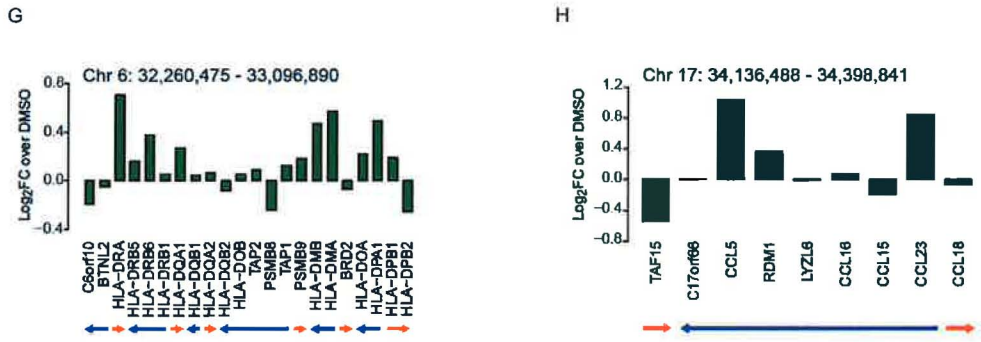

Figure 3.5. Inhibition of H3K9me2 patterning in HSPCs results in up-regulation of multi-lineage gene expressions and affects transcriptional regulation of certain gene clusters. **(A)** Tissue classifications of genes that were significantly changed in expression by UNC0638 with the Uniprot-tissue database. **(B)** Gene expression profiling performed using the Broad Institute's Molecular Signatures database. Genes that were considered differentially expressed were compared to the Novartis normal tissue compendium. Multi-lineage genes up-regulated by UNC0638 were shown. **(C)** qPCR analysis confirmed the microarray results that UNC0638 treatment largely increased genes of diverse lineages but had mild effect on HSC-related genes or AHR. *Student's t-test, $p < 0.01$. **(D-H)** Clusters of genes that were significantly changed in expression by UNC0638. Looking for genes in close proximity in the differential expression set identified these clusters. Fold change represents gene expression change between $CD34^+$ HSPCs treated with UNC0638 compared to DMSO control. Arrows indicate transcription directions.

3.6 Inhibition of H3K9me2 patterning promotes primitive cell phenotypes and expansion of CD34$^+$ cells, which is further enhanced by SR1

To examine the possibility that G9a/GLP inhibition may delay or block adoption of HSPC cell fates, we performed a series of UNC0638 treatments on *ex vivo* cultures of CD34$^+$ HSPCs followed by flow analysis of CD34 and lineage cell surface markers (Fig. 3.6). During a two-week time course, we observed that UNC0638 treatment increased the proportion of CD34$^+$ cells (23.6% in UNC0638-treated vs. 9.2% in the cytokines alone) while diminishing differentiated CD15$^+$ cells (Fig. 3.6A). UNC0638 treatment also led to increases in the number of total nucleated cells (TNCs) and CD34$^+$ cells, with 1 μM UNC0638 having the best expansion effect (Fig. 3.6B). Moreover, UNC0638 treated HSCs also better retained CD49f, a marker associated with long-term repopulating HSCs (Notta et al. 2011) (Fig. 3.6C). These experiments were repeated multiple times with CD34$^+$ cells derived from bone marrow of normal donors or peripheral blood of G-CSF mobilized donors with similar effects. Molecular studies revealed that G9a and GLP had similar expression in CD34$^+$ primitive cells and CD34$^-$ differentiated cells (Fig. 3.6D), and that UNC0638 treatment led to global loss of H3K9me2 (~2- to 4-fold) in HSPCs and a lesser decrease in H3K9me1 (~1.4-fold) without affecting H3K9me3 levels or the expression of G9a, consistent with direct inhibition of its catalytic activity (Fig. 3.6E-K).

To further evaluate the effect of UNC0638 in promoting primitive HSPCs, we compared and combined it with treatments of SR1, a small molecule inhibitor

of AHR, which was recently shown to promote expansion of human HSPCs in *ex vivo* cultures (Boitano et al. 2010). Flow analysis revealed that single treatments with UNC0638 and SR1 enhanced the proportion of more primitive HSPCs (Fig. 3.6A), indicated by: $CD34^+$, $CD38^{lo}$, $CD90^+$, and $CD45RA^-$ (Majeti et al. 2007; Manz et al. 2002) compared to the no-drug control on day 14. SR1 treatments reproduced previously published results. Remarkably, co-treatment with SR1 and UNC0638 approximately doubled the effect of either drug alone for retention of $CD34^+CD38^{lo}$ and $CD34^+CD90^+$ cells, resulting in $CD34^+$ retention as high as 84% after 14 days of culture, compared to only 12% in untreated controls. Similar results were obtained from $CD34^+$ cells from G-CSF mobilized and bone marrow cells from multiple donors (Fig. 3.7A and data not shown).

To determine the cause of increase in $CD34^+$ cells, we performed cumulative cell counts and viability assays for the total nucleated cells produced by HSPC cultures for 21 or 31 days, as well as total $CD34^+$ cells produced during the same time period. The results demonstrated that the increase in proportion of $CD34^+$ cells was due to increased expansion of $CD34^+$ cells. Notably, double treatment increased G-CSF mobilized $CD34^+$ expansion >120-fold by day 17 and bone marrow $CD34^+$ cells nearly 400-fold by day 31, while individual treatments and mock controls were considerably less potent (Fig. 3.7C and data not shown). Importantly, the live-dead cell ratio did not change significantly between mock and treatments (Fig. 3.6L), demonstrating that the increased cell counts were not due to increase in cell survival. Moreover, carboxyfluorescein succinimidyl ester (CFSE) dye retention assays revealed that by day 7 all cells in culture had

undergone at least four cell divisions, including $CD34^+$ cells (Fig. 3.6M). Thus, SR1/UNC0638 treatments did not result in maintenance of large numbers of quiescent cells. However, treated cultures did exhibit better dye retention, suggestive of expansion of slower dividing primitive cells (Cheng et al. 2000; Zhang et al. 2006).

Similar results were obtained using different media formulations, with or without serum and altered cytokine conditions (e.g., using EPO instead of TPO or EPO plus TPO) (Birkmann et al. 1997) (Fig. 3.6N,O), albeit overall $CD34^+$ retention varied by treatment. Moreover, another substrate-competitive inhibitor of G9a/GLP, BIX01294 (Kubicek et al. 2007), phenocopied UNC0638 treatments for $CD34^+$ retention (Fig. 3.6P), while the use of a N-methyl analog of UNC0638, UNC0737, which is highly similar in structural but over 300-fold less potent against G9a/GLP than UNC0638 (Vedadi et al. 2011), had no effect on HSPC expansion (data not shown). Both results further suggest that UNC0638 inhibition is specific to G9a/GLP activity.

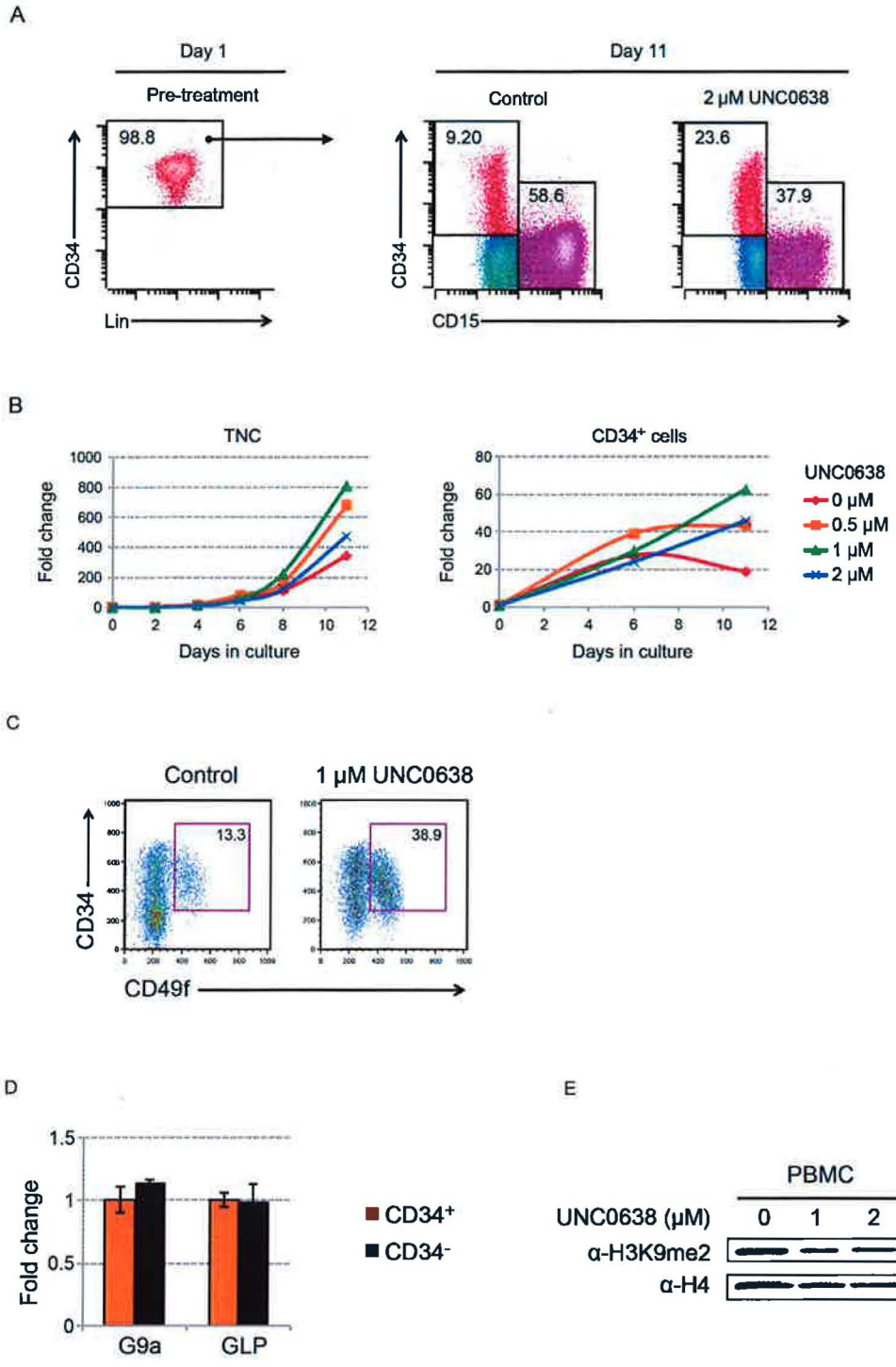
A
Day 1
Pre-treatment
98.8
CD34
Lin
Day 11
Control
2 μM UNC0638
9.20
58.6
23.6
37.9
CD34
CD15
B
TNC
Fold change
Days in culture
CD34+ cells
Fold change
Days in culture
UNC0638
0 μM
0.5 μM
1 μM
2 μM
C
Control
1 μM UNC0638
13.3
38.9
CD34
CD49f
D
Fold change
G9a
GLP
CD34+
CD34-
E
PBMC
BM
UNC0638 (μM)
0 1 2 0 2
α-H3K9me2
α-H4

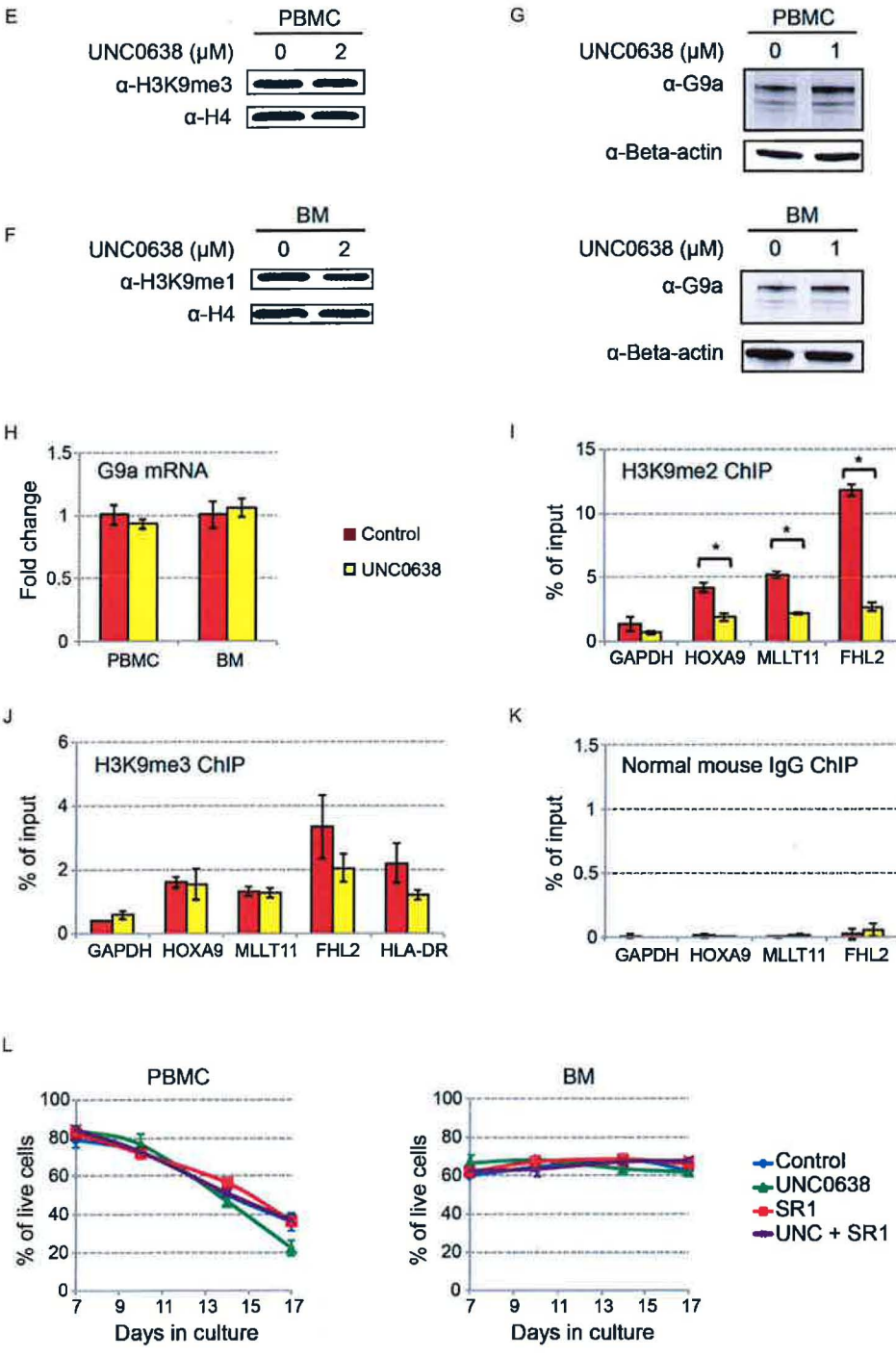
E
PBMC
UNC0638 (μM) 0 2
α-H3K9me3
α-H4
F
BM
UNC0638 (μM) 0 2
α-H3K9me1
α-H4
G
PBMC
UNC0638 (μM) 0 1
α-G9a
α-Beta-actin
BM
UNC0638 (μM) 0 1
α-G9a
α-Beta-actin
H
G9a mRNA
Fold change
Control
UNC0638
PBMC
BM
I
H3K9me2 ChIP
% of input
GAPDH HOXA9 MLLT11 FHL2 HLA-DR
J
H3K9me3 ChIP
% of input
GAPDH HOXA9 MLLT11 FHL2 HLA-DR
K
Normal mouse IgG ChIP
% of input
GAPDH HOXA9 MLLT11 FHL2 HLA-DR
L
PBMC
BM
% of live cells
Days in culture
Control
UNC0638
SR1
UNC + SR1

M

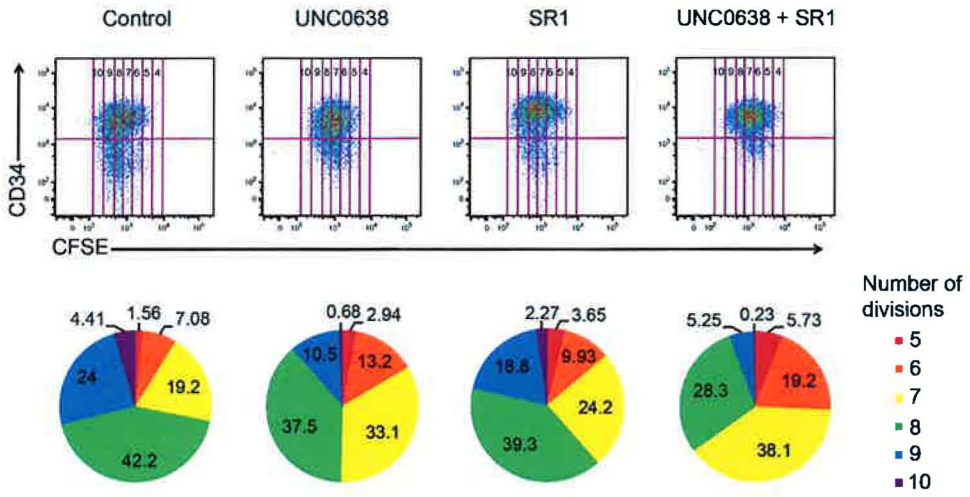

N

Percentage of CD34$^+$ cells on day 12

	Control	UNC 0638	SR1	UNC +SR1
TPO	30.1	42.9	65.4	81.7
EPO	1.06	8.25	3.48	10.2
TPO + EPO	3.68	20.0	7.68	30.0

O

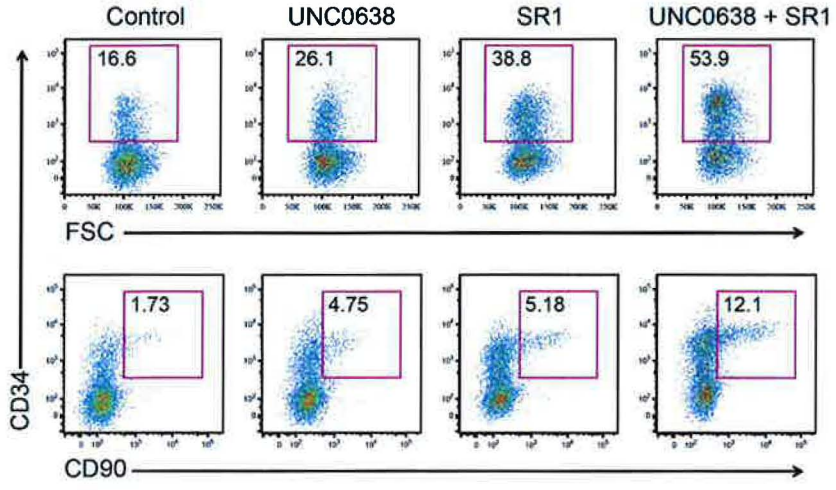

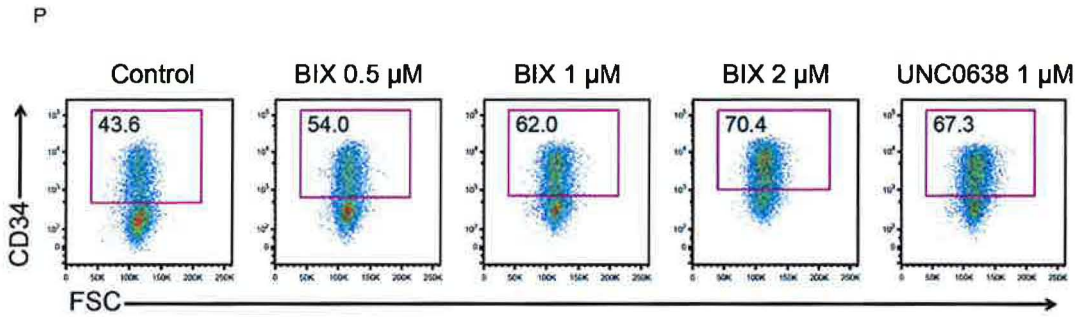

Figure 3.6. Inhibition of H3K9me2 patterning promotes primitive cell phenotypes and expansion of $CD34^+$ cells. **(A)** Flow analysis of day 1 vs. day 11 bone marrow (BM) $CD34^+CD38^{lo}$ cells. $CD34^+CD38^{lo}$ cells were cultured with or without UNC0638 for 11 days. Multi-color flow analysis was performed on CD34 (HSPC maker) and CD15 (differentiated granulocyte marker). Lineage markers include: CD3 (T-cell), CD11b (monocyte/granulocyte), CD14 (monocyte), CD15, CD19 (B-cell), CD56 (natural killer cell) and CD235a (erythrocyte) (Baum et al., 1992; Manz et al., 2002). Colors shown are: red, $CD34^+$; magenta, $CD15^+$; blue, $HLA\text{-}DR^{hi}$; cyan, $HLA\text{-}DR^{lo}$; green, $CD13^{hi}$. Data are representative of multiple independent experiments using G-CSF-mobilized peripheral blood mononuclear cell (PBMC) or BM derived $CD34^+$ cells. **(B)** UNC0638 from 0.5 µM to 2 µM increased the number of both total nucleated cells (TNCs) and $CD34^+$ cells, with 1 µM having the greatest expansion effect on $CD34^+$ cells. **(C)** mRNA expression of G9a and GLP in CD34 HSPCs vs. CD34 differentiated cells. **(E-G)** Western blot analysis of G-CSF mobilized peripheral blood mononuclear cell (PBMC) or bone marrow (BM) derived $CD34^+$ cells treated or untreated with UNC0638 for 48 hours. Total histone H4 or beta-actin were used as loading controls. **(H)**

Relative expression of G9a mRNA in PBMC and BM $CD34^+$ cells treated (yellow) or untreated (red) with 2 μM UNC0638 for 48 hours. **(I-K)** ChIP-qPCR measuring levels of H3K9me2 (G) and H3K9me3 (H) at GAPDH and several HSPC-related genes. Normal mouse IgG was used as negative control (I). Red, DMSO control; yellow, UNC0638. *Student's t-test, $p < 0.01$. **(L)** Percentage of live/dead cells was determined by flow cytometry. Results are presented as mean +/- SD (n = 3). Control, blue diamonds; UNC0638, green triangles; SR1, red squares; UNC0638 plus SR1, purple crosses. **(M)** CFSE labeled $CD34^+$ cells were cultured with DMSO control, 1 μM UNC0638, 1 μM SR1, or 1 μM UNC0638 plus 1 μM SR1 for 7 days. Gates were drawn based on day 1 CFSE fluorescence. Numbers indicate cell divisions. Percentages of total cells with 5 to 10 divisions are indicated in the pie charts. **(N)** Percentage of BM $CD34^+$ cells in serum-free media with three different growth-factor combinations (100 ng/ml TPO, 3 U/ml EPO, or 100 ng/ml TPO plus 3 U/ml EPO; all media also contained 100 ng/ml SCF, 100 ng/ml Flt3L, and 100 ng/ml IL-6.), and four treatments (DMSO control, 1 μM UNC0638, 1 μM SR1, or 1 μM UNC0638 plus 1 μM SR1). **(O)** Flow analysis of CD34 and CD90 in $CD34^+$ cells cultured 8 days in medium containing 10% serum. **(P)** Flow analysis comparing treatments of BIX01294 (BIX) and UNC0638. Data shown here are day 12 PBMC $CD34^+$ cells.

3.7 SR1 and UNC0638 have divergent effects on HSPC expansion and gene expressions

Given the observed differences in HSPC responses to SR1 and UNC0638 single treatments, we further investigated the mechanism of SR1- and UNC0638-dependent HSPC expansion on different HSPCs subpopulations. We began by analyzing CD45RA positive and negative progenitor pools, since UNC0638 increased the proportion of $CD34^+CD45RA^-$ cells while SR1 increased the proportion of $CD34^+CD45RA^+$ cells (Fig. 3.7A). To this end, we purified $CD34^+CD45RA^-$ and $CD34^+CD45RA^+$ populations from day-4 HSPC cultures, which had not previously been treated with SR1 or UNC0638, and performed expansion assays on the isolated cells (Fig. 3.7D). The results revealed that UNC0638 had no effect on the $CD34^+CD45RA^+$ subpopulation, while SR1 preferentially stimulates its expansion. By contrast, both drugs had similar effects on $CD34^+CD45RA^-$ cells (~8-fold peak expansion) and combined treatment resulted in 13-fold peak expansion (Fig. 3.7D).

To further refine this experiment, expansion assays were performed on five pools of myeloid progenitors available in the HSPC culture system: HSCs, MPPs, CMPs, MEPs and GMPs (Fig. 3.7E). Progenitor pools were isolated by FACS and then expanded with or without SR1 and UNC0638. In these assays, SR1/UNC0638 co-treatment most dramatically affected the primitive HSCs (i.e., $CD34^+CD90^+CD38^{lo}CD45RA^-$)—the $CD34^+$ cells expanded ~50-fold after 14 days in SR1/UNC0638, compared to ~6-fold expansion for untreated controls.

Moreover, single treatments were less effective than co-treatment, except for the CD45RA$^+$ GMP pool, where UNC0638 had no effect (Fig. 3.7E).

We next examined SR1- and UNCC0638-dependent changes in HSPC gene expressions to help determine the degree of similarity in their molecular mechanisms of action. We performed gene expression analysis for single treated and co-treated CD34$^+$ HSPCs. The results revealed a degree of divergence for singly treated HSPCs by cluster and multidimensional scaling analysis (Fig. 3.7F,G). In fact, there was little overlap between single treatments and few over all genes that showed significant changes (Fig. 3.7H). These results suggest that UNC0638 and SR1 act through different mechanisms.

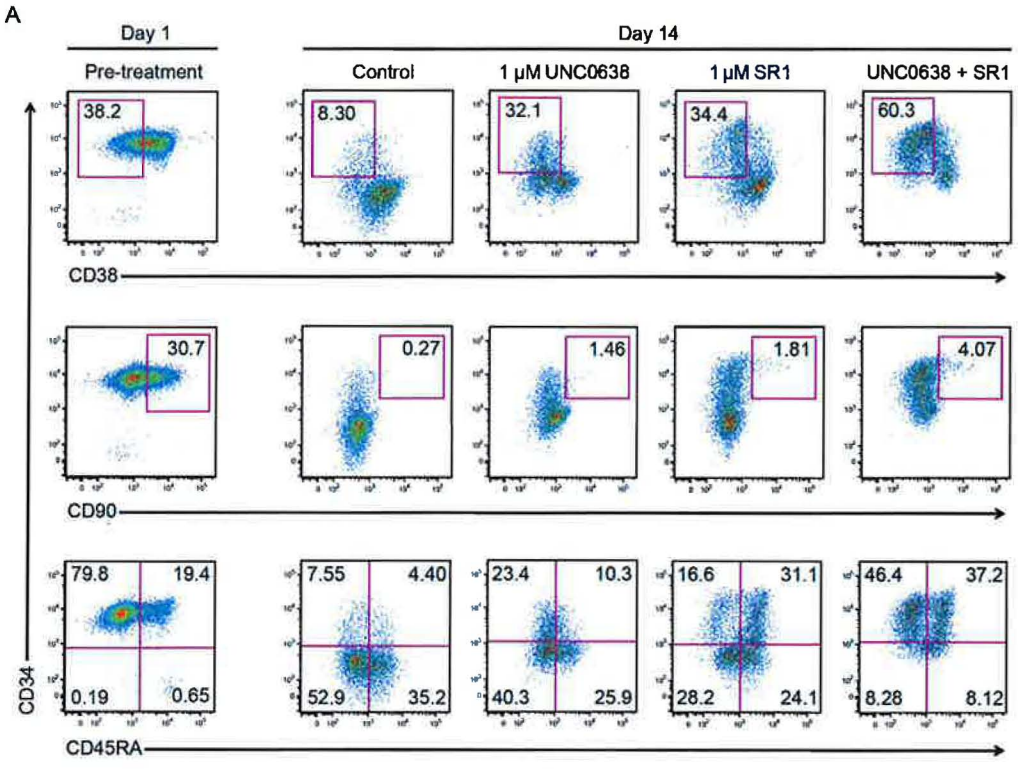

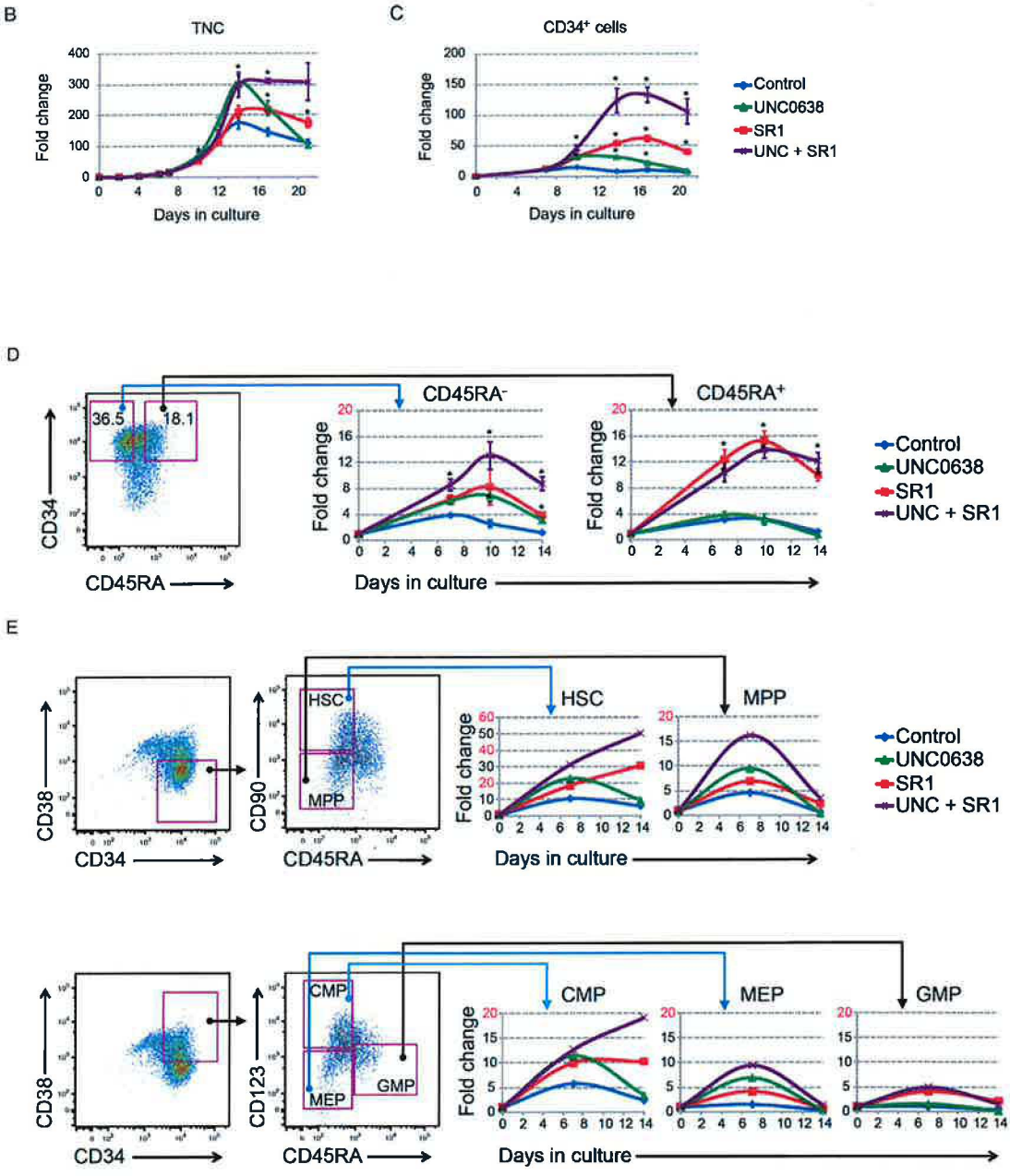
B
TNC
Fold change
Days in culture
C
CD34+ cells
Fold change
Days in culture
Control
UNC0638
SR1
UNC + SR1
D
36.5
18.1
CD34
CD45RA
CD45RA-
CD45RA+
Fold change
Days in culture
Control
UNC0638
SR1
UNC + SR1
E
CD38
CD34
HSC
MPP
CD90
CD45RA
HSC
MPP
Fold change
Days in culture
Control
UNC0638
SR1
UNC + SR1
CD38
CD34
CMP
MEP
GMP
CD123
CD45RA
CMP
MEP
GMP
Fold change
Days in culture

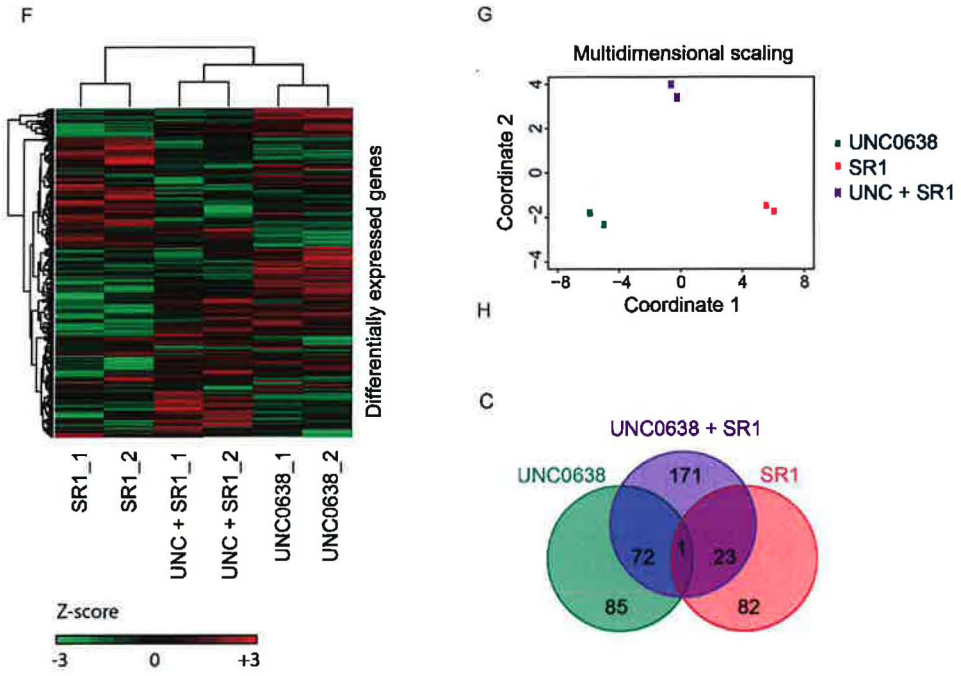

Figure 3.7. UNC0638 and SR1 additively enhanced retention of primitive HSPCs. **(A)** Flow analysis of PBMC $CD34^+$ cells on day 1 (pre-treatment) or day 14 cultured with control (0.01% DMSO), UNC0638, SR1 or UNC0638/SR1 dual treatment. Primitive HSPCs are detected by $CD34^+CD38^{lo}$ (top panels), $CD34^+CD90^+$ (middle panels), and $CD34^+CD45RA^-$ (bottom panels). **(B-C)** Fold expansion of total nucleated cells (B) and $CD34^+$ cells (C) from control (blue diamonds), UNC0638 (green triangles), SR1 (red squares), or UNC0638 plus SR1 (purple crosses) treated conditions (n = 3). *Student's t-test, $p < 0.01$. **(D)** Unfractionated CD34+ cells were expanded in normal culture condition for 4 days and then sorted into two populations: CD34+CD45RA- and CD34+CD45RA+,

which contain HSC/MPP/CMP/MEP and GMP, respectively. Mean fold expansion of CD34+ cells from sorted CD34+CD45RA- or CD34+CD45RA+ cells was calculated (n = 3). *Student's t-test, $p < 0.01$. **(E)** Unfractionated $CD34^+$ cells were expanded in normal culture condition for 4 days and then sorted into 5 defined populations (HSC, MPP, CMP, MEP, and GMP) using known cell surface markers. Mean fold expansion of $CD34^+$ cells from each sorted population was calculated. Control, blue diamonds; 1 μM SR1, red squares; 1 μM UNC0638, green triangles; 1 μM UNC0638 plus 1 μM SR1, purple crosses. **(F-H)** PBMC $CD34^+$ cells were treated with control, UNC0638, SR1 or UNC0638 and SR1 for 48 hours and then subjected to gene expression microarray analysis. **(F)** Supervised clustering of these 434 differentially expressed genes arising from treatments in HSPCs ($P<0.001$). "_1" and "_2" indicate independent experiments of two donors. **(G)** Multi-dimensional scaling of 434 differentially expressed genes between treatment conditions. **(H)** Venn diagram showing extent of overlap in differential gene expression arising from UNC0638, SR1, and UNC0638/SR1 treatment of HSPCs. $p < 0.001$.

3.8 UNC0638 and SR1 treated HSPCs better retain ability to engraft and repopulate *in vivo* in mouse and dog

These results suggest that both UNC0638 and SR1 treatments are capable of enhancing the *ex vivo* expansion of $CD34^+$ populations and combining the two compounds multiplies the effect of either one alone. In order to demonstrate retention of stem cell activity *in vivo*, we performed engraftment and repopulation experiments using SR1 and UNC0638 expanded HSPCs in small and large animal models of HSC transplantation.

We first measured SCID-repopulating cells (SRC) in expanded human HSPC cultures using limiting dilution assays (LDA) in immune compromised mice (Szilvassy et al. 1990). In these assays, day 14 expanded HSPCs in mock, single or co-treated conditions were injected into sub-lethally irradiated NOD/Scid/IL-2 receptor-γ null (NSG) mice (n = 5). Eight weeks post-injection, percentages of human $CD45^+$ cells in mouse bone marrow were examined to determine SRC frequency. By this assay, single drug treatments resulted ~2-fold in increase in the number of SRCs over mock treatment, while co-treatment resulted in ~5-fold increase (Fig. 3.8A). Importantly, human $CD45^+$ cells contained both myeloid ($CD33^+$) and lymphoid ($CD19^+$) cells, indicating that the expanded cells retained multilineage reconstitution potential *in vivo*. However, it should be note that in control experiments, in which freshly isolated G-mobilized $CD34^+$ were injected into NSG mice, as few as 200,000 $CD34^+$ cells displayed engraftment and multilineage differentiation in mice (n=5), whereas no mouse was engrafted with 200,000 UNC0638/SR1 expanded day-14 $CD34^+$ cells (n=5). This suggests that

while SR1/UNC0638 treatment does enhance retention of primitive stem cell markers and stem cell activity compared to the no-drug control expanded cells, the overall stem cell activity as measured in this surrogate assay still diminishes when compared to unexpanded cells.

We next examined the effects of SR1/UNC0638 treatment on HSC activity during expansion of canine $CD34^+$ cells, as previous studies conducted over four decades show that the outcomes of HSC transplantation in dogs accurately predict the outcomes in human patients (Ostrander and Giniger 1997; Thomas and Storb 1999). To this end, a recipient dog was given 9.2 Gray total body irradiation (TBI), a myeloablative dose, and then infused with autologous day-14 SR1/UNC0638 expanded HSPCs, $1.7x10^7$ total nucleated cells/kg. To evaluate reconstitution, absolute neutrophil counts (ANC) were monitored daily until complete hematopoietic recovery for 84 days post-transplantation. Remarkably, transplantation of SR1/UNC0638 expanded cells led to full recovery of the recipient. (Georges et al. 2010) (Fig. 3.8B). These results are consistent with the notion that SR1/UNC0638 expansion, at the very least, sustains canine HSC activity during 14-day expansion of HSPCs. This is in contrast to an unpublished study (n=4), in which canine $CD34^+$ HSPCs cultured for 7-10 days in cytokines only, failed to engraft in dogs conditioned with 9.2 Gy TBI (Mielcarek M., personal communication).

These results strongly suggested that SR1/UNC0638 co-treatment allow retention of primitive HSCs during *in vitro* expansion. It holds promise for expanding HSPCs for transplantation purposes (Dahlberg et al. 2011).

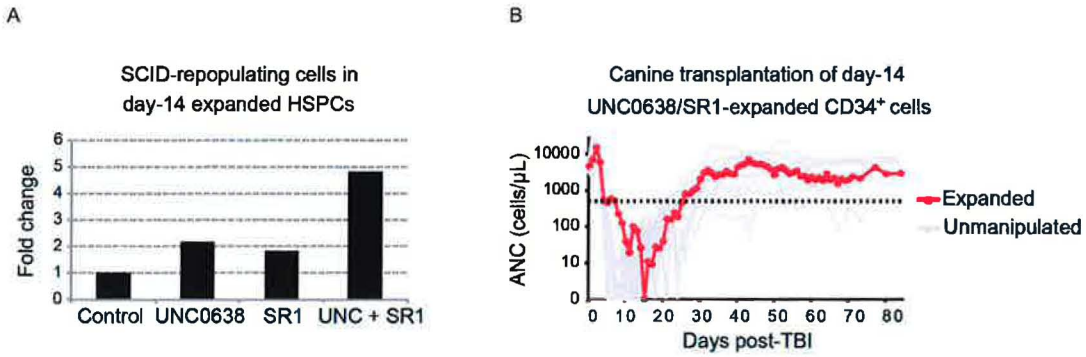

Figure 3.8. UNC0638 and SR1 treated HSPCs better retain ability to engraft and repopulate *in vivo* in mouse and dog. **(A)** Engraftments of human day-14 expanded HSPCs in immunodeficient mice. Frequency of SCID-repopulating cells (SRC) was calculated by Poisson statistics (n = 5). The number of SRCs in each group was calculated by multiplying its frequency by the total cell number at day 14. **(B)** Engraftment kinetics of absolute neutrophil count (ANC) in dog H501 that received 9.2 Gray TBI and $1.7x10^7$/kg expanded autologous $CD34^+$ cells, which were cultured for 14 days in UNC0638 and SR1 (red line). As a positive control (grey lines), shown is ANC recovery after major histocompatibility complex matched littermate or unrelated cord blood progenitor cell transplantation with unmanipulated cells in 13 dogs after 9.2 Gy TBI infused with cell doses comparable to H501. Dotted line indicates ANC = 500 cells per µl.

3.9 Discussion

Here, we examined roles for G9a/GLP activity in normal human HSPCs using an *in vitro* culture and differentiation system and a newly developed chemical probe targeting G9a/GLP, UNC0638 (Vedadi et al. 2011). Our studies have led to several unexpected findings. First, they reveal that G9a/GLP-dependent H3K9me2 patterning is progressive during HSPC lineage commitment: H3K9me2 marks are nucleated at 79% of CpG islands in $CD34^+$ HSPCs and then spread to surrounding regions during differentiation to form characteristic H3K9me2 territories in euchromatic regions of all chromosomes. Second, they suggest that G9a/GLP and H3K9me2 patterning may help restrict transcription of multi-lineage genes during HSPC differentiation. Third, they show that UNC0638 treatment in G-CSF mobilized peripheral blood and bone marrow derived $CD34^+$ HSPCs promotes retention of primitive HSCs *in vitro*, and that this effect is enhanced by co-treatment with the AHR inhibitor SR1 (Boitano et al. 2010). Fourth, they demonstrate that UNC0638 and SR1 target primitive HSCs, but do so through different mechanisms, as judged by differences in expansion effects on committed progenitors and gene expression profiles after treatments (Fig. 3.9). Taken together, these results suggest that G9a/GLP-dependent H3K9me2 patterning plays key roles in early lineage commitment of adult HSPCs. However, these results also raise several questions regarding G9a/GLP function and H3K9me2 marks in HSPCs.

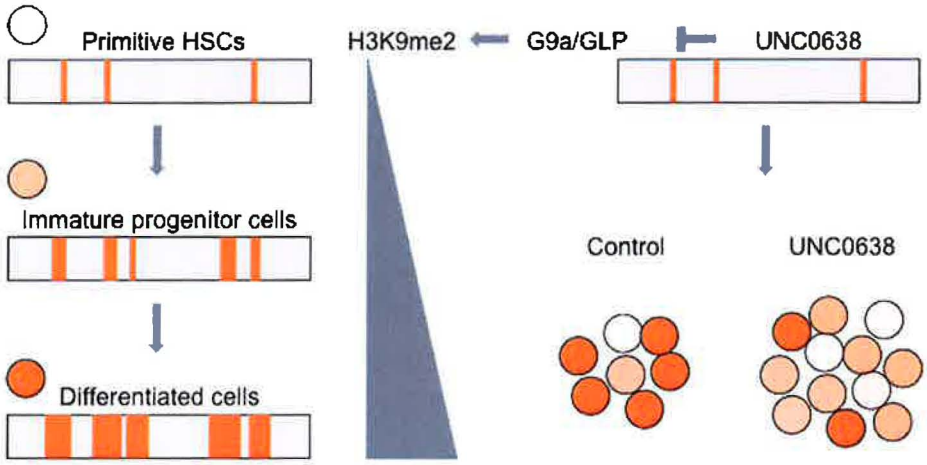

Figure 3.9. Summary of findings. Primitive HSCs display fewer and smaller H3K9me2 marks than immature progenitor cells. H3K9me2 developed in progenitor cells were transmitted and further expanded in differentiated cells. This progressive H3K9me2 patterning requires the histone methyltransferase activity of G9a/GLP. Inhibition of G9a/GLP by UNC0638 reverses H3K9me2 to a similar level as in the HSCs, and leads to better retention and expansion of the primitive cells.

Key among these is: what specific roles do H3K9me2 marks play during HSPC lineage specification? During mammalian development G9a/GLP activity gives rise to large organized chromatin K9me2 modifications (LOCKs) regions of up to 4.9 Mb (Wen et al. 2009), which have been proposed to facilitate retention of higher order chromatin structure and epigenetic memory. LOCKs show apparent tissue specific patterns based on examination of H3K9me2 marks in mouse brain, liver, and human placenta (Wen et al. 2009). Our results are

consistent with formation of LOCKs-like H3K9me2 territories during human hematopoiesis and, moreover, support roles for H3K9me2 in development of higher order chromatin structures during HSPC lineage specification. G9a/GLP-dependent H3K9me2 marks arise in HSPC nuclei as "speckles", which likely indicates the formation of organized chromatin structures during lineage commitment. Furthermore, UNC0638 treatment affects expression of multiple genes appearing in chromosome gene clusters in HSPCs (e.g., 6p21, 11p15, 17q11), suggesting that H3K9me2 facilitates formation of local chromosome structures at these loci. For example, G9a/GLP-H3K9me2 has been shown to facilitate silencing of HBE1, HBG1, and HBG2 during mammalian development by altering chromatin secondary structure of LCR and the fetal hemoglobin genes (Chaturvedi, et al. 2009). Expression of these genes is de-repressed in UNC0638-treated HSPCs. Thus, the results are consistent with the notion that UNC0638 treatment partially blocks formation of higher order chromatin structure in HSPCs.

Another question is how H3K9me2 marks arise in committed hematopoietic cells. Since G9a/GLP-dependent H3K9 methylation can occur *de novo*, pre-existing epigenetic marks are not required (Collins and Cheng 2010). Our results show that H3K9me2 nucleation sites in HSPCs most strongly overlap with CpG islands, perhaps suggesting a functional link between H3K9me2 and DNA methylation. Since CGIs are generally hypomethylated in HSPCs (Hodges et al. 2011), one possibility is that G9a/GLP and DNMT activity are coordinated such that H3K9me2 marks are laid down by default only where CpGs are

unmethylated (i.e., in CGIs). Alternately, specificity factors might target G9a/GLP to CGIs. For example, in ESCs G9a/GLP bind to UHRF1, which, in turn, binds to hemi-methylated CpG sites (Kim et al. 2009).

One intriguing implication of our results is that the absence of H3K9me2 marks in HSCs may facilitate adoption of alternate chromatin and chromosomal structures required for lineage commitment and specification. This would be consistent with the concept that HSCs harbor open chromatin structure that results promiscuous transcription (Akashi et al. 2003), which is incompatible with the presence of H3K9me2 chromatin territories.

This work also has important implications for clinical uses of human HSCs. One of the long-standing roadblocks limiting application of HSCs has been our inability to effectively expand and/or immortalize HSC *ex vivo* (Dahlberg et al. 2011). Initial attempts at *ex vivo* expansion of HSPCs focused on cytokine stimulation to support survival and proliferation of lineage-committed progeny in the hope of expanding true HSCs as well (Dahlberg et al. 2011; Sauvageau et al. 2004). However, these attempts have largely failed to enhance *in vivo* engraftment in patients.

One notable exception is stimulation of Notch signaling in cord blood units (Ohishi et al. 2002; Delaney et al. 2010), which allows more rapid myeloid reconstitution in patients with post-transplantation cytopenias. However, it appears that Notch-expanded cord blood units may be depleted of long-term repopulating HSCs (Dahlberg et al. 2011), and, as a result, are given in combination with naïve cord blood units to provide stem cells to improve long-

term engraftment. Moreover, Notch-driven expansion only affects fetal cord blood stem cells but has no effect on adult human HSC expansion (Dahlberg et al. 2011).

However, Cooke and colleagues recently discovered that SR1, a small molecular inhibitor of the aryl hydrocarbon receptor, promotes expansions of $CD34^+$ human HSPCs in *ex vivo* cultures (Boitano et al. 2010). Our SR1 trials similarly support these findings in adult stem cells, although SR1 treatment did not dramatically affect expression of AHR-pathway targets, as previously reported (Boitano et al. 2010).

Our studies with UNC0638 revealed that this drug on its own had effects similar to SR1 with respect to retention of $CD34^+$ HSPCs and also HSPC engraftment activity in immunocompromised mice. Moreover, examination of SR1 and UNC0638 treatment revealed that each affects both common and distinct populations of HSPCs, with most dramatic effects observed on primitive HSCs. The mechanisms giving rise to their expansion effects were clearly divergent based on transcriptional profiling and there was no evidence of cross regulation of either AHR-pathway and/or G9a/GLP gene expression.

We envision several clinical applications of SR1/UNC0638 treatments. First is in the expansion of HSCs for transplantation. There are many cases were transplantation products are critically limited (e.g., young or small donors, prior treatment of the donor, or failure to mobilize). Second is in accelerating transplantation recovery. Post-transplantation cytopenias, including neutropenias and thrombocytopenias, are commonplace, and lead to life threatening infections

or bleeding and result in costly, extended hospitalization (Dahlberg et al. 2011). Our results from modeling transplantation of SR1/UNC0638 cultures in a canine model suggest that combining day-14 expanded cultures with non-manipulated HSPCs may help bridge post-transplantation neurtropenia, in addition to providing long term engraftment. Third, it is conceivable that UNC0638 has the potential benefit to patients with beta-hemoglobinopathies by reactivating the embryonic and fetal hemoglobin, whose activation is associated with milder symptoms (Akinsheye et al. 2011). Lastly, we envision that SR1 and UNC0638 may be combined with additional experimental manipulations to practically immortalize single HSC for unlimited expansion while retaining developmental potential, similar to ESCs or induced pluripotent stem cells.

In conclusion, our data strongly suggest that G9a/GLP-mediated H3K9me2 patterning is required for HSPC lineage specification and its inhibition leads to delayed differentiation and retention of the HSPCs. These findings should prove useful for clinical and experimental applications limited by current techniques to maintain HSPCs *in vitro*.

CHAPTER 4

SMALL MOLECULAR INHIBITOR OF G9A/GLP, UNC0638, PROMOTES MEGAKARYOPOIESIS FROM HUMAN HSPC

4.1 UNC0638 promotes $CD41^+/CD42^+$ megakaryocytes from $CD34^+$ HSPCs

We performed a 14-parameter flow analysis on differentiation markers, including granulocyte marker CD15, and megakaryocyte marker CD41. We found that while the majority of $CD34^-$ cells differentiated from SR1 treated HSPCs are $CD15^+$, $CD34^-$ cells generated from UNC0638 treated HSPCs are largely $CD15^-$ (Fig. 4.1A). On the other hand, UNC0638 expanded the $CD41^+$ cells to a significant greater extent compared to the control and SR1 (Fig. 4.1B). With the treatment of UNC0638, we achieved an over 4000-fold increase in the number of $CD41^+$ cells from $CD34^+$ HSPCs—16-fold more compared to the control (Fig. 4.1C). These phenotypes are consistent with our previous observation that UNC0638 acted on $CD45RA^-$ megakaryocyte/erythrocyte lineages while SR1 acted on $CD45RA^+$ granulocyte/monocyte lineages (Fig. 3.7A). It suggested that although both UNC0638 and SR1 retained primitive HSPCs *in vitro*, they each have preferences in regarding to lineage specification when these cells differentiate. These results also emphasized the value of combining UNC0638

and SR1 to expand human HSPCs for transplantation purposes to ensure the regeneration of all blood lineages.

We then examined the effect of UNC0638 on megakaryocytes maturation by two sequentially expressed megakaryocyte markers, CD41 (earliest megakaryocytic marker) and CD42 (late megakaryocytic marker). Megakaryocyte progenitors are $CD41^+CD42^-$, while mature megakaryocytes are $CD41^+CD42^+$. On day 1, more than 90% of the starting $CD34^+$ HSPCs are $CD41^-CD42^-$, with 6.6% $CD41^+CD42^-$ cells and less than 0.5% $CD41^+CD42^+$ cells (Fig. 4.1D). On day 7 in TPO-containing medium, treatment of UNC0638 resulted in 12.1% $CD41^-CD42^+$ cells and 24.3% $CD41^+CD42^+$ cells, which are twice as many as the control and SR1 (Fig. 4.1E). On day 12, 17.7% of UNC0638 treated $CD34^+$ cells became $CD41^+CD42^-$ and 41.8% became $CD41^+CD42^+$, which is more than 3 fold compared to the control and SR1 (Fig. 4.1F). We also showed that BIX01294, an UNC0638 analogy, has similar effect as UNC0638 (Fig. 4.1G).

To further characterize which progenitor population UNC0638 is affecting, we sorted five HSPC pools (HSC, MPP, CMP, MEP, and GMP), treated with UNC0638 separately and did flow analysis on CD41 and CD42 on day 12 (Fig. 4.1H). We found that UNC0638 stimulates megakaryopoiesis and promotes the maturation of megakaryocytes from all HSPC pools except for the GMP, which is consistent with known developmental potential of these populations.

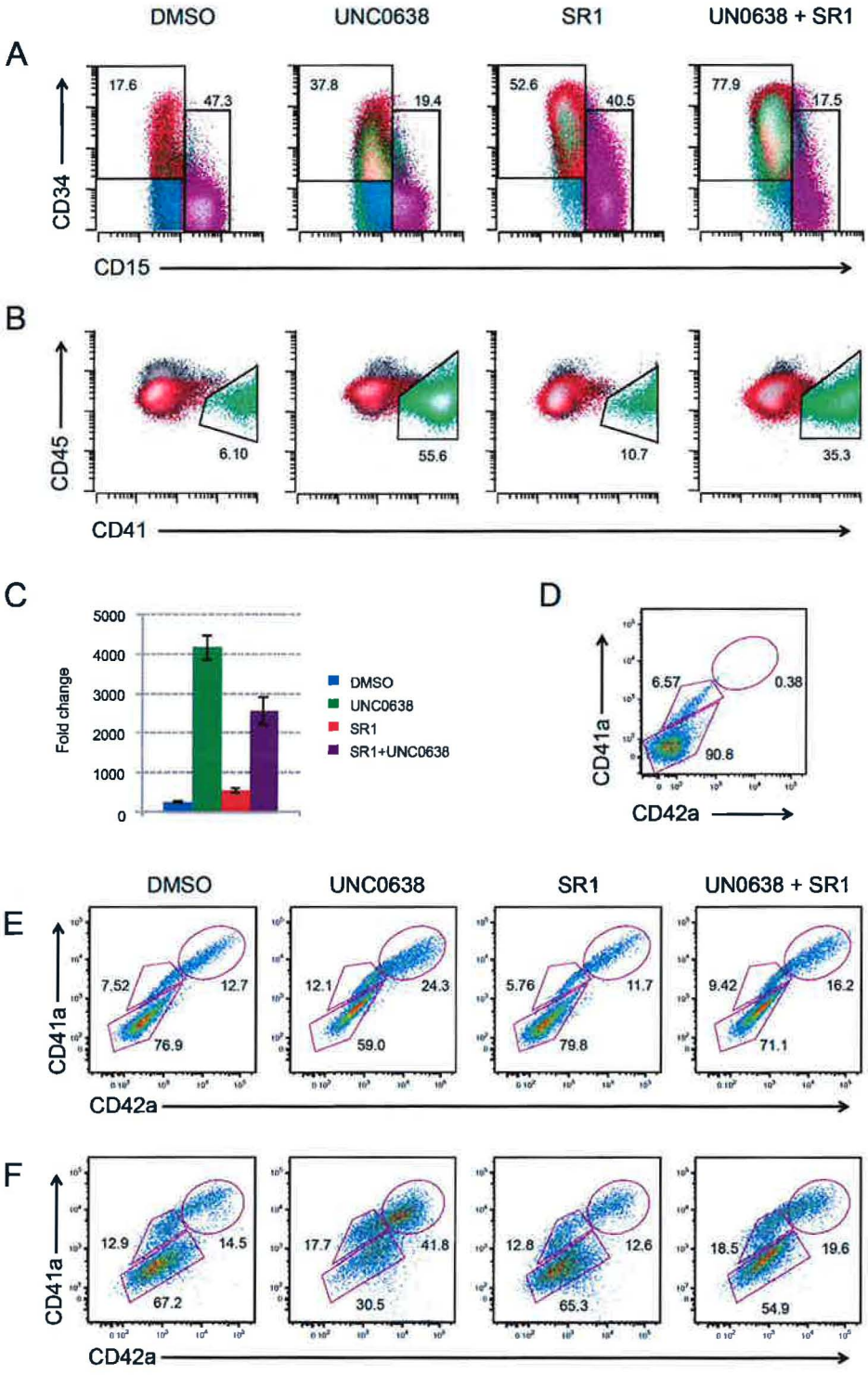
DMSO
UNC0638
SR1
UN0638 + SR1
A
17.6
47.3
37.8
19.4
52.6
40.5
77.9
17.5
CD34
CD15
B
6.10
55.6
10.7
35.3
CD45
CD41
C
5000
4000
3000
2000
1000
0
Fold change
DMSO
UNC0638
SR1
SR1+UNC0638
D
6.57
0.38
90.8
CD41a
CD42a
E
7.52
12.7
76.9
12.1
24.3
59.0
5.76
11.7
79.8
9.42
16.2
71.1
CD41a
CD42a
F
12.9
14.5
67.2
17.7
41.8
30.5
12.8
12.6
65.3
18.5
19.6
54.9
CD41a
CD42a

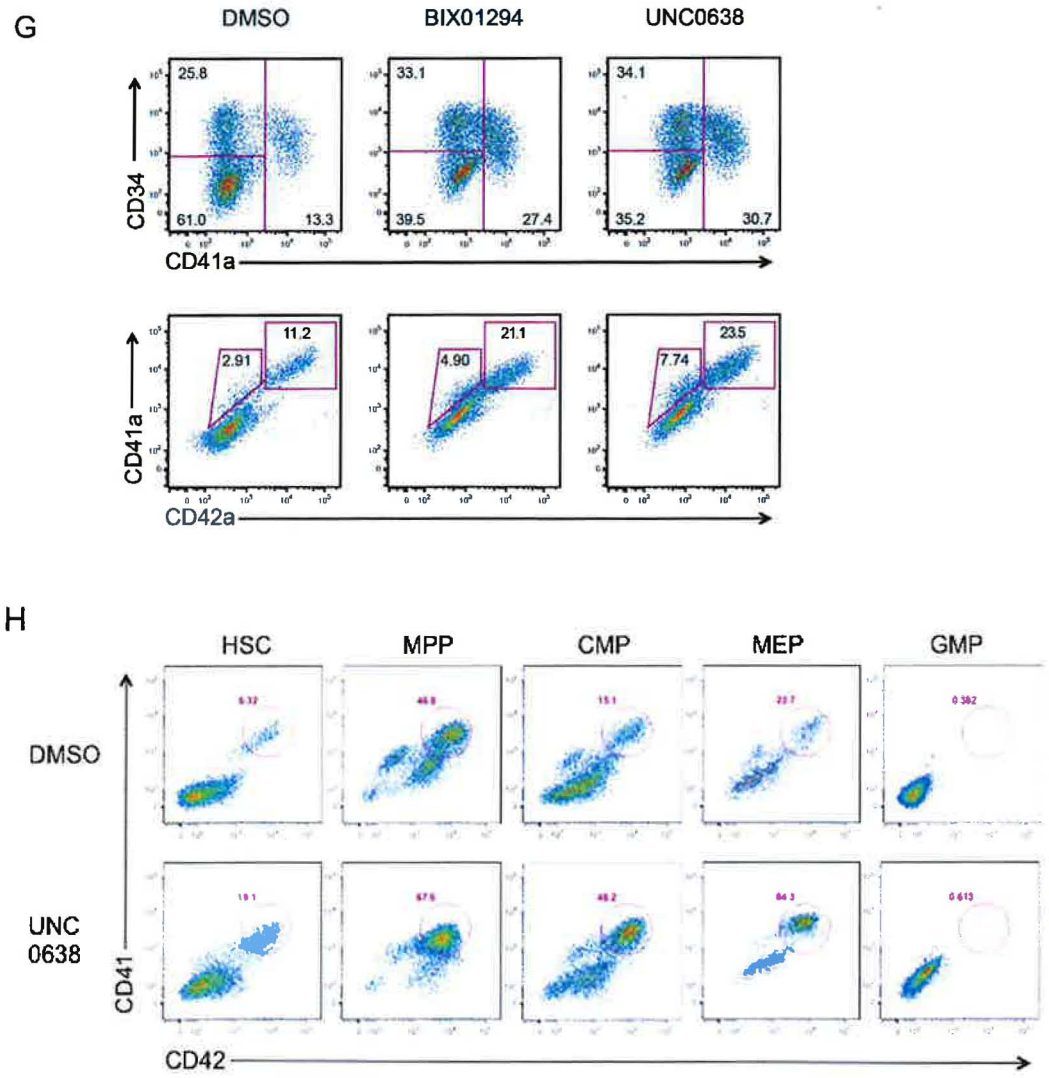

Figure 4.1. UNC0638 promotes megakaryopoiesis. **(A and B)** Flow analysis of $CD34^+$ cells cultured in serum-free medium for 14 days revealed a significant increase of $CD41^+$ and decrease of $CD15^+$ cells with the treatment of UNC0638. **(C)** Fold increase of $CD41^+$ cells from $CD34^+$ cells on day 14. **(D-F)** CD41 and CD42 expression on day 1 (D), day 7 (E) and day 12 (F). **(G)** BIX01294 has similar effect as UNC0638. **(H)** UNC0638 treatment promotes $CD41^+CD42^+$ megakaryocytes from HSC, MPP, CMP, MEP but not GMP.

4.2 UNC0638 inhibits non-meg lineage differentiation

First, to test whether UNC0638 also promotes erythropoiesis, we added 2 U/ml of erythropoietin (EPO) into the culture medium and did flow analysis of CD41 and CD235a (erythrocyte glycophorin a). Our results indicated that UNC0638 increased the percentage of $CD41^+$ but decreased the percentage of $CD235a^+$ cells (Fig. 4.2A). It suggests that UNC0638 may promote megakaryopoiesis at the expense of erythropoiesis.

To examine the effect of UNC0638 on other hematopoietic lineages, I performed an experiment to induce differentiation of $CD34^+$ cells into a number of lineages by adding different cytokines. For all cultures, SCF, IL-6 and Flt3L were added to support cell growth. In addition, in separate cultures, TPO was added to induce megakaryopoiesis ($CD41^+CD42^+$), EPO was added to induce erythropoiesis ($CD235a^+$), GM-CSF for granulocyte and monocyte differentiation ($CD15^+$ and $CD14^+$, respectively) and IL-3 for myeloid cells in general. Flow cytometry and cell counting were performed 12 days post treatment on different lineage markers.

A

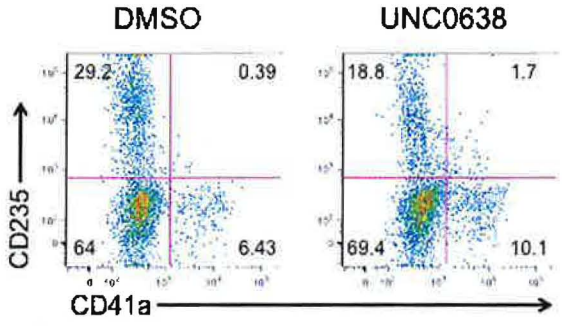

B

	34+%	41+42+%	235a+%	15+%	14+%	33+%	Total cell # fold change
SF6	23.5 | 55.1	1.0 | 8.0	0 | 0	58.0 | 31.5	6.6 | 5.0	96.5 | 95.4	42.3 | 20.4
SF6+TPO	31.2 | 55.2	7.3 | 34.4	0 | 0.2	40.8 | 11.5	4.6 | 2.3	91.2 | 90.7	114.9| 122.1
SF6+IL-3	24.6 | 30.8	3.5 | 13.7	4.8 | 8.1	29.9 | 18.4	5.9 | 3.7	92.4 | 92.1	206.4| 213.9
SF6+GM-CSF	22.8 | 26.3	2.3 | 7.3	7.6 | 4.6	34.1 | 26.4	2.0 | 1.8	66.5 | 86.0	222 | 144.6
SF6+EPO	5.4 | 37.7	0.5 | 3.7	71.3 | 42.2	9.1 | 8.1	1.8 | 1.4	12.9 | 30.5	159.3 | 65.7

Figure 4.2. UNC0638 promote megakaryopoiesis at the expense of other lineages. **(A)** $CD34^+$ cells were cultured with TPO and EPO and treated or untreated with UNC0638 for 7 days and examined for their expression of CD41 and CD235a by flow. **(B)** $CD34^+$ cells were culture with diverse cytokines. Percentage of lineage positive cells in each condition was analyzed, and cell number was counted on day 12. Cytokiens used: SF6: SCF + FL + IL-6, each at 100 ng/ml; TPO, IL-3, GM-CSF each at 100 ng/ml; EPO at 0.1 U/ml. Red: DMSO; blue: UNC0638. Purple boxes indicate significant changes.

4.3 $CD41^+CD42^-$ megakaryocyte progenitor cells generated in UNC0638 are bi-potent

To test whehter the $CD41^+CD42^-$ cells generated in UNC0638 are bi-potent megakaryocyte progenitors, which have the potential to give rise to both megakaryocytic and erythrocytic lineages, we cultured human G-mobilized $CD34^+$ cells in our standard medium with 1 μM UNC0638 for 12 days, and sorted the progenies into three populations: $CD41^+CD42^+$ that contains mature megakaryocytes, $CD41^+CD42^-$ that contains MEPs, and $CD41^-CD42^-$ that contains immature progenitors and cells of non-megakaryocytic lineages (Fig. 4.3A). We then put them each back to culture with the same TPO medium or with a red blood cell (RBC) expansion medium, which has SCF, IL-3, IGF-1, dexamethasone and 2 U/ml EPO. Flow analysis on CD41, CD42 and CD235a was performed 7 days after re-plating. We hypothesized that if the sorted population contains HSCs and/or MEPs, they should have bi-potency, meaning that they can generate $CD41^+CD42^+$ mature megakaryocytes in TPO medium and $CD41^-CD235^+$ RBCs in EPO medium. As predicted, over 90% sorted $CD41^+CD42^+$ cells broke up into small platelet-like cells, which stay $CD41^+CD42^+$ in both TPO and EPO media (Fig. 4.3B,C bottom panels). On the contrary, 77.4% of the $CD41^+CD42^-$ MEPs further differentiated into $CD41^+CD42^+$ mature megakaryocytes in TPO medium and 50.1% of them lost CD41 expression and became $CD41^-CD235^+$ erythrocytes in EPO medium (Fig. 4.3B,C middle panels), proving that these cells are bi-potent. $CD41^-CD42^-$ cells that contains immature progenitors also had the ability to generate some $CD41^+CD42^+$ cells in TPO

medium (11.5%) and erythrocytes in EPO medium (38.7%) (Fig. 4.3B,C upper pannels).

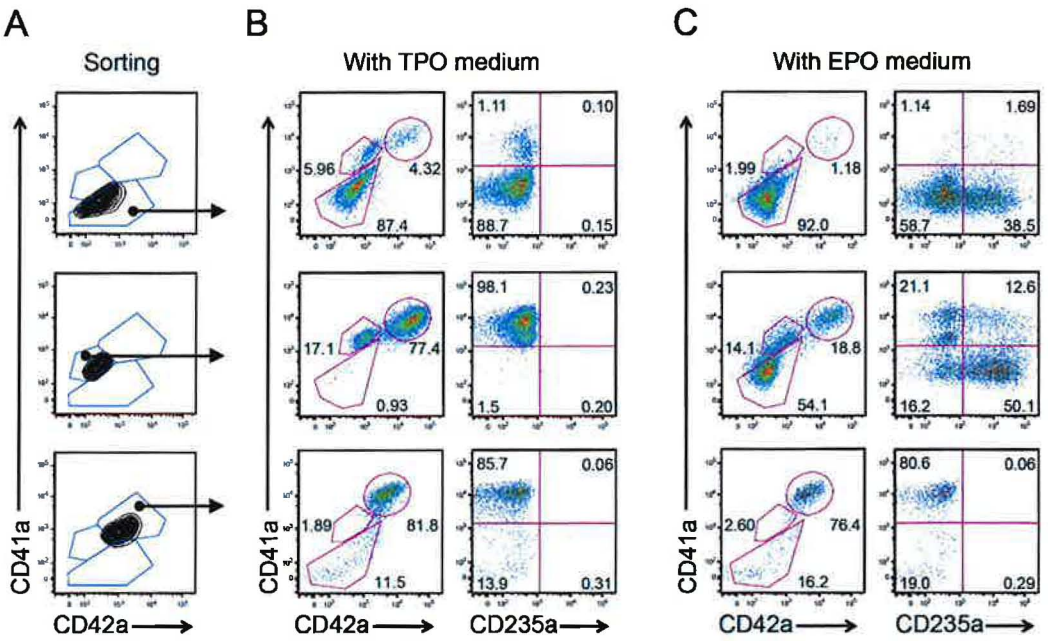

Figure 4.3. Megakaryocyte progenitors generated in UNC0638 are bi-potent. **(A)** CD34+ cells were culture with UNC0638 for 12 days and then sorted into 3 populations: $CD41^{-}CD42^{-}$ (immature progenitors and cells of non-megakaryocytic lineages), $CD41^{+}CD42^{-}$ (MEP), and $CD41^{+}CD42^{+}$ (mature megakaryocyte). Sorted cells were replated in TPO- **(B)** or EPO- **(C)** containing medium for 7 days before flow analysis. Both $CD41^{-}CD42^{-}$ and $CD41^{+}CD42^{-}$ cells had the ability to generate $CD41^{+}CD42^{+}$ cells in TPO medium and $CD235a^{+}$ erythrocytes in EPO medium, with the most from $CD41^{+}CD42^{-}$ cells. Whereas, over 90% $CD41^{+}CD42^{+}$ cells broke up into small platelet-like cells, which stay $CD41^{+}CD42^{+}$ in both TPO and EPO media.

4.4 Megakaryocytes generated in UNC0638 can penetrate endothelial cell vessel wall and release platelets in a 3D-culture system

To confirm whether the large number of megakaryocytes generated with UNC0638 are functional, we cultured them in an engineered microvessel system, which mimics the *in vivo* microenvironment (Zheng et al., 2013). In this experiment, human $CD41^{+}CD42^{+}$ mature megakaryocytes sorted from day 10 culture of $CD34^{+}$ HSPCs with continuos UNC0638 treatment were mixed with collagen gel, and together were molded against a micropatterned silicone rubber stamp to form a microfluidic network. Human umbilical vein endothelial cells (HUVECs) were then seeded along the vessel wall. Normal endothelial cell medium with TPO was flowing in the vessel by gravity. Three days after culture, microvessles were fixed and stained for CD31 (endothelial cells), CD41 (megakaryocytes) and DAPI (nuclei).

We found that megakaryocytes migrated from the collagen matrix to the vessle wall and were tightly associated with the HUVECs. Moreover, some megakaryocytes were able to penetrate the microvessel and release platelets into the vessel lumen (Fig. 4.4A,B). We also observed pro-platelets that were released into vessel wall (Fig. 4.4C,D). These results suggested that UNC0638 generated megakaryocytes can produce platelets in a 3D-culture system. Further functions of culture-generated megakaryocytes will be tested *in vivo* in immunodeficient mice.

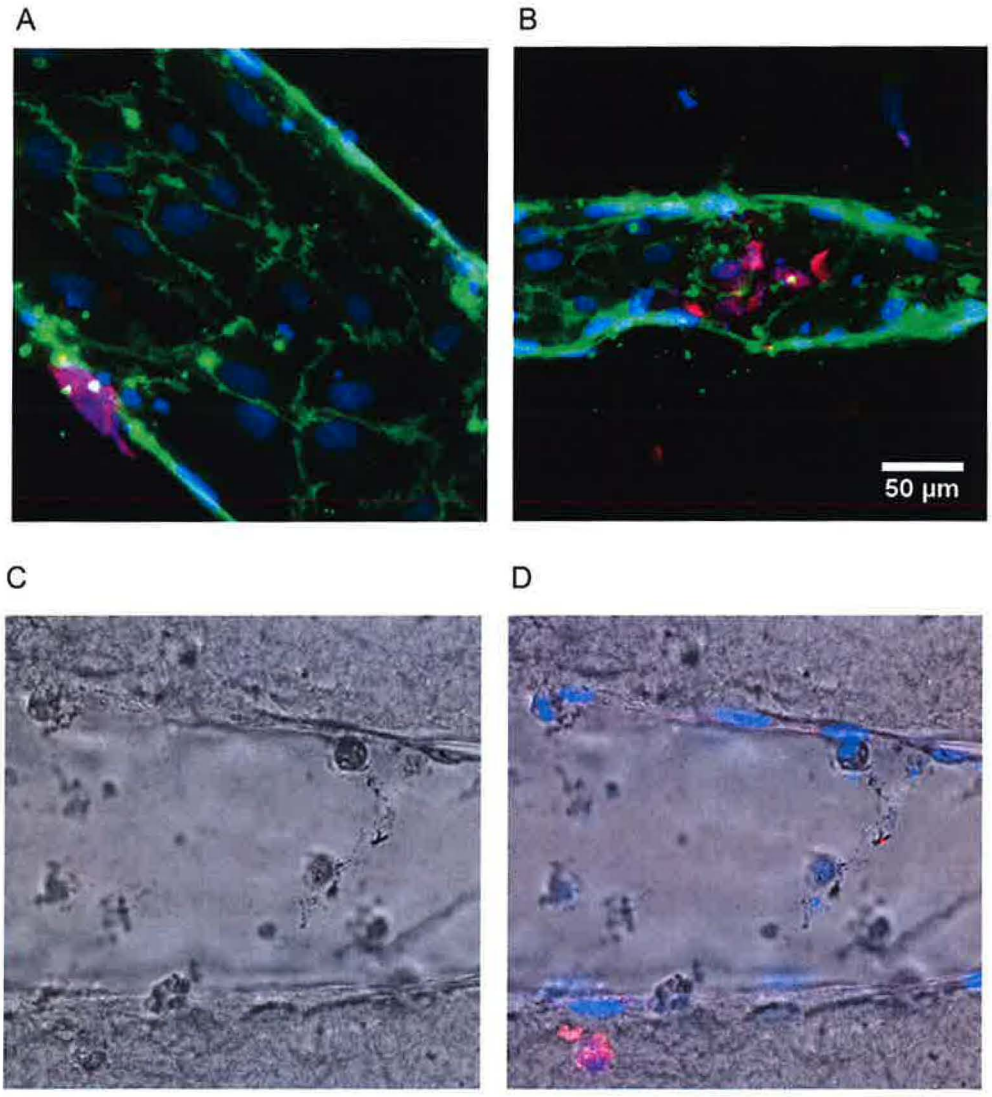

Figure 4.4. $CD41^{+}CD42^{+}$ megakaryocytes generated in UNC0638 penetrate the microvessel and release platelets. **(A)** Megakaryocyte penetrates the vessel wall and releases platelets in the vessel. **(B)** Megakaryocyte completely penetrated into the microvessel. **(C, D)** Pro-platelets observed that are released into vessel wall. Green: CD31 (endothelial cells on the vessel wall); red: CD41 (megakaryocytes and platelets); blue: DAPI (nuclei).

4.5 Discussion

Megakaryocytes are generated from HSCs through a complex process, including cellular enlargement, multiple endomitosis, membrane system development and cytoplasmic fragmentation (Patel et al., 2005). Since the discovery of TPO (Bartley et al. 1994), great efforts have been made to generate megakaryocytes *ex vivo* from $CD34^+$ cells (Lannutti et al., 2005; Chen et al., 2009; Liu et al., 2010). With the inhibition of H3K9me2 by UNC0638, we observed higher expression of megakaryocyte markers CD41 and CD42 using human adult $CD34^+$ cells, and increased number of large cells using dog whole bone marrow. In a 3-dimensional culture system, UNC0638 generated megakaryocytes were able to migrate and interact with endothelial cells and produce platelets in the microvessel.

These results add to the growing approaches for future development of an *in vito* platelets production system. It also sheds light on the role of epigenetic modifications in regulation of hematopoiesis. We hypothesize that the balance between histone H3K9 methylation and demethylation may be involved in critical steps of megakaryopoiesis. In fact, two recent studies using genome-wide meta-analysis have identified a histone H3K9 demethylase JMJD1C, among several other novel genes, has crucial roles in megakaryopoiesis (Gieger et al., 2011) and platelet aggregation (Johnson et al., 2010). Silencing of JMJD1C in zebrafish led to ablation of both megakaryopoiesis and erythropoiesis (Gieger et al., 2011).

Inhibition of G9a/GLP by UNC0638 may have similar effect as JMJD1C in megakaryopoiesis.

However, it is of note that we did not detect lineage specific pattern of H3K9me2, and its distribution in megakaryocytes and T-cells is identical. Genes up-regulated in HSPCs by UNC0638 treatment are not megakaryocyte specific either. The precious role of G9a/GLP and H3K9me2 on megakaryopoiesis requires further investigations, and the molecular mechanism, by which UNC0638 preferentially induces the megakaryocytic lineage, needs to be determined.

Although our results are strongly suggestive of a mechanism whereby UNC0638 blocks G9a/GLP-H3K9me2 activity to affect HSC differentiation, G9a/GLP also have non-histone methylation targets. *Known* non-histone targets include: ACINUS (Rathert et al., 2008), CDYL1 (Rathert et al., 2008), WIZ (Rathert et al., 2008), C/EBP-β (Pless et al., 2008), p53 (Huang et al., 2010), and Reptin (Lee et al., 2010) (Collins and Cheng, 2010; Shinkai and Tachibana, 2011). Among these genes, C/EBP-β has been shown to be involved in granulopoiesis in stress conditions (Hirai et al., 2006).

Previous studies also found that a nuclear factor kappa B (NF-κB) transcription factor RelB interacts with G9a. G9a dimethylates H3K9 in target gene, which further recruits heterochromatin protein 1 (HP1) and Dnmt3 and causes heterochromatin formation (Chen et al. 2009). Additionally, GLP can recognize and bind to methylated RelA, and lead to chromatin condensation at NF-kB-dependent target genes (Chang et al. 2011). Thus, UNC0638 treatment in

$CD34^+$ cells may negatively affect the NF-κB signaling pathway, as it was found that DNA binding activity of NF-κB and IKK was downregulated in megakaryocytes (Zhang et al. 2002).

Considering those possibilities, at this time, we cannot formally exclude non-histone G9a/GLP targets as being key regulators responsible for the megakaryocytic phenotypes. However, regardless of precise mechanism of UNC0638 function, this work should have important implications for clinical expansion of human megakaryocytes *in vitro*.

CHAPTER 5

IDENTIFICATION OF GENES GOVERNING LINEAGE COMMITMENT OF HUMAN COMMON MYELOID PROGENITOR CELLS BY SHRNA SCREENING

5.1 Create an shRNA library that can achieve satisfactory transfection efficiency and stable knockdown in $CD34^+$ cells

I first tested a number of lenti- and retro-viral vectors and found that a retroviral vector (MLP) (Fig. 5.1A), which utilizes a MSCV promoter, produce robust infection efficiencies and gene silencing, and outperforms lenti-based platforms in HSPCs (which appear to trigger an innate-immunity response that blocks silencing).

Our shRNA library contains ~ 8000 shRNAs, with an average of ~2 shRNAs per gene, targeting 390 E3-ubiquitin ligases, 784 kinases, and 1013 transcription factors (Paddison et al., 2004). shRNAs were cloned into MLP from pGIPZ. We have achieved ~ 10% transduction efficiency using concentrated MLP retrovirus in $CD34^+$ HSPCs. shRNAs against a control gene, PTEN, showed ~ 60% knockdown of gene expression in both $CD34^+$ and $CD34^-$ cells (Fig. 5.1B).

A

B

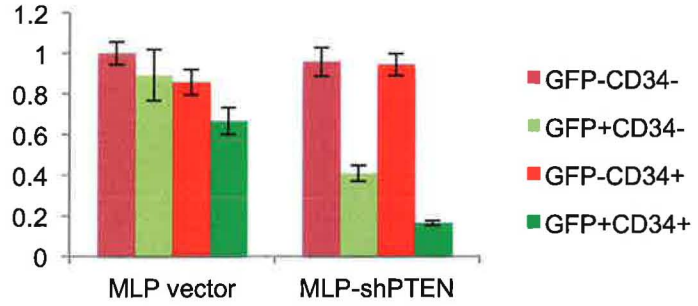

Figure 5.1. MSCV-LTRmiR30-PIG (MLP) based shRNA library. **(A)** Our shRNAs are designed based on the structure of an endogenous miRNA, miR-30. Pooled shRNA library is cloned into the XhoI and EcoRI sites of an MSCV-based retroviral vector (MLP). **(B)** MLP retrovirual vector facilitates RNAi in human $CD34^+$ HSPCs. Cells were infected with MLP retrovirus carrying a PTEN shRNA, sorted for GFP and $CD34^{+/-}$ 72 hours post-infection, and used for Q-PCR detection of PTEN expression in the four populations.

5.2 Conduct a screen with the shRNA library in CMPs

For the screen (Fig. 5.2), donor derived $CD34^+$ cells were thawed and cultured for 1 day in myeloid expansion medium and sorted for $CD34^+CD123^+CD45RA^-$ (CMP population). Next, sorted cells were infected with concentrated viral supernatants of pooled human MLP-shRNA library to produce ~ 1 million infected cells and allowed to outgrow for 4 days in myeloid expansion media. Transduction efficiency was kept low (~ 10%) to ensure only one shRNA per cell. 4 days post infection, ~ 10 million GFP^+ cells were sorted into four populations: $CD34^+CD123^+CD45RA^-$ (CMP), $CD34^+CD123^-CD45RA^-$ (MEP), $CD34^+CD123^-CD45RA^+$ (GMP), and $CD34^-$ (committed cells).

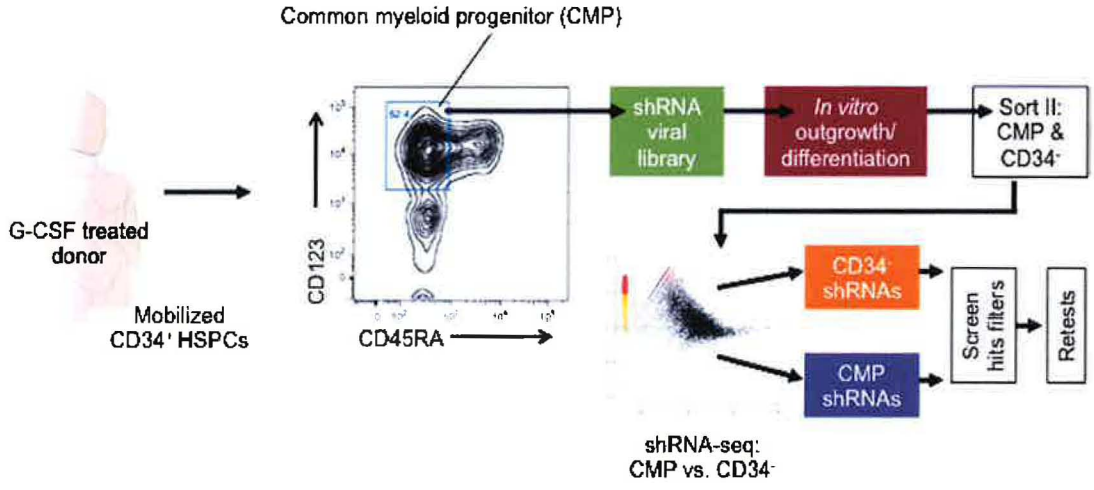

Figure 5.2. A screen for shRNAs promoting expansion or differentiation of HSPC-derived CMPs. 28 of the screen hits are expression QTLs for mouse HSC activity which >40 have published functions associated with hematopoiesis or leukemia.

5.3 Determine relative representations of shRNAs in $CD34^+$ CMPs vs. $CD34^-$ differentiated cells

For each population, shRNAs were amplified using half-shRNA PCR strategy (i.e. 5' vector primer + 3' miR30-shRNA loop primer) from genomic DNA representing ~ 2 million cells (~ 33 µg). Illumina sequencing adaptors were ligated onto purified shRNA PCR products (Illumina kit) and used for high-throughput sequencing-by-synthesis (HT-SBS) on an Illumina HiSeq 2000 sequencer (Genomics facility, FHCRC). The resulting reads (~ 40 million per replicate) were mapped onto a reference library containing library shRNA sequences and filtered to include only those with phred-based mapped quality of 37, representing about 79% of reads for each replicate. Mapped reads tallied and compared using two R/Bioconductor packages. edgeR, developed for RNA-seq analysis, and limma, developed for microarray analysis (Smyth 2005). Both comparisons subtract control from experimental replicated to calculate logFC and use the Benjamini-Hochberg FDR calculation to adjust p-vales for multiple comparisons.

We found ~ 322 shRNAs enriched in the $CD34^-$ (i.e. lineage committed cells) and ~ 290 shRNAs enriched in $CD34^+$ CMP population (LogFC>5, FDR<0.05). We further filtered these hits based on:

(1) Literature mining: hematopoietic/hematopoietic malignancy function (11% hits)

(2) Interactions with other screen hits—direct protein-protein only (9% hits)

(3) Enriched expression in human HSC, blood progenitor, and/or leukemia (> 5% hits)

(4) Mouse HSC eQTLs (Gerrits et al. 2008; Bystrykh et al. 2005) (5% hits)

The last category is worth noting. HSCs eQTLs were identified by De Haan and colleagues using a "genetical genomic". They mapped mouse QTLs associated with in HSC frequency and progenitor division rates (which were shown to be cell autonomous traits) from recombinant inbreed lines of two laboratory mouse strains (C57BL/6 and DBA/2) harboring heritable differences in these traits (Bystrykh et al. 2005). Next, gene expression levels in HSC and progenitor populations were examined from the recombinant inbred lines to find transcripts that co-vary with HSC QTLs (i.e. eQTLs). By this method, they were able to identify >500 HSC eQTLs and, thus, candidate genes and pathways involved in HSC turnover. However, they were not able to demonstrate requirement for eQTLs gene candidates. When we compare our screen hits with their eQTLs, 28 genes were directly in common. Among these, we have prioritized ones that also score by other metrics.

Based on these criteria, we found 15 hits and will examine their roles in promoting HSPC activity and/or hematopoietic lineage formation (Table 5.1).

Screen hits	shRNA phenotype	Mouse HSC eQTL	Screen hit protein/ gene interaction	Known hematopoietic phenotype	Predicted role in blood progenitors
CDH1	↓ CD34+	✓	-	HSC pol size	G1/S entry
EWSR1	↓ CD34+	✗	LRRC15	HSC quiescence	INK4A repression
GRIN2C	↓ CD34+	✓	-	Unknown	Glutamate signaling
GRIN2D	↓ CD34+	✓	-	Megakaryopoiesis	Glutamate signaling
NLK	↓ CD34+	✓	TCF7L2	MDS, AML	Cytokine signaling
NR0B1	↓ CD34+	✓	NR5A2 EWSR1	Unknown	Progenitor gene regulation
NR5A2	↓ CD34+	✓	NR0B1	Unknown	Progenitor gene regulation
PIK3CD	↓ CD34+	✓	RUNX1	AMkL, CLL	Survival
RBAK	↓ CD34+	✗	-	HSC expressed	E2F repression
TBL1X	↓ CD34+	✗	HDAC3 TBL1XR1	Unknown	Progenitor gene regulation
TBL1XR1	↓ CD34+	✗	TBL1X	Unknown	Progenitor gene regulation
EGR1	↑ CD34+	✗	-	HSC quiescence	Progenitor gene regulation
MS4A3	↑ CD34+	✗	-	HSC quiescence	G1/S entry
NUMB	↑ CD34+	✓	AAK1	HSC differentiation	Cytokine signaling
RNF138	↑ CD34+	✗	-	Unknown	Differentiation

Table 5.1. Selected candidate HSPC shRNA screen hits. ↓ $CD34^+$ means shRNAs enriched in $CD34^-$ cells; ↑ $CD34^+$ means shRNAs enriched in CMP.

5.4 Create a smaller pool of shRNAs for a secondary screening

Our normal procedure in validating an RNAi screen is to first crudely estimate true-false positive frequency by randomly testing 10-20 screen hits. From our experience performing RNAi screens in human cell lines, embryonic stem cells (Schaniel et al. 2009), neural stem cells and glioma stem cells (Ding et al. 2013), true positive validation frequencies range from 5%-50%. Given the expense of acquiring biological blood progenitor samples, we carefully analyzed screen hits in order to enrich for true positives.

For re-test, we first created a pool of 335 shRNAs, targeting 41 genes, whose shRNAs were over-represented in CMPs. These shRNAs were cherry-picked from our archive shRNA plates, and cloned into the MLP retroviral vector as a pool. The secondary screen will be conducted in the same way as the primary screen. qPCR will be performed to measure relative representation of shRNAs in $CD34^+$ CMP vs. $CD34^-$ differentiated cells. This rescreen will identify true/false positive hits.

5.5 Validate and characterize candidate commitment or self-renewal genes

Positive hits from the secondary screen will be tested by flow cytometry analysis of cell surface markers (e.g. CD34, CD90, CD123, CD45RA, CD41, CD15, CD235a) to determine knockdown effects of single genes on $CD34^+$ HSPCs. Further tests will also include CFU activity assays, long-term initiating cell (LTC-IC) assays, and *in vivo* in a canine transplantation model (on-going).

5.6 Discussion

This study will serve as a basis for other *in vitro* RNAi screens in normal and malignant blood stem cells derived from human donors and patients. If successful, we will identify novel genes and molecular pathways required for human HSPC activity, which, in turn, can be exploited by scientists and clinicians at the Hutch and elsewhere to facilitate *ex vivo* and *in vivo* manipulations of highly desirable human hematopoietic stem/progenitor cells.

However, we still need to verify that the screen knockdown phenotypes can translate to CFU and engraftment assays. Constitutive knockdown may block developmental pathways required for colony formation or successful engraftment. Another problem we have encountered is achieving reliable infection efficiency and durable gene silencing in human $CD34^+$ cells. This problem, along with access to source material, likely accounts for the lack of published RNAi screens in human and mouse HSPCs. After initial examination of our standard lenti- and retro-shRNA expression vector, we have found that an MSCV-retroviral-based system provided sustained knockdown and robust reporter gene expression in $CD34^+$ cells. Thus our initial screen was performed in this system. However, since this system only productively infects dividing cells, it is not ideal for assay quiescent or slow dividing stem cell populations. Therefore, we are also testing other lentiviral systems with alternative promoter, reporter and shRNA configurations, in $CD34^+$ cells.

Moreover, this screen will also serve as the basis for *in vivo* RNAi screens in canine model of HSPC transplantation. We have now completed construction of the dog shRNA library, named SHAGi (Short Hairpin Activated Gene Inhibition) dog library. First, as a proof of principle study, we transduced dog bone marrow cells with shRNAs targeting dog EPO receptor, and plated these cells in CFU assays. We found that cells transduced with EPO receptor shRNAs generated significantly less CFU-E than cells transduced with a control vector. We will further test the efficacy of this library and ultimately examine the stem cell activity *in vivo* in a canine transplantation model.

In addition, we have a ~ 16,000 human ORFeome library, which is also being replicated for cherry picking schemes. ORFs corresponding to ~ 100 screen hits chosen for shRNA retest, will be cherry-picked from this library, and rescreened in the same format. In this scheme, we seek to identify ORFs that show the opposite biological effect of their cognate shRNA; for these will be candidate genes that are "necessary and sufficient" for stem cell activity.

CHAPTER 6

DISCUSSION AND FUTURE DIRECTION

6.1 Discussion

Over 50 years of bone marrow transplantation (BMT) have proved that human hematopoiesis is supported by a population of multipotent HSCs, which are capable of self-replicating and generating progenies that can differentiate into various blood cell lineages throughout life. However, achieving a broader application of BMT with greater success is limited by our ability to control their cell fate decisions.

One challenge is that HSCs do not self-renewal *in vitro* and thus have very limited quantity for both clinical and research purposes. A lot of evidence suggests that the number of HSCs infused strongly correlates with post-transplantation outcomes (Dahlberg et al., 2011). Numerous approaches are under investigation to expand HSCs *in vitro*, including (1) mimicking the *in vivo* HSC niche, for example using HSC-supportive stromal cells (Goerner et al. 2000; Li et al. 2007), (2) novel cytokines, such as Angiopoietin-like 5 (Angptl5) and IGFBP2 (Zhang et al. 2008), (3) novel culture strategy (Csaszar et al. 2012), (4) genetic modification, such as overexpression of the homeobox gene HOXB4

(Antonchuk et al., 2002; Amsellem et al., 2003), and (5) epigenetic regulations (Milhem et al., 2004; Nishino et al., 2011). However, although many of tnem have reported *ex vivo* stem cell expansion, few, if any, actually involve expansion through true self-replication and retention of stem cell potential.

Another challenge is to direct the commitment of multipotent HSPCs into a particular lineage to treat lineage-specific cytopenia. For example, to induce produce and expand large number of autologous megakaryocytes *ex vivo* from HSPCs, which can then be infused into patients. This will help overcome thrombocytopenia post BMT and reduce the need for platelet transfusion. This requires greater insights into the molecular mechanisms that can enhance megakaryocytic lineage commitment from progenitor cells.

Our studies have found that treating human HSPCs with a small molecular inhibitor of G9a/GLP histone methyltransferases, UNC0638, promotes retention of primitive cell phenotypes *in vitro*, which is correlated with more stem cell activity *in vivo*. Moreover, UNC0638 treated HSPCs preferentially give rise to the megakaryocytic lineage over other myeloid lineages when they differentiate. Molecular studies found that UNC0638 treatment removes H3K9me2 marks throughout the genome to a similar level as in the primitive HSCs. However, the precious role of G9a/GLP and H3K9me2 in HSPC lineage commitment, and whether this megakaryocyte-specific phenotype is due to H3K9me2 or non-histone targets of G9a/GLP, need further investigations.

We also conducted an shRNA library screen in human HSPCs. This study will not only identify genes required for HSCP self-renewal and lineage

commitment but more importantly will serve as a basis for future library screening approaches in HSPCs (e.g. modifiers of UNC0638 expansion, human ORFeome library, miRNAs).

To better understand the complex regulatory network that governs HSPC fate determination, we are also studying other factors in human hematopoiesis, including DNA methylation, miRNAs, and chromatin structures.

6.2 DNA methylation profiling of human HSPCs

In this on-going study, we examined and compared DNA methylation status of at > 485,000 CpG sites throughout the genome of human HSC, MEP, GMP, megakaryocyte (Meg) and unfractionated $CD34^+$ cells treated or untreated with UNC0638. It covers 99% of RefSeq genes, with an average of 17 CpG sites per gene, and 96% of CpG islands. We found that DNA methylation status of different populations was clusterd by their lineages—MEP and Meg showed similar methylation patterns with more significant differences in the Meg population (Fig. 6.1A). We also compared UNC0638 treated $CD34^+$ cells with control DMSO treated $CD34^+$ cells but did not detect a significant difference. We also identified genes that were differentially methylated in different populations (Fig. 6.1B), and these patterns correlate with their known functions in hematopoiesis. For examples, CD34 is a cell surface maker of primitive HSPCs, and it is less methylated in the most primitive HSCs, and heavily methylated in differentiated Megs. On the other hand, Meg related genes GATA1, GATA2, and MPL (TPO receptor) had decreased DNA methylation in MEP and Meg

populations (Fig. 6.1B). It is interesting to note that DNA methylation level of DNMT3A itself was also increased as the cells differentiate into Megs (Fig. 6.1B).

A

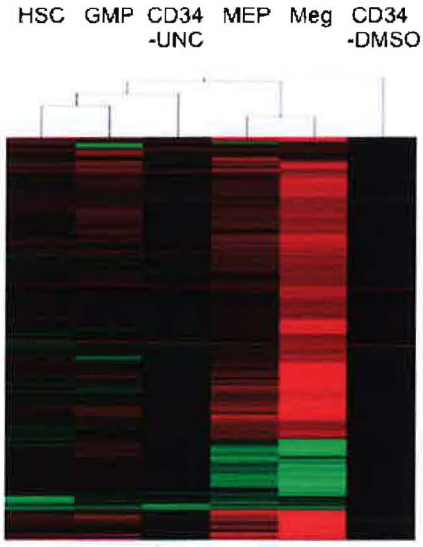

B

HSC	GMP	CD34-U	MEP	Meg	CD34-D	
0.89	1.40	1.00	1.21	2.21	1	CD34
1.05	1.11	0.98	0.60	0.48	1	GATA1
1.07	1.22	1.00	0.53	0.27	1	GATA1
0.53	3.21	0.90	1.22	0.58	1	GATA2
0.95	1.94	1.16	0.64	0.49	1	MPL
1.13	0.49	0.95	1.02	1.59	1	RUNX1
0.94	0.84	1.09	1.45	2.04	1	ITGA2B
1.00	1.12	1.09	1.79	2.78	1	DNMT3A
1.03	1.21	1.11	1.45	3.50	1	DNMT3A
1.02	1.85	0.79	3.09	5.73	1	PU.1

Figure 6.1. DNA methylation profiling. (A) Shown are probes that were 2-fold different between the CD34-DMSO control in at least one other sample. Red: more methylated compared to CD34-DMSO control; green: less methylated compared to CD34-DMSO control. (B) Sample genes with differential methylation status in different lineages.

Further analysis will include where the methylation marks are located (e.g. CGIs and shores), overlap of DNA methylation with other genomic elements (e.g. gene promoter, enhancer, SINE, LINE), gene set enrichment analysis. We have also done RNA-seq of the same populations, and will compare gene expression

level to DNA methylation level to determine if these two are negatively correlated as DNA methylation is believed to repress gene expression. These analyses will help us understand the role of DNA methylation in human hematopoiesis, and may identify novel genes involved in HSPC lineage commitment.

6.3 Role of miRNAs in human hematopoiesis

We also performed a miRNA sequencing, to examine their expression levels in human HSC, MEP, GMP, megakaryocyte (Meg) and unfractionated $CD34^+$ cells treated or untreated with UNC0638. We found a number of miRNAs that were differentially expressed in different cell populations (Fig. 6.2). Some of these miRNAs have known functions in the hematopoietic system. For example, miR-125b, which has higher expression in HSCs than immature progenitor cells and committed Megs, was found to expand the mouse HSCs when overexpressed (Ooi et al. 2010). miR-10a was also found to be higher expressed in the stem cell fraction (Bissels et al. 2011), which is consistent with our results.

One miRNA that showed dramatic change in GMP vs. MEP and Meg lineages is miR-486. It was also confirmed by qPCR array that miR-486 was significantly up-regulated in Meg and erythrocyte lineages, and was down-regulated in the GMP lineage. miR-486 was located within the last intron of a erythrocyte gene Ankyrin-1 on chromosome 8 (Small et al. 2010). It was also found to regulate the NF-κB signaling pathway (Song et al. 2012).

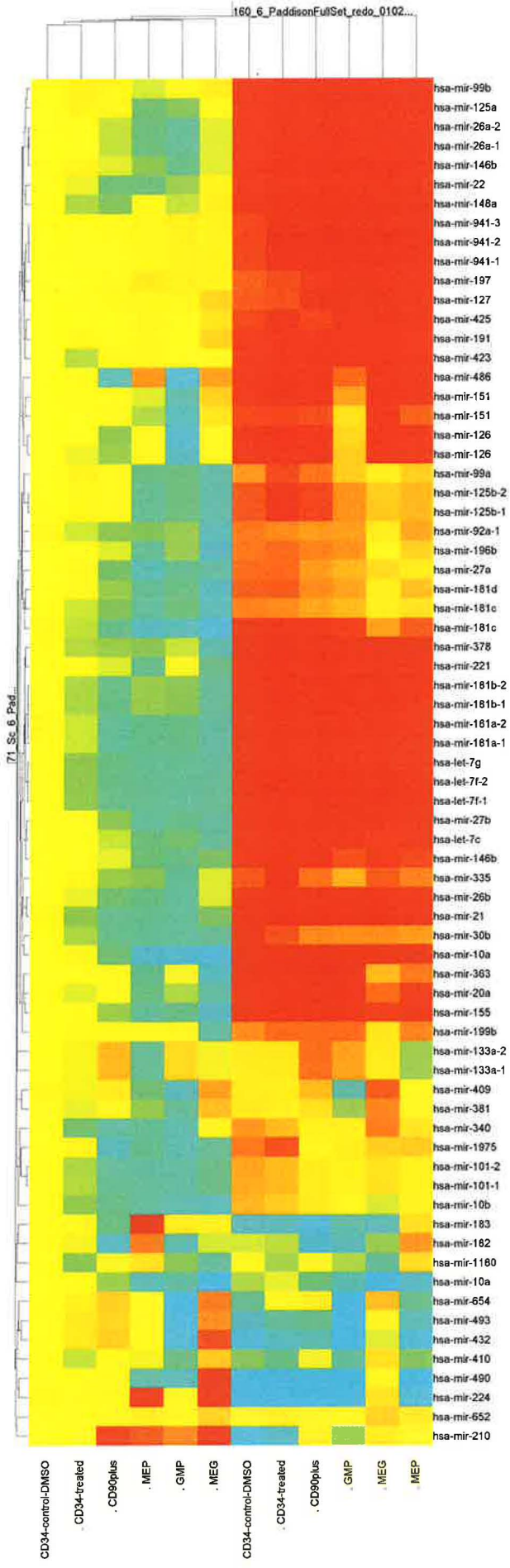

Figure 6.2. Heatmap of the top 71 differentially expressed miRNAs. The left 6 lanes of the map are relative levels of the miRNAs in the different samples compared to $CD34^{+}$-DMSO control cells. The right 6 lanes are absolute expression levels of expression of these miRNAs. Red: high expression, cyan: low expression. Expression levels were confirmed by miRNA qPCR arrays.

The roles of miR-486 and other interesting miRNAs in HSPC and megakaryocytic commitment will be further studied using miRNA mimics and antagomirs for transient expression/knockdown, and expression vectors and miRNA sponges for long-term effects. Flow cytometry and CFU assays will then be performed to examine cell phenotypes and functions.

6.4 Studying higher-order chromatin structure by FAIRE-seq and 3C

We have showed that HSPC differentiation is accompanied by a progressive increase of H3K9me2, and H3K9me2 marks in HSPC nuclei appear as "speckles" (Fig. 3.1 and Fig. 3.4). UNC0638 treatment largely removes the H3K9me2 mark throughout the genome and affects expression of multiple gene clusters (Fig. 3.5). These data suggest that H3K9me2 may facilitate formation/organization of higher-order chromatin structure in HSPCs. However, it is not clear that how chromatin structure and conformation change during lineage commitment, and whether they are altered by removal of H3K9me2.

To answer these questions, we first collaborated with Dr. Schones's lab at City of Hope to perform a FAIRE-seq (formaldehyde-assisted isolation of regulatory elements coupled with high-throughput sequencing, Fig. 6.3) (Giresi and Lieb 2009; Auerbach et al. 2009; Gaulton et al. 2010; Song et al. 2011) on UNC0638 treated or untreated $CD34^+$ cells to map open chromatin regions in these cells. In this experiment, $CD34^+$ cells were treated with UNC0638 or DMSO control for 48 hours, and crosslinked with formaldehyde. Sonication was then performed on cell lysates, and DNA was extracted using phenol-chloroform. DNA

fragments of ~ 100-350 bp were selected and sequenced. It was found that DNA regions identified by FAIRE-seq are associated with open chromatin structure, and overlap with TSS, H3K4me3, and CGIs (Auerbach et al. 2009). Therefore, using this method, we can test whether removal of the repressive marker H3K9me2 opens the chromatin, and if so, on what locations. If this method proves applicable in our system, we can then use it to study changes in chromatin structure as the HSPCs undergo lineage specification.

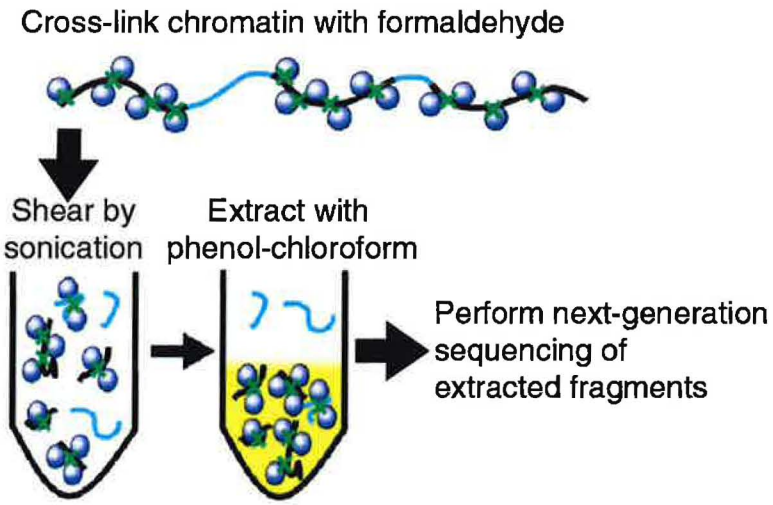

Figure 6.3. FAIRE-seq procedure.

(Figure adapted from Gaulton et al. 2010)

We will also utilize a chromosome conformation capture (3C) technique (Dekker et al. 2002) to study the organization of chromosomes during HSPC commitment. It is suggested that chromosomal activities are related to their spatial conformations. For example, it was found that gene-rich regions are

relatively more distant from the nuclear membrane than gene-poor regions (Cremer et al. 2003). It was also suggested that H3K9me2 might play a role in chromosome reposition during ESC differentiation by interacting with the nuclear lamina (Wen et al. 2009). Using 3C, we will be able to analyze the spatial organization of chromosomes in HSPC and lineage committed cells, and whether it is regulated by H3K9me2.

These studies will reveal genetic and epigenetic factors driving HSPC commitment decisions. Ultimately our goal is to facilitate *ex vivo* and *in vivo* manipulations of human HSPCs to control lineage commitment.

REFERENCES

Akashi K, He X, Chen J, Iwasaki H, Niu C, Steenhard B, Zhang J, Haug J, Li L. 2003. Transcriptional accessibility for genes of multiple tissues and hematopoietic lineages is hierarchically controlled during early hematopoiesis. *Blood* **101**: 383-389.

Akashi K, Traver D, Miyamoto T, Weissman IL. 2000. A clonogenic common myeloid progenitor that gives rise to all myeloid lineages. *Nature* **404**: 193-197.

Akinsheye I, Alsultan A, Solovieff N, Ngo D, Baldwin CT, Sebastiani P, Chui DH, Steinberg MH. 2011. Fetal hemoglobin in sickle cell anemia. *Blood* **118**: 19-27.

Ali N, Karlsson C, Aspling M, Hu G, Hacohen N, Scadden DT, Larsson J. 2009. Forward RNAi screens in primary human hematopoietic stem/progenitor cells. *Blood* **113**: 3690-3695.

Allis CD, Jenuwein T, Reinberg D, Caparros ML. 2007. Epigenetics. *New York: Cold Spring Harbor Laboratory Press.*

Amsellem S, Pflumio F, Bardinet D, Izac B, Charneau P, Romeo PH, Dubart-Kupperschmitt A, Fichelson S. 2003. Ex vivo expansion of human hematopoietic stem cells by direct delivery of the HOXB4 homeoprotein. *Nat Med* **9**: 1423-1427.

Antonchuk J, Sauvageau G, Humphries RK. 2002. *HOXB4*-induced expansion in adult hematopoietic stem cells ex vivo. *Cell* **109**: 39-45.

Attema JL, Papathanasiou P, Forsberg EC, Xu J, Smale ST, Weissman IL. 2007. Epigenetic characterization of hematopoietic stem cell differentiation using miniChIP and bisulfite sequencing analysis. *Proc Natl Acad Sci USA* **104**: 12371-12376.

Auerbach RK, Euskirchen G, Rozowsky J, Lamarre-Vincent N, Moqtaderi Z, Lefrançois P, Struhl K, Gerstein M, Snyder M. 2009. Mapping accessible chromatin regions using Sono-Seq. *Proc Natl Acad Sci* **106**: 14926-14931.

Aza-Blanc P, Cooper CL, Wagner K, Batalov S, Deveraux QL, Cooke MP. 2003. Identification of modulators of TRAIL-induced apoptosis via RNAi-based phenotypic screening. *Mol Cell* **12**: 627-637.

Bannister AJ, Schneider R, Kouzarides T. 2002. Histone methylation: dynamic or static? *Cell* **109**: 801-806.

Barroga CF. 2008. Thrombopoietin regulates c-Myb expression by modulating micro RNA 150 expression. *Exp Hematol* **36**: 1585–1592.

Bartley TD, Bogenberger J, Hunt P, Li YS, Lu HS, Martin F, Chang MS, Samal B, Nichol JL, Swift S, et al. 1994. Identification and cloning of a megakaryocyte growth and development factor that is a ligand for the cytokine receptor Mpl. *Cell* **77**: 1117-1124.

Bartz SR, Zhang Z, Burchard J, Imakura M, Martin M, Palmieri A, Needham R, Guo J, Gordon M, Chung N, et al. 2006. Small interfering RNA screens reveal enhanced cisplatin cytotoxicity in tumor cells having both BRCA network and TP53 disruptions. *Mol Cell Biol* **26**: 9377-9386.

Bauer DE, Orkin SH. 2011. Update on fetal hemoglobin gene regulation in hemoglobinopathies. *Curr Opin Pediatr* **23**: 1-8.

Baum CM, Weissman IL, Tsukamoto AS, Buckle AM, Peault B. 1992. Isolation of a candidate human hematopoietic stem-cell population. *Proc Natl Acad Sci USA* **89**: 2804-2808.

Beerman I, Bock C, Garrison BS, Smith ZD, Gu H, Meissner A, Rossi DJ. 2013. Proliferation-Dependent Alterations of the DNA Methylation Landscape Underlie Hematopoietic Stem Cell Aging. *Cell Stem Cell* pii: S1934-5909(13)00020-9.

Ben-Ami O, Pencovich N, Lotem J, Levanon D, Groner Y. 2009. A regulatory interplay between miR-27a and Runx1 during megakaryopoiesis. *Proc Natl Acad*

Sci **106**: 238–243.

Berns K, Hijmans EM, Mullenders J, Brummelkamp TR, Velds A, Heimerikx M, Kerkhoven RM, Madiredjo M, Nijkamp W, Weigelt B, et al. 2004. A large-scale RNAi screen in human cells identifies new components of the p53 pathway. *Nature* **428**: 431-437.

Bhutani N, Burns DM, Blau HM. 2011. DNA demethylation dynamics. *Cell* **146**: 866-872.

Birkmann J, Oez S, Smetak M, Kaiser G, Kappauf H, Gallmeier WM. (1997). Effects of recombinant human thrombopoietin alone and in combination with erythropoietin and early-acting cytokines on human mobilized purified CD34+ progenitor cells cultured in serum-depleted medium. Stem Cells *15*, 18-32.

Bissels U, Bosio A, Wagner W. 2012. MicroRNAs are shaping the hematopoietic landscape. *Haematologica* **97**: 160-167.

Boitano AE, Wang J, Romeo R, Bouchez LC, Parker AE, Sutton SE, Walker JR, Flaveny CA, Perdew GH, Denison MS, et al. 2010. Aryl Hydrocarbon Receptor Antagonists Promote the Expansion of Human Hematopoietic Stem Cells. *Science* **329**: 1345-1348.

Bystrykh L, Weersing E, Dontje B, Sutton S, Pletcher MT, Wiltshire T, Su AI, Vellenga E, Wang J, Manly KF, et al. 2005. Uncovering regulatory pathways that affect hematopoietic stem cell function using 'genetical genomics'. *Nat Genet* **37**: 225-232.

Calvanese V, Fernández AF, Urdinguio RG, Suárez-Alvarez B, Mangas C, Pérez-García V, Bueno C, Montes R, Ramos-Mejía V, Martínez-Camblor P, et al. 2012. A promoter DNA demethylation landscape of human hematopoietic differentiation. *Nucleic Acids Res* **40**: 116-131.

Challen GA, Sun D, Jeong M, Luo M, Jelinek J, Berg JS, Bock C, Vasanthakumar A, Gu H, Xi Y et al. 2011. Dnmt3a is essential for hematopoietic stem cell differentiation. *Nat Genet* **44**: 23-31.

Chang Y, Levy D, Horton JR, Peng J, Zhang X, Gozani O, Cheng X. 2011. Structural basis of SETD6-mediated regulation of the NF-kB network via methyl-lysine signaling. *Nucleic Acids Res* **39**: 6380-6389.

Chaturvedi CP, Hosey AM, Palii C, Perez-Iratxeta C, Nakatani Y, Ranish JA, Dilworth FJ, Brand M. 2009. Dual role for the methyltransferase G9a in the maintenance of beta-globin gene transcription in adult erythroid cells. *Proc Natl Acad Sci USA* **106**: 18303-18308.

Chen TW, Yao CL, Chu IM, Chuang TL, Hsieh TB, Hwang SM. 2009. Large generation of megakaryocytes from serum-free expanded human CD34+ cells. *Biochem Biophys Res Commun* **378**: 112-117.

Chen X, El Gazzar M, Yoza BK, McCall CE. 2009. The NF-kappaB factor RelB and histone H3 lysine methyltransferase G9a directly interact to generate epigenetic silencing in endotoxin tolerance. *J Biol Chem* **284**: 27857-27865.

Chen X, Skutt-Kakaria K, Davison J, Ou Y, Choi E, Malik P, Loeb K, Wood B, Georges G, Torok-Storb B, Paddison JP. 2012. G9a/GLP-dependent histone H3K9me2 patterning during human hematopoietic stem cell lineage commitment. *Genes and Development* **26**: 2499-2511.

Cheng T, Rodrigues N, Shen H, Yang Y, Dombkowski D, Sykes M, Scadden DT. (2000). Hematopoietic stem cell quiescence maintained by p21cip1/waf1. Science *287*, 1804-1808.

Christensen JL, Weissman IL. 2001. Flk-2 is a marker in hematopoietic stem cell differentiation: a simple method to isolate long-term stem cells. *Proc Natl Acad Sci* **98**: 14541-14546.

Christophersen NS, Helin K. 2010. Epigenetic control of embryonic stem cell fate. *J Exp Med* **207**: 2287-2295.

Cocozza S, Akhtar MM, Miele G, Monticelli A. 2011. CpG islands undermethylation in human genomic regions under selective pressure. *PLoS One*. **6**: e23156.

Collins R, Cheng X. 2010. A case study in cross-talk: the histone lysine methyltransferases G9a and GLP. *Nucleic Acids Res* **38**: 3503-3511.

Collins RE, Northrop JP, Horton JR, Lee DY, Zhang X, Stallcup MR, Cheng X. 2008. The ankyrin repeats of G9a and GLP histone methyltransferases are mono- and dimethyllysine binding modules. *Nat Struct Mol Biol* **15**: 245-250.

Copelan EA. 2006. Hematopoietic stem-cell transplantation. *N Engl J Med* **354**: 1813-26.

Cremer M, Küpper K, Wagler B, Wizelman L, von Hase J, Weiland Y, Kreja L, Diebold J, Speicher MR, Cremer T. 2003. Inheritance of gene density-related higher order chromatin arrangements in normal and tumor cell nuclei. *J Cell Biol* **162**: 809–820.

Csaszar E, Kirouac DC, Yu M, Wang W, Qiao W, Cooke MP, Boitano AE, Ito C, Zandstra PW. 2012. Rapid expansion of hHSCs by automated control of inhibitory feed back signaling. *Cell Stem Cell* **10**: 218–229.

Cui K, Zang C, Roh TY, Schones DE, Childs RW, Peng W, Zhao K. 2009. Chromatin Signatures in Multipotent Human Hematopoietic Stem Cells Indicate the Fate of Bivalent Genes during Differentiation. *Cell Stem Cell* **4**: 80-93.

Dahlberg A, Delaney C, Bernstein ID. 2011. Ex vivo expansion of human hematopoietic stem and progenitor cells. *Blood* **117**: 6083-6090.

Deaton AM, Bird A. 2011. CpG islands and the regulation of transcription. *Genes Dev* **25**: 1010-1022.

Dekker J, Rippe K, Dekker M, Kleckner N. 2002. Capturing chromosome conformation. *Science* **295**: 1306-1311.

Delaney C, Heimfeld S, Brashem-Stein C, Voorhies H, Manger RL, Bernstein ID. 2010. Notch-mediated expansion of human cord blood progenitor cells capable of rapid myeloid reconstitution. *Nat Med* **16**: 232-236.

Ding Y, Hubert CG, Herman J, Corrin P, Toledo CM, Skutt-Kakaria K, Vazquez J, Basom R, Zhang B, Risler JK, et al. 2013. Cancer-Specific requirement for BUB1B/BUBR1 in human brain tumor isolates and genetically transformed cells. *Cancer Discov* **3**: 198-211.

Doulatov S, Notta F, Laurenti E, Dick JE. 2012. Hematopoiesis: a human perspective. *Cell Stem Cell* **10**: 120-136.

Eichler EE, Hoffman SM, Adamson AA, Gordon LA, McCready P, Lamerdin JE, Mohrenweiser HW. 1998. Complex beta-satellite repeat structures and the expansion of the zinc finger gene cluster in 19p12. *Genome Res* **8**: 791-808.

Ema H, Sudo K, Seita J, Matsubara A, Morita Y, Osawa M, Takatsu K, Takaki S, Nakauchi H. 2005. Quantification of self-renewal capacity in single hematopoietic stem cells from normal and Lnk-deficient mice. *Dev Cell* **8**: 907-914.

Elbashir SM, Harborth J, Lendeckel W, Yalcin A, Weber K, Tuschl T. 2001. Duplexes of 21-nucleotide RNAs mediate RNA interference in cultured mammalian cells. *Nature* **411**: 494-498.

Estève PO, Chin HG, Smallwood A, Feehery GR, Gangisetty O, Karpf AR, Carey MF, Pradhan S. 2006. Direct interaction between DNMT1 and G9a coordinates DNA and histone methylation during replication. *Genes Dev* **20**: 3089-3103.

Feldman N, Gerson A, Fang J, Li E, Zhang Y, Shinkai Y, Cedar H, Bergman Y. 2006. G9a-mediated irreversible epigenetic inactivation of Oct-3/4 during early embryogenesis. *Nat Cell Biol* **8**: 188-194.

Fire A, Xu S, Montgomery MK, Kostas SA, Driver SE, Mello CC. 1998. Potent and specific genetic interference by double-stranded RNA in Caenorhabditis elegans. *Nature* **391**: 806–811.

Friedman AD. 2007. Transcriptional control of granulocyte and monocyte development. *Oncogene* **26**: 6816-6828.

Fuchs E, Tumbar T, Guasch G. 2004. Socializing with the Neighbors: Stem Cells and Their Niche. *Cell* **116**: 769–778.

Gandhi MJ, Drachman JG, Reems JA, Thorning D, Lannutti BJ. 2005. A novel strategy for generating platelet-like fragments from megakaryocytic cell lines and human progenitor cells. *Blood Cells Mol Dis* **35**: 70-73.

Gardiner-Garden M, Frommer M. 1987. CpG islands in vertebrate genomes. *J Mol Biol* **196**: 261-282.

Gaspar-Maia A, Alajem A, Meshorer E, Ramalho-Santos M. 2011. Open chromatin in pluripotency and reprogramming. *Nat Rev Mol Cell Biol* **12**: 36-47.

Gaulton KJ, Nammo T, Pasquali L, Simon JM, Giresi PG, Fogarty MP, Panhuis TM, Mieczkowski P, Secchi A, Bosco D, et al. 2010. A map of open chromatin in human pancreatic islets. *Nat Genet* **42**: 255-259.

Georgantas RW 3rd, Hildreth R, Morisot S, Alder J, Liu CG, Heimfeld S, Calin GA, Croce CM, Civin CI. 2007. CD34+ hematopoietic stem-progenitor cell microRNA expression and function: A circuit diagram of differentiation control. *Proc Natl Acad Sci* **104**: 2750–2755.

Georges GE, Lesnikov V, Baran SW, Aragon A, Lesnikova M, Jordan R, Laura Yang YJ, Yunusov MY, Zellmer E, Heimfeld S, et al. 2010. A preclinical model of double- versus single-unit unrelated cord blood transplantation. *Biol Blood Marrow Transplant* **16**: 1090-1098.

Gerrits A, Dykstra B, Otten M, Bystrykh L, de Haan G. 2008. Combining transcriptional profiling and genetic linkage analysis to uncover gene networks operating in hematopoietic stem cells and their progeny. *Immunogenetics* **60**: 411-422.

Gieger C, Radhakrishnan A, Cvejic A, Tang W, Porcu E, Pistis G, Serbanovic-Canic J, Elling U, Goodall AH, Labrune Y, et al. 2011. New gene functions in megakaryopoiesis and platelet formation. *Nature* **480**: 201-208.

Ginder GD, Gnanapragasam MN, Mian OY. 2008. The role of the epigenetic signal, DNA methylation, in gene regulation during erythroid development. *Curr Top Dev Biol* **82**: 85-116.

Giresi PG, Lieb JD. 2009. Isolation of active regulatory elements from eukaryotic chromatin using FAIRE (Formaldehyde Assisted Isolation of Regulatory Elements). *Methods* **48**: 233-239.

Graf L, Heimfeld S, Torok-Storb B. 2001. Comparison of gene expression in CD34+ cells from bone marrow and G-CSF-mobilized peripheral blood by high-densiity oligonucleotide array analysis. *Biol Blood Marrow Transplant* **7**: 486-494.

Graf L, Iwata M, Torok-Storb B. 2002. Gene expression profiling of the functionally distinct human bone marrow stromal cell lines HS-5 and HS-27a. *Blood* **100**: 1509-1511.

Greenbaum AM, Link DC. 2010. Mechanisms of G-CSF-mediated hematopoietic stem and progenitor mobilization. *Leukemia* **16**: 1-7.

Goerner M, Roecklein B, Torok-Storb B, Heimfeld S, Kiem HP. 2000. Expansion and transduction of nonenriched human cord blood cells using HS-5 conditioned medium and FLT3-L. *J Hematother Stem Cell Res* **9**: 759-765.

Gomes I, Sharma TT, Edassery S, Fulton N, Mar BG, Westbrook CA. 2002. Novel transcription factors in human CD34 antigen-positive hematopoietic cells. *Blood* **100**: 107-119.

Goodnough LT, Shander A, Brecher ME. 2003. Transfusion medicine: looking to the future. Lancet 361: 161-169.

Gutiérrez L, Tsukamoto S, Suzuki M, Yamamoto-Mukai H, Yamamoto M, Philipsen S, Ohneda K. 2008. Ablation of Gata1 in adult mice results in aplastic crisis, revealing its essential role in steady-state and stress erythropoiesis. *Blood* **111**: 4375-4385.

Gyory I, Wu J, Fejér G, Seto E, Wright KL. 2004. PRDI-BF1 recruits the histone H3 methyltransferase G9a in transcriptional silencing. *Nat Immunol* **5**: 299-308.

Hannon GJ. 2002. RNA interference. *Nature* **418**: 244-251.

Hanson BA. 2011. HiveR: 2D and 3D Hive Plots for RR package 0.2-1

He L, Hannon GJ. 2004. MicroRNA: Small RNAs with a big role in gene regulation. *Nat Rev Genet* **5**: 522-531.

Hirai H, Zhang P, Dayaram T, Hetherington CJ, Mizuno S, Imanishi J, Akashi K, Tenen DG. 2006. C/EBPbeta is required for 'emergency' granulopoiesis. *Nat Immunol* **7**: 732-739.

Hodges E, Molaro A, Dos Santos CO, Thekkat P, Song Q, Uren PJ, Park J, Butler J, Rafii S, McCombie WR, et al. 2011. Directional DNA methylation changes and complex intermediate states accompany lineage specificity in the adult hematopoietic compartment. *Mol Cell* **44**: 17-28.

Hope KJ, Cellot S, Ting SB, MacRae T, Mayotte N, Iscove NN, Sauvageau G. 2010. An RNAi screen identifies Msi2 and Prox1 as having opposite roles in the regulation of hematopoietic stem cell activity. *Cell Stem Cell* **7**: 101-113.

Hu M, Krause D, Greaves M, Sharkis S, Dexter M, Heyworth C, Enver T. 1997. Multilineage gene expression precedes commitment in the hemopoietic system. *Genes Dev* **11**: 774-785.

Huang J, Dorsey J, Chuikov S, Pe´rez-Burgos L, Zhang X, Jenuwein T, Reinberg D, Berger SL. 2010. G9a and Glp methylate lysine 373 in the tumor suppressor p53. *J Biol Chem* **285**: 9636–9641.

Ikegami K, Iwatani M, Suzuki M, Tachibana M, Shinkai Y, Tanaka S, Greally JM, Yagi S, Hattori N, Shiota K. 2007. Genome-wide and locus-specific DNA hypomethylation in G9a deficient mouse embryonic stem cells. *Genes Cells* **12**: 1-11.

Ivanova NB. 2002. A stem cell molecular signature. *Science* **298**: 601-604.

Johnson AD, Yanek LR, Chen MH, Faraday N, Larson MG, Tofler G, Lin SJ, Kraja AT, Province MA, Yang Q, et al. 2010. Genome-wide meta-analyses

identifies seven loci associated with platelet aggregation in response to agonists. *Nat Genet* **42**: 608-613.

Kim JK, Estève PO, Jacobsen SE, Pradhan S. 2009. UHRF1 binds G9a and participates in p21 transcriptional regulation in mammalian cells. *Nucleic Acids Res* **37**: 493-505.

Kirito K, Fox N, Kaushansky K. 2004. Thrombopoietin Induces HOXA9 Nuclear Transport in Immature Hematopoietic Cells: Potential Mechanism by Which the Hormone Favorably Affects Hematopoietic Stem Cells. *Mol Cell Biol* **24**: 6751–6762.

Kittler R, Putz G, Pelletier L, Poser I, Heninger AK, Drechsel D, Fischer S, Konstantinova I, Habermann B, Grabner H, et al. 2004. An endoribonuclease-prepared siRNA screen in human cells identifies genes essential for cell division. *Nature* **432**: 1036-1040.

Klusmann JH, Li Z, Böhmer K, Maroz A, Koch ML, Emmrich S, Godinho FJ, Orkin SH, Reinhardt D. 2010. miR-125b-2 is a potential oncomiR on human chromosome 21 in megakaryoblastic leukemia. *Genes Dev* **24**: 478-490.

Kolasinska-Zwierz P, Down T, Latorre I, Liu, T., Liu, X.S., Ahringer, J. 2009. Differential chromatin marking of introns and expressed exons by H3K36me3. *Nat Genet* **41**: 376-381.

Kondo M, Scherer DC, King AG, Manz MG, Weissman IL. 2001. Lymphocyte development from hematopoietic stem cells. *Curr Opin Genet Dev* **11**: 520-526.

Kubicek S, O'Sullivan RJ, August EM, Hickey ER, Zhang Q, Teodoro ML, Rea S, Mechtler K, Kowalski JA, Homon CA, et al. 2007. Reversal of H3K9me2 by a small-molecule inhibitor for the G9a histone methyltransferase. *Mol Cell* **25**: 473-481.

Kumano K, Chiba S, Shimizu K, Yamagata T, Hosoya N, Saito T, Takahashi T, Hamada Y, Hirai H. 2001. Notch1 inhibits differentiation of hematopoietic cells by sustaining GATA-2 expression. *Blood* **98**: 3283-3289.

Lannutti BJ, Blake N, Gandhi MJ, Reems JA, Drachman JG. 2005. Induction of polyploidization in leukemic cell lines and primary bone marrow by Src kinase inhibitor SU6656. *Blood* **105**: 3875-2878.

Laslo P, Pongubala JM, Lancki DW, Singh H. 2008. Gene regulatory networks directing myeloid and lymphoid cell fates within the immune system. *Semin Immunol* **20**: 228-235.

Laslo P, Spooner CJ, Warmflash A, Lancki DW, Lee HJ, Sciammas R, Gantner BN, Dinner AR, Singh H. Multilineage transcriptional priming and determination of alternate hematopoietic cell fates. *Cell* **126**, 755-766 (2006)

Lee JS, Kim Y, Kim IS, Kim B, Choi HJ, Lee JM, Shin HJ, Kim JH, Kim JY, Seo SB, et al. 2010. Negative regulation of hypoxic responses via induced Reptin methylation. *Mol Cell* **39**: 71–85.

Li N, Feugier P, Serrurrier B, Latger-Cannard V, Lesesve JF, Stoltz JF, Eljaafari A. 2007. Human mesenchymal stem cells improve ex vivo expansion of adult human CD34+ peripheral blood progenitor cells and decrease their allostimulatory capacity. *Exp Hematol* **35**: 507-515.

Litt MD, Simpson M, Gaszner M, Allis CD, Felsenfeld G. 2001. Correlation between histone lysine methylation and developmental changes at the chicken beta-globin locus. *Science* **293**: 2453-2455.

Liu B, Ohishi K, Yamamura K, Suzuki K, Monma F, Ino K, Nishii K, Masuya M, Sekine T, Heike Y, et al. 2010. A potential activity of valproic acid in the stimulation of interleukin-3-mediated megakaryopoiesis and erythropoiesis. *Exp Hematol* **38**: 685-695.

Luis TC, Weerkamp F, Naber BA, Baert MR, de Haas EF, Nikolic T, Heuvelmans S, De Krijger RR, van Dongen JJ, Staal FJ. 2009. Wnt3a dediciency irreversibly impairs hematopoietic stem cell self-renewal and leads to defects in progenitor cell differentiation. *Blood* **15**: 546-554.

MacKeigan JP, Murphy LO, Blenis J. 2005. Sensitized RNAi screen of human kinases and phosphatases identifies new regulators of apoptosis and chemoresistance. *Nat Cell Biol* **7**: 591-600.

Majeti R, Park CY, Weissman IL 2007. Identification of a hierarchy of multipotent hematopoietic progenitors in human cord blood. *Cell Stem Cell* **1**: 635-645.

Malik S, Bhaumik SR. 2010. Mixed lineage leukemia: histone H3 lysine 4 methyltransferases from yeast to human. *FEBS J* **277**: 1805-1821.

Månsson R, Hultquist A, Luc S, Yang L, Anderson K, Kharazi S, Al-Hashmi S, Liuba K, Thorén L, Adolfsson J, et al. 2007. Molecular evidence for hierarchical transcriptional lineage priming in fetal and adult stem cells and multipotent progenitors. *Immunity* **26**: 407-419.

Manz MG, Miyamoto T, Akashi K, Weissman IL. 2002. Prospective isolation of human clonogenic common myeloid progenitors. *Proc Natl Acad Sci USA* **99**: 11872-11877.

Meissner A. 2010. Epigenetic modifications in pluripotent and differentiated cells. *Nat Biotechnol* **28**: 1079-1088.

Milhem M, Mahmud N, Lavelle D, Araki H, DeSimone J, Saunthararajah Y, Hoffman R. 2004. Modification of hematopoietic stem cell fate by 5aza 2'deoxycytidine and trichostatin A. *Blood* **103**: 4102-4110.

Miyamoto T, Iwasaki H, Reizis B, Ye M, Graf T, Weissman IL, Akashi K. 2002. Myeloid or lymphoid promiscuity as a critical step in hematopoietic lineage commitment. *Dev Cell* **3**: 137-147.

Morrison SJ, Weissman IL.1994. The long-term repopulating subset of hematopoietic stem cells is deterministic and isolatable by phenotype. *Immunity* **1**: 661-673.

Napoli C, Lemieux C, Jorgensen R. 1990. Introduction of a chimeric chalcone synthetase gene in Petunia results in reversible cosuppression of homologous genes in trans. *Plant Cell* **2**: 279–289.

Nash RA, Gooley T, Davis C, Appelbaum FR. 1996. The problem of thrombocytopenia after hematopoietic stem cell transplantation. *Oncologist* **1**: 371-380.

Ng CE, Yokomizo T, Yamashita N, Cirovic B, Jin H, Wen Z, Ito Y, Osato M. 2010. A Runx1 intronic enhancer marks hemogenic endothelial cells and hematopoietic stem cells. *Stem Cell* **28**: 1869-181.

Nishino T, Wang C, Mochizuki-Kashio M, Osawa M, Nakauchi H, Iwama A. 2011. Ex vivo expansion of human hematopoietic stem cells by garcinol, a potent inhibitor of histone acetyltransferase. *PLoS One* **6**: e24298.

Noma K, Allis CD, Grewal SI. 2001. Transitions in distinct histone H3 methylation patterns at the heterochromatin domain boundaries. *Science* **293**: 1150-1155.

North TE, de Bruijn MF, Stacy T, Talebian L, Lind E, Robin C, Binder M, Dzierzak E, Speck NA. 2002. Runx1 expression marks long-term repopulating hematopoietic stem cells in the midgestation mouse embryo. *Immunity* **16**: 661-672.

Notta F, Doulatov S, Laurenti E, Poeppl A, Jurisica I, Dick JE. 2011. Isolation of single human hematopoietic stem cells capable of long-term multilineage engraftment. *Science* **333**: 218-221.

Novershtern N, Subramanian A, Lawton LN, Mak RH, Haining WN, McConkey ME, Habib N, Yosef N, Chang CY, Shay T, et al. 2011. Densely interconnected transcriptional circuits control cell states in human hematopoiesis. *Cell* **144**: 296-309.

O'Connell RM, Chaudhuri AA, Rao DS, Gibson WS, Balazs AB, Baltimore D. 2010. MicroRNAs enriched in hematopoietic stem cells differentially regulate long-term hematopoietic output. *Proc Natl Acad Sci* **107**: 14235-14240.

O'Geen H, Echipare L, Farnham PJ. 2011. Using ChIP-seq technology to generate high-resolution profiles of histone modifications. *Methods Mol Biol* **791**: 265-286.

Ohishi K, Varnum-Finney B, Bernstein ID. 2002. Delta-1 enhances marrow and thymus repopulating ability of human CD34(+)CD38(-) cord blood cells. *J Clin Invest* **110**: 1165-1174.

Ooi AG, Sahoo D, Adorno M, Wang Y, Weissman IL, Park CY. 2010. MicroRNA-125b expands hematopoietic stem cells and enriches for the lymphoid-balanced and lymphoid-biased subsets. *Proc Natl Acad Sci* **107**: 21505-21510.

Orkin SH, Zon LI. (2008). Hematopoiesis: an evolving paradigm for stem cell biology. *Cell* **132**: 631-644.

Ostrander EA, Giniger E. 1997. Semper fidelis: what man's best friend can teach us about human biology and disease. *Am J Hum Genet* **61**: 475-480.

Paddison PJ, Hannon GJ. 2002. RNA interference: the new somatic cell genetics? *Cancer Cell* **2**: 17-23.

Paddison PJ, Silva JM, Conklin DS, Schlabach M, Li M, Aruleba S, Balija V, O'Shaughnessy A, Gnoj L, Scobie K, et al. 2004. A resource for large-scale RNA-interference-based screens in mammals. *Nature* **428**: 427-431.

Patel SR, Hartwig JH, Italiano JE Jr. 2005. The biogenesis of platelets from megakaryocyte proplatelets. *J Clin Invest* **115**: 3348-3354.

Perry JM, Li L. 2007. Disrupting the stem cell niche: good seeds in bad soil. *Cell* **129**: 1045-1047.

Peters AH, Kubicek S, Mechtler K, O'Sullivan RJ, Derijck AA, Perez-Burgos L, Kohlmaier A, Opravil S, Tachibana M, Shinkai Y, et al. 2003. Partitioning and plasticity of repressive histone methylation states in mammalian chromatin. *Mol Cell* **12**: 1577-1589.

Pless O, Kowenz-Leutz E, Knoblich M, Lausen J, Beyermann M, Walsh MJ, Leutz A. 2008. G9a-mediated lysine methylation alters the function of CCAAT/enhancer-binding protein-beta. *J Biol Chem* **283**: 26357–26363.

Rao DD, Vorhies JS, Senzer N, Nemunaitis J. 2009. siRNA vs. shRNA: Similarities and differences. *Adv. Drug Deliv. Rev.* **61**: 746–759.

Rathert P, Dhayalan A, Murakami M, Zhang X, Tamas R, Jurkowska R, Komatsu Y, Shinkai Y, Cheng X, Jeltsch A. 2008. Protein lysine methyltransferase G9a acts on nonhistone targets. *Nat Chem Biol* **4**: 344–346.

Reems JA. 2011. A journey to produce platelets in vitro. *Transfusion* **51**: 169S-176S.

Renström J, Kröger M, Peschel C, Oostendorp RA. 2010. How the niche regulates hematopoietic stem cells. *Chem Biol Interact* **184**: 7-15.

Rice JC, Briggs SD, Ueberheide B, Barber CM, Shabanowitz J, Hunt DF, Shinkai Y, Allis CD. 2003. Histone methyltransferases direct different degrees of methylation to define distinct chromatin domains. *Mol Cell* **12**: 1591-1598.

Romania P, Lulli V, Pelosi E, Biffoni M, Peschle C, Marziali G. 2008. MicroRNA 155 modulates megakaryopoiesis at progenitor and precursor level by targeting Ets-1 and Meis1 transcription factors. *Br J Haematol* **143**: 570–580.

Roopra A, Qazi R, Schoenike B, Daley TJ, Morrison JF. 2004. Localized domains of G9a-mediated histone methylation are required for silencing of neuronal genes. *Mol Cell* **14**: 727-738.

Sauvageau G, Iscove NN, Humphries RK. 2004. In vitro and in vivo expansion of hematopoietic stem cells. *Oncogene* **23**: 7223-7232.

Saxonov S, Berg P, Brutlag DL. 2006. A genome-wide analysis of CpG dinucleotides in the human genome distinguishes two distinct classes of promoters. *Proc Natl Acad Sci USA* **103**: 1412-1417.

Schaniel C, Ang YS, Ratnakumar K, Cormier C, James T, Bernstein E, Lemischka IR, Paddison PJ. 2009. Smarcc1/Baf155 couples self-renewal gene repression with changes in chromatin structure in mouse embryonic stem cells. *Stem Cells* **27**: 2979-2991.

Serwold T, Ehrlich LI, Weissman IL. 2009. Reductive isolation from bone marrow and blood implicates common lymphoid progenitors as the major source of thymopoiesis. *Blood* **113**: 807-815.

Shearstone JR, Pop R, Bock C, Boyle P, Meissner A, Socolovsky M. 2011. Global DNA demethylation during mouse erythropoiesis in vivo. *Science* **334**: 799-802.

Shi Y, Desponts C, Do JT, Hahm HS, Schöler HR, Ding S. (2008a). Induction of pluripotent stem cells from mouse embryonic fibroblasts by Oct4 and Klf4 with small-molecule compounds. *Cell Stem Cell* **3**: 568-574.

Shi Y, Do JT, Desponts C, Hahm HS, Schöler HR, Ding S. (2008b). A Combined Chemical and Genetic Approach for the Generation of Induced Pluripotent Stem Cells. *Cell Stem Cell* **2**: 525-528.

Shivdasani RA, Mayer EL, Orkin SH. 1995. Absence of blood formation in mice lacking the T-cell leukaemia oncoprotein tal-1/SCL. *Nature* **373**: 432-434.

Shivdasani RA, Orkin SH. 1996. The transcriptional control of hematopoiesis. *Blood* **87**: 4025-4039.

Silva JM, Li MZ, Chang K, Ge W, Golding MC, Rickles RJ, Siolas D, Hu G, Paddison PJ, Schlabach MR, et al. 2005. Second-generation shRNA libraries covering the mouse and human genomes. *Nat Genet* **37**: 1281-1288.

Small EM, O'Rourke JR, Moresi V, Sutherland LB, McAnally J, Gerard RD, Richardson JA, Olson EN. 2010. Regulation of PI3-kinase/Akt signaling by muscle-enriched microRNA-486. *Proc Natl Acad Sci* **107**: 4218-4223.

Smith AR, Wagner JE. 2009. Alternative haematopoietic stem cell sources for transplantation: place of umbilical cord blood. *Br J Haematol* **147**: 246-261.

Song L, Lin C, Gong H, Wang C, Liu L, Wu J, Tao S, Hu B, Cheng SY, Li M, et al. 2012. miR-486 sustains NF-κB activity by disrupting multiple NF-κB-negative feedback loops. *Cell Res* **23**: 274-289.

Song L, Zhang Z, Grasfeder LL, Boyle AP, Giresi PG, Lee BK, Sheffield NC, Gräf S, Huss M, Keefe D, et al. 2011. Open chromatin defined by DNaseI and FAIRE identifies regulatory elements that shape cell-type identity. *Genome Res* **21**: 1757-1767.

Sorrentino BP. 2004. Clinical strategies for expansion of hematopoietic stem cells. *Nat Rev Immunol* **4**: 878-888.

Stier S, Cheng T, Dombkowski D, Carlesso N, Scadden DT. 2002. Notch1 activation increases hematopoietic stem cell self-renewal in vivo and favors lymphoid over myeloid lineage outcome. *Blood* ***99***: 2369-2378.

Su RC, Brown KE, Saaber S, Fisher AG, Merkenschlager M, Smale ST. 2004. Dynamic assembly of silent chromatin during thymocyte maturation. *Nat Genet* **36**: 502-506.

Suh HC, Gooya J, Renn K, Friedman AD, Johnson PF, Keller JR. 2006. C/EBPalpha determines hematopoietic cell fate in multipotential progenitor cells by inhibiting erythroid differentiation and inducing myeloid differentiation. *Blood* **107**: 4308-4316.

Szilvassy SJ, Humphries RK, Lansdorp PM, Eaves AC, Eaves CJ. 1990. Quantitative assay for totipotent reconstituting hematopoietic stem cells by a competitive repopulation strategy. *Proc Natl Acad Sci USA* **87**: 8736-8740.

Tachibana M, Matsumura Y, Fukuda M, Kimura H, Shinkai Y. 2008. G9a/GLP complexes independently mediate H3K9 and DNA methylation to silence transcription. *EMBO J* **27**: 2681-2690

Tachibana M, Sugimoto K, Nozaki M, Ueda J, Ohta T, Ohki M, Fukuda M, Takeda N, Niida H, Kato H, et al. 2002. G9a histone methyltransferase plays a dominant role in euchromatic histone H3 lysine 9 methylation and is essential for early embryogenesis. *Genes Dev* **16**: 1779-1791.

Tahiliani M, Koh KP, Shen Y, Pastor WA, Bandukwala H, Brudno Y, Agarwal S, Iyer LM, Liu DR, Aravind L, Rao A. 2009. Conversion of 5-methylcytosine to 5-

hydroxymethylcytosine in mammalian DNA by MLL partner TET1. *Science* **324**: 930-935.

Tammen SA, Friso S, Choi SW. 2012. Epigenetics: The link between nature and nurture. *Mol Aspects Med* http://dx.doi.org/10.1016/j.mam.2012.07.018.

Thomas ED, Storb R. 1999. The development of the scientific foundation of hematopoietic cell transplantation based on animal and human studies. In Hematopoietic Cell Transplantation, E.D. Thomas, K.G. Blume, S.J. Forman, eds. (Blackwell Science Inc), pp. 1–11.

Vakoc CR, Mandat SA, Olenchock BA, Blobel GA. 2005. Histone H3 lysine 9 methylation and HP1γ are associated with transcription elongation through mammalian chromatin. *Mol Cell* **19**: 381-391.

Vedadi M, Barsyte-Lovejoy D, Liu F, Rival-Gervier S, Allali-Hassani A, Labrie V, Wigle TJ, Dimaggio PA, Wasney GA, Siarheyeva A, et al. 2011. A chemical probe selectively inhibits G9a and GLP methyltransferase activity in cells. *Nat Chem Biol* **7**: 566-574.

Wen B, Wu H, Shinkai Y, Irizarry RA, Feinberg AP. 2009. Large histone H3 lysine 9 dimethylated chromatin blocks distinguish differentiated from embryonic stem cells. *Nat Genet* **41**: 246-250.

Westbrook TF, Martin ES, Schlabach MR, Leng Y, Liang AC, Feng B, Zhao JJ, Roberts TM, Mandel G, Hannon GJ, et al. 2005. A genetic screen for candidate tumor suppressors identifies REST. *Cell* **121**: 837-48.

Wierenga AT, Vellenga E, Schuringa JJ. 2010. Down-regulation of GATA1 uncouples STAT5-induced erythroid differentiation from stem/progenitor cell proliferation. *Blood* **115**: 4367-4376.

Williams K, Christensen J, Pedersen MT, Johansen JV, Cloos PA, Rappsilber J, Helin K. 2011. TET1 and hydroxymethylcytosine in transcription and DNA methylation fidelity. *Nature* **473**: 343-348.

Wilson A, Trumpp A. Bone-marrow haematopoietic-stem-cell niches. *Nat Rev Immunol* **6**: 93-106.

Zhang CC, Kaba M, Iizuka S, Huynh H, Lodish HF. 2008. Angiopoietin-like 5 and IGFBP2 stimulate ex vivo expansion of human cord blood hematopoietic stem cells as assayed by NOD/SCID transplantation. *Blood* **111**: 3415-3423.

Zhang J, Grindley JC, Yin T, Jayasinghe S, He XC, Ross JT, Haug JS, Rupp D, Porter-Westpfahl KS, Wiedemann LM, et al. 2006. PTEN maintains haematopoietic stem cells and acts in lineage choice and leukaemia prevention. *Nature* **441**: 518-522.

Zhang Y, Sun S, Wang Z, Thompson A, Kaluzhny Y, Zimmet J, Ravid K. 2002. Signaling by the Mpl receptor involves IKK and NF-kappaB. *J Cell Biochem* **85**: 523-535.

Zheng Y, Chen J, Craven M, Choi NW, Totorica S, Diaz-Santana A, Kermani P, Hempstead B, Fischbach-Teschl C, López JA, Stroock AD. 2013. In vitro microvessels for the study of angiogenesis and thrombosis. *Proc Natl Acad Sci* **110**: 2670-2675.

Zon LI. 2001. Hematopoiesis: A Developmental Approach. *New York: Oxford University Press, Inc*